Journal of Double Star Observations

VOLUME 19 NUMBER 4 Oct 1, 2023

Inside this issue:

Inside this issue:

Double Star Measurements with a 12-inch Newtonian Telescope, Annual Report of 2022

Joerg S. Schlimmer
64342 Seeheim-Jugenheim, Germany
Email: js@epsilon-lyrae.de

Abstract

This report shows the results of 323 double star measurements from 2022. During the observations some new components of known double stars and 6 new double stars could be found.

1. Introduction

In 2022 323 double stars were measured. As in previous years, pairs with large magnitude differences were of interest. Especially the double stars discovered by the British astronomer Espin were chosen for observation. An short overview about Espin's double stars cand be found in the author's annual report from 2021 (Schlimmer 2022). During the observations some new components from known double stars and 6 new double stars were discovered and will be discussed.

2. Equipment and Methods

Observations were done with a 12-inch Newtonian telescope in combination with a QHY5L II CMOS color camera. Focal length is 1500 mm, reproduction scale is about 0.52 arc seconds per pixel. In cases of separation < 3" focal length were sometimes magnified with a Barlow lens. Calibration of the telescope setup was described in detail in the previous annual report of 2021 (Schlimmer, 2022).

For each measurement a video with 100 or 200 frames were recorded. Every frame is like a single measurement. Data analyses were done with REDUC software (Losse, 2016). For each frame separation and position angel will be automatically analyzed by the ELI interface. The standard deviation for measurements of the separation is usually smaller than ± 0.15 arc seconds. The standard deviation for measurements of position angel depends on the separation of both components. For double stars with separation of about 5 arc seconds the standard deviation for position angle is usually ±1 degree.

3. Discoveries

During the observations some new components and 6 new double stars could be found which aren't listed in the WDS catalog. The nature of those isn't known. In the case where proper motion of both components is known but different it can be assumed that they are optical double stars.

3.1 New component of WDS04582+3503, BU 1390, (98 Tau)

BU 1390 AB was discovered by Burnham in 1912. AC was already discovered in 1891 by him, but there is no registration about his observations of 98 Tau in his famous *General Catalogue of 1290 double stars discovered from 1871 to 1899* (Burnham, 1900). During the author's observation of BU 1390 a new component next to the primary could be found. Compared with the brightness of component B the brightness of the new component can be estimated at 14 mag. Separation is 28.0'', position angel is about 109°. Figure 1 shows a stacked image of 100 frames. Exposure time was 1s.

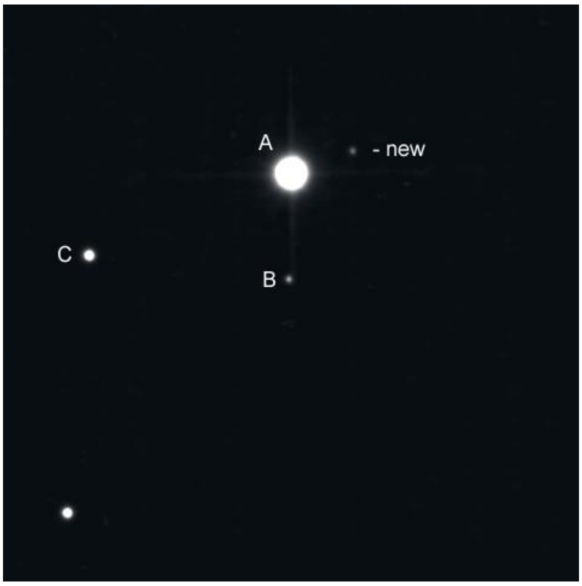

Figure 1 : 98 Tau, (BU 1390), stacked image of 100 frames. Exposure time was 1s.

3.2 A new double star TYC2085-280-1

In a distance of 216'' from ES 469 (WDS17467+2759) a new double star can be found. Identifier of the primary component is TYC2085-280-1, its brightness is 12.15 mag. A second component appears in 6.8'' at an angle of 341°. Its brightness its about 12.7 mag. Figure 2 shows the neighborhood of ES 469 and TYC2085-280-1 from SIMBAD catalog with inlay of stacked frames of TYC2085-280-1 made by the measurement. Coordinates are 17 46 23.8 +27 57 26.3. Its nature is uncertain.

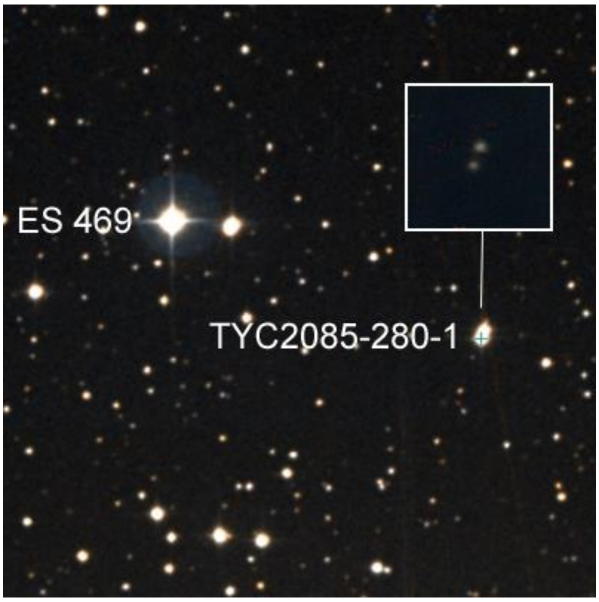

Figure 2 : ES 469 and TYC2085-280-1 from SIMBAD catalog with inlay of stacked frames of TYC2085-280-1 from observation

3.3 New optical double star TYC4209-01624-1 and TYC 4209-1724-1

In a distance of about 17’ from 36 Dra an optical pair TYC4209-01624-1 / TYC 4209-1724-1 could be found. Brightness of TYC4209-01624-1 is 8.93 mag, proper motion is –3.628 / -5.766 mas/yr. Brightness of the secondary component is 11.44 mag, its proper motion is -10.086 / -7.344 mas/yr. Separation of both is 32.36’’, position angle is 263.8°. Coordinates of TYC4209-01624-1 are 18 15 26.4 +64 09 35.1. Because of different proper motions of both components there is no physical relationship between them.

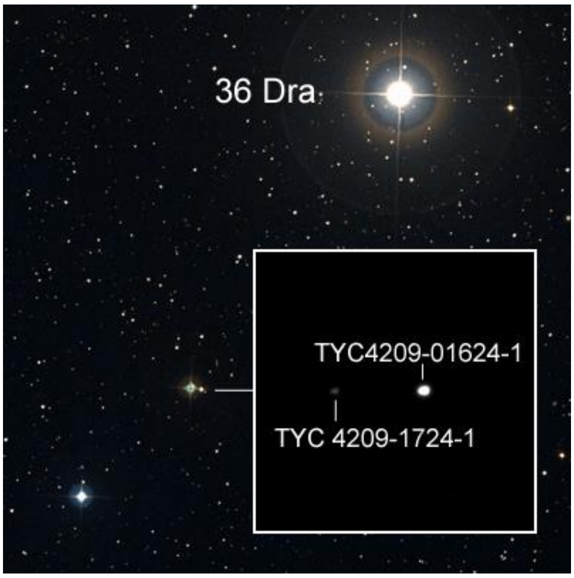

Figure 3 : TYC4209-01624-1 and TYC 4209-1724-18 from SIMBAD catalog with inlay of stacked frames from observation

3.4 New optical double star HD336458 and HD336459 next to WDS18349+2701, ES 477

Only 115’’ from ES 477 (WDS18349+2701) an nice optical pair with HD336458 and HD336459 can be found. Brightness are 10.34 and 10.69 mag, so they can be easily observed. Separation is 27.8’’ position angle is 252.4°. Proper motion of both components is very different, so it can be assumed that there is no physical relationship between them. Coordinates of HD336458 are 18 34 43.9 +26 59 56.9.

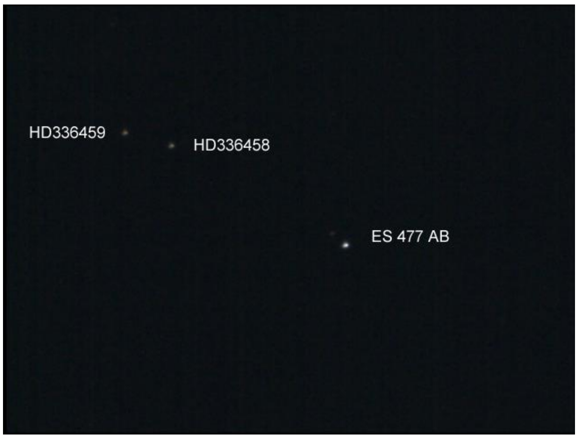

Figure 4 : ES 477 (WDS18349+2701) and HD336458 / HD336459. Image is stack of 100 frames

3.5 Three new components in WDS18569+3112, ES 2422

ES 2422 was discovered in 1930by Espin. His 2 known components has a brightness of 8.96 and 12.00 mag and are in a distance of 5.7''. During observation of ES 2422 the author found 3 further components. First one in a separation of 23.7'' with a position angle of 249.6°. Brightness is about 13 mag. Second new component can be found in a distance of 31.9'' with an angle of 317.2°. Brightness is about 12.5 mag. Third new component has more less the same brightness like component B. Separation is only 13.4'', position angle is 321.2°.

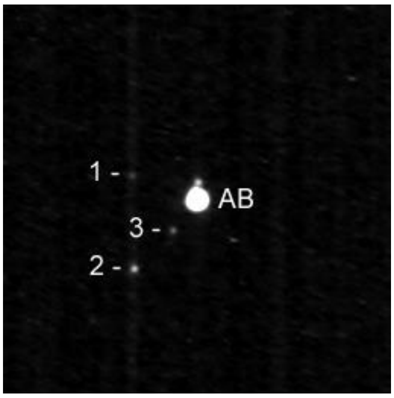

Figure 5 : ES 2422 with 3 new components, labeled by numbers. Image is stack of 100 frames.

3.6 A new triple star next to WDS23154+5516, STI2963

In a distance of 84'' from STI2963 a new triple star system can be found. The brightness of component A with 12 mag is similar to the primary of STI2963, B has a brightness of about 13 mag. Separation between both is 7.9'' position angle is 345.8°. In a distance of 18.8'' at an angle of 303.4° component C can be found. Brightness is about 14 mag. The nature of the triple star system is uncertain.

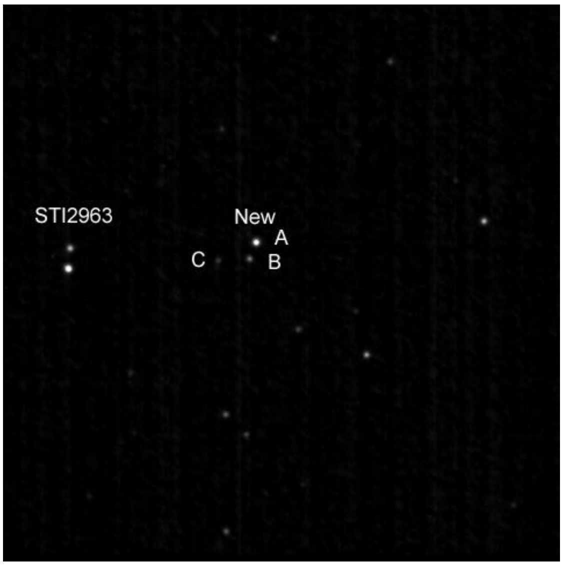

Figure 6 : New triple star system next to STI2963

3.7 New double star HD 23616 next to ES 1044, WDS23271+5302

In a distance of 160''from ES 1044 a new double star can be found. Primary is HD 23616 which has a brightness of 10.23 mag, secondary is a not identified star in a distance of 12.25''. Position angle is 164.5°. Brightness of the secondary is 12.2 mag. Coordinates of HD 23616 are 23 27 28.8 +53 03 48.0. The nature of this double star is uncertain.

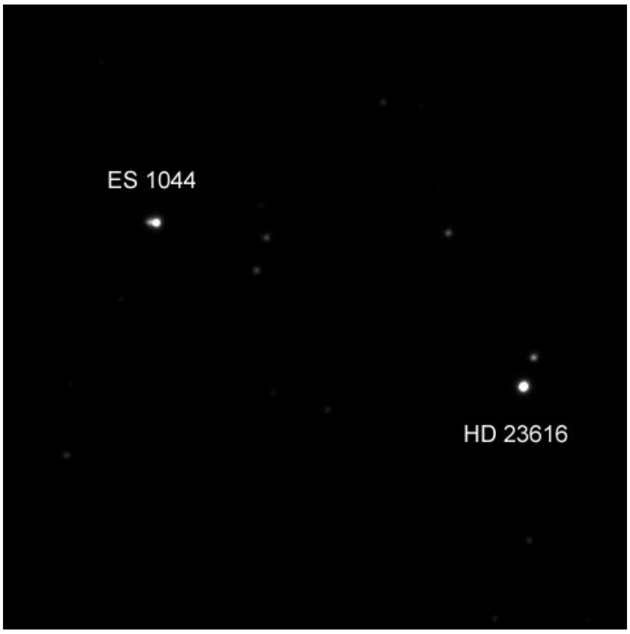

Figure 7 : ES 1044 and HD 23616 with companion.

3.8 A new double star USNO-B1 1422-0565068 and USNO-B1 1421-0552384

About 4' from WDS 23361+5211 (TDT4121) a new double star can be found. With a brightness of 11.4 mag USNO-B1 1422-0565068 is the primary, while USNO-B1 1421-0552384 in 3.95'' is the secondary with a brightness of 12.3 mag. Position angle is 14.4°. Proper motion of the primary is -10 in RA and -4 mas in DE, proper motion of the secondary isn't known. The new double star can be found at 23 35 39.9 in RA and +52 12 11.8 in DE. The nature of this double star is uncertain.

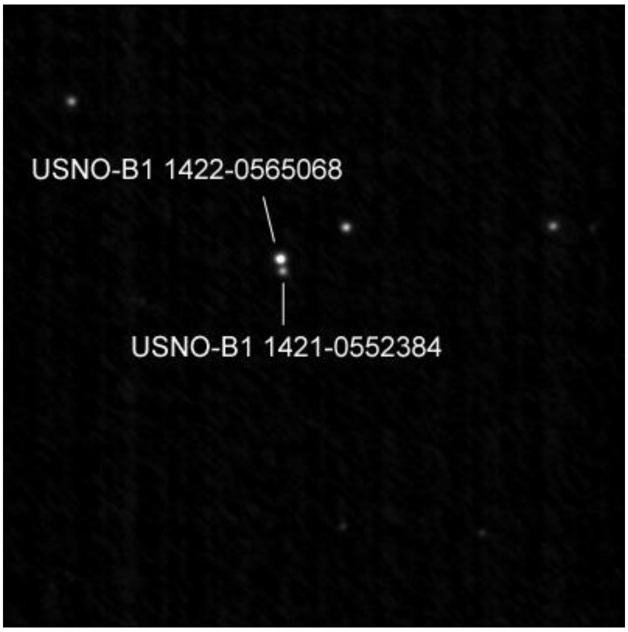

Figure 8 : USNO-B1 1422-0565068 and USNO-B1 1421-0552384

4. Observation Data

The following table shows the measurements of separation and position angle of 323 double stars from 2022. Brightness and coordinates are taken from *The Washington Double Star Catal*og (Mason et al., 2020). Date is given in Julian years. N gives the numbers of observation nights. Usually, every double star will be observed only for one night (N=1).

Table 1: Measurements of 2022

RA+DEC	**Name**	**MAGS**	**PA**	**SEP**	**Date**	**N**	**Notes**
03001+4323	ES 1511	10.5,11.7	281.3	6.72	2022.120	1	
03119+4146	ES 1513	10.58,11.7	92.7	7.40	2022.120	1	
03164+5050	ES 769	10.23,12.1	139.1	5.42	2022.120	1	
04010+3415	ES 237	9.82,11.17	331.0	3.09	2022.120	1	
04026+5304	ES 1066	10.9,11.1	115.1	5.65	2022.120	1	
04075+6009	ES 1715	8.73,10.6	165.1	5.86	2022.120	1	
04078+6220	ES 2603AB	6.91,12.9	255.3	6.41	2022.120	1	NGC1502
04078+6220	STF 485AC	6.91,13.5	0.8	11.18	2022.120	1	NGC1502
04078+6220	STF 485AE	6.91,6.94	305.2	17.91	2022.120	1	NGC1502
04078+6220	STF 484GH	9.63,10.5	133.4	5.55	2022.120	1	NGC1502
04078+6220	HLM 3LM	10.4,11.4	216.6	5.99	2022.120	1	NGC1502
04078+6220	HZG 2OP	9.49,10.69	229.2	17.37	2022.120	1	NGC1502
04089+6231	ES 1882	9.33,12.4	278.2	7.31	2022.120	1	
04091+4801	ES 1223	10.21,12.1	112.3	3.73	2022.120	1	
04477+4744	ES 1318	10.2,11.3	156.7	2.21	2022.167	1	
04537+4737	ES 1227	9.86,11.3	239.2	4.12	2022.162	1	
04582+2503	BU 1390AB	5.81,13.3	357.7	45.28	2022.162	3	
04582+2503	NEW	5.81/14	109.3	28.00	2022.162	2	See section 3.1
05020+4349	BU 554AB	2.99,14.0	226.2	29.33	2022.222	1	Eps Aur
05020+4349	BU 554AC	2.99,11.26	276.0	43.17	2022.222	1	
05020+4349	BU 554AD	2.99,13.4	317.5	44.92	2022.222	1	
05020+4349	SMR 25AG	2.99,14.	15.2	99.52	2022.222	1	
05020+4349	SMR 25AI	2.99,13.5	140.9	111.86	2022.222	1	
05020+4349	SMR 25AJ	2.99,13.5	159.9	132.44	2022.222	1	
05039+3223	ES 412	8.3,13.1	275.0	5.13	2022.162	1	
05046+4232	ES 1621	9.92,12.3	193.4	4.13	2022.162	1	
05058+3540	ES 331	9.27,11.7	326.8	8.05	2022.167	1	
05132+4429	ES 1373AB	9.50,10.6	85.9	5.61	2022.167	1	
05143+6127	ES 1963	9.09,12.8	269.7	3.59	2022.162	1	
05144+5424	ES 889	10.0,11.4	319.3	7.91	2022.167	1	
05145-0812	STF 668A,BC	0.3,6.8	202.8	9.46	2022.136	1	Rigel
05167+4600	HJ 2256AF	0.08,10.21	134.2	104.72	2022.222	1	
05173+5335	ES 2610	9.51,10.13	52.4	45.00	2022.167	1	
05212+5023	ES 2613	9.38,10.1	123.6	8.81	2022.167	1	

05247+3723	BU 888AB	5.16,12.0	163.4	7.47	2022.162	1	
05272+1758	STT 107AB	5.39,11.1	306.8	10.13	2022.162	2	
05274+5422	ES 891	9.40,12.6	67.3	6.90	2022.167	1	
05280+4110	ES 1724	10.67,12.9	48.4	2.90	2022.167	1	
05314+4152	ES 1625	10.6,11.6	80.3	3.14	2022.181	1	
05316+3843	ES 2216	11.4,11.6	125.8	3.35	2022.181	1	
05320-0018	STFA 14AC	2.41,6.83	0.7	52.46	2022.110	1	
05323+4924	STF 718AB	7.47,7.54	72.2	7.78	2022.181	1	
05329+4912	ES 1072	10.3,11.4	0.28	3.39	2022.181	1	
05332+6212	ES 1887	9.28,10.4	106.3	5.37	2022.181	1	
05365+3903	ES 2152	10.31,11.8	312.6	7.16	2022.181	1	
05407-0157	STF 774AB	1.88,3.70	168.3	2.07	2022.110	1	
05407-0157	STF 774AC	1.88,9.55	10.2	58.18	2022.110	1	
05424+3831	ES 2217	10.30,10.55	131.0	3.97	2022.181	1	
05469+0931	J 251	5.79,11.9	304.8	16.67	2022.162	1	
05515+3909	H 5 90	3.97,11.40	206.5	55.56	2022.222	1	
05533+3725	ES 284	10.4,12.4	182.9	4.67	2022.222	1	
05574+0002	BU 1190AC	6.95,12.1	100.9	6.58	2022.162	1	
05597+3713	STT 545AB	2.60,7.2	301.6	3.705	2022.222	1	
06039+4754	ES 1233	9.2,11.0	208.7	2.94	2022.222	1	
06148+1909	HJ 2302AB	5.20,11.2	179.0	5.64	2022.162	2	
06288-0702	STF 919AB	4.62,5.00	132.1	7.34	2022.181	1	
06288-0702	STF 919AC	4.62,5.39	126.8	9.54	2022.181	1	
06288-0702	STF 919BC	5.00,5.32	107.0	2.63	2022.181	1	
06367+4404	ES 582AB	11.29,11.66	79.3	23.92	2022.222	1	
06367+4404	ES 582BC	11.66,14.4	301.8	6.60	2022.222	1	
06410+0954	STF 950AC	4.66,9.9	14.4	16.60	2022.181	2	AB,C
06410+0954	D 11EP	8.86,10.4	46.0	3.88	2022.181	2	
06425+3902	SIN 119AC	8.34,11.3	28.9	15.41	2022.222	1	
06451-1643	AGC 1AB	-1.47,8.44	64.8	11.27	2022.175	8	Sirius
06505+5327	ES 899	10.0,11.2	314.5	2.90	2022.222	1	
07277+2208	ES 2625AB	6.98,12.4	26.4	11.63	2022.222	1	
07303+4136	ES 586	8.26,11.2	23.1	13.45	2022.222	1	
08358+0637	STF1245AB	5.98,7.16	24.9	10.09	2022.235	1	
08397+0546	STF1255AB	7.33,8.56	30.5	25.93	2022.235	1	
08468+0625	STF1273AB,C	3.49,6.66	313.8	2.78	2022.235	1	
08484+0550	AGC 3	4.36,11.9	146.8	12.20	2022.235	1	
08534+0513	A 2752	8.99,11.01	229.6	5.11	2022.235	1	
09036+4903	ES 72	9.29,12.3	301.0	13.33	2022.402	1	
09098+5340	ES 715	10.36,11.7	232.5	7.77	2022.402	2	
09144+0219	HJ 2489AB	3.85,9.9	255.8	20.64	2022.235	1	
09188+3648	STF1334AB	3.92,6.09	222.0	2.54	2022.416	1	3000mm
09234+5136	ES 718AB	10.16,12.5	28.1	7.86	2022.402	1	
09257+3837	ES 298AB	9.99,12.4	319.8	8.42	2022.402	1	
09257+3837	ES 298AC	9.99,11.09	320.8	93.61	2022.402	1	
09257+3837	ES 298CD	11.09,12.1	173.9	3.80	2022.402	1	
09368+5755	ES 1783AB	10.04,10.75	240.8	120.54	2022.402	1	

09368+5755	ES 1783Ba,Bb	11.1,11.9	9.0	2.02	2022.402	1	
09412+0954	H 6 76AB	3.56,10.83	48.9	97.79	2022.345	1	
09447+3218	ES 2347	10.72,11.0	251.4	7.95	2022.402	1	
09504+4245	ES 1244	10.24,11.07	242.1	2.06	2022.416	1	3000mm
09538+4658	ES 913	10.2,11.3	337.3	7.62	2022.402	1	
10009+4631	ES 914	10.46,12.8	327.3	5.85	2022.345	1	
10050+4634	ES 1149	9.33,12.7	249.6	7.98	2022.345	1	
10084+1158	STFB 6AB	1.40,8.24	308.1	176.51	2022.345	1	
10185+3630	HJ 2525	11.80,12.00	67.4	13.60	2022.345	1	
10258+3237	ES 432	11.06,11.62	165.7	2.64	2022.402	1	
10262+3628	ES 302	11.22,12.7	345.9	2.66	2022.345	1	
10303+6321	ES 1905AB	8.59,12.64	67.0	41.2	2022.345	1	
10443+3739	ES 2634	10.90,11.52	234.4	9.44	2022.402	1	
10479+3958	ES 1543	10.0,12.5	7.9	3.34	2022.416	1	
10532+4359	ES 2635AB	9.54,10.3	34.5	9.62	2022.416	1	
10562+4802	ES 2636	8.90,9.62	149.4	42.68	2022.416	1	
10590+3256	ES 2283AB	11.13,12.62	106.9	5.64	2022.416	1	
11141+2031	STT 573AB	2.54,10.87	341.6	208.60	2022.345	1	
11141+2031	BU 1282AC	2.54,12.69	28.6	98.96	2022.345	1	
11323+3323	ES 2284	11.0,11.1	76.2	2.94	2022.416	1	
11381+3246	ES 2285AB	11.01,12.39	331.2	10.78	2022.416	1	
11491+1434	BU 604AD	2.14,8.49	193.7	235.82	2022.345	1	
12081+5528	STF1603AB	7.82,8.26	83.5	22.22	2022.424	1	
12104+5455	ES 73AB	9.05,11.6	29.7	37.77	2022.424	1	
12104+5455	ES 73BC	11.6,12.1	306.9	3.06	2022.424	1	
12269+2816	SMR 58	4.4,12.	205.6	15.77	2022.402	1	
12280+4753	ES 2642	10.15,10.41	258.0	28.22	2022.424	1	
12347+4808	ES 924	11.07,11.72	219.4	4.17	2022.424	1	
12353+3634	ES 2166	12.4,12.7	357.9	4.78	2022.424	1	
12397+4028	ES 1402AB	10.6,11.6	27.1	3.78	2022.424	2	
12406+4017	HJ 2617AB	8.41,9.61	1.4	5.69	2022.424	1	
12417-0127	STF1670AB	3.48,3.53	356.2	3.15	2022.408	3	3000mm
12439+5349	ES 729	9.1,12.6	226.9	8.81	2022.424	1	
13119+2753	STT 578	4.30,12.1	178.6	134.67	2022.402	1	
13149+4847	PKO 10	12.00,11.90	269.7	20.38	2022.444	1	
13152+4838	ES 732	10.93,10.98	88.2	3.39	2022.444	1	
13239+5456	STF1744AB	2.23,3.88	152.9	14.41	2022.424	1	
13265+4233	ES 2645	10.99,11.10	210.9	21.94	2022.444	1	
13486+4821	BU 802	7.56,11.78	221.1	3.25	2022.444	1	
13529+4744	ES 960AB	10.7,11.9	270.4	4.43	2022.444	1	
14375+4743	ES 609AB	10.23,11.9	15.2	4.51	2022.444	1	
14375+4743	ES 609AC	10.23,10.22	117.9	78.64	2022.444	1	
14380+5135	STF1863	7.71,7.80	57.6	0.63	2022.405	1	
14439+4743	ES 962AB	8.7,11.3	267.2	11.44	2022.444	1	
14573+4806	ES 2647	9.44,12.4	118.5	9.06	2022.444	1	
15054+4809	BU 1086	5.57,13.3	252.2	6.49	2022.444	1	
15127+4835	ES 2648AB	7.28,11.25	340.7	26.24	2022.444	1	

15135+3244	ES 2476	10.5,11.5	212.7	2.56	2022.444	1	
15151+3318	SMR 32AB	12.76,11.21	337.5	27.80	2022.444	1	
15151+3318	SMR 32AC	12.76,12.90	70.2	37.51	2022.444	1	
15151+3318	SMR 32BC	11.21,12.90	105.8	47.69	2022.444	1	
15185+5159	BEM 18	10.3,12.0	13.5	8.68	2022.454	1	
15198+5245	ES 741AB	9.78,11.8	233.6	8.91	2022.454	1	
15200+4603	ES 75AB,C	11.02,10.74	35.7	4.42	2022.454	1	
15222+4508	ES 2649	9.55,10.14	5.2	25.75	2022.454	1	
15351+4150	ES 1553	11.40,11.78	151.6	2.69	2022.454	1	
15409+5009	ES 626	9.2,9.2	275.6	8.17	2022.454	1	
16003+5856	STF2006AB	8.48,9.96	180.3	1.50	2022.539	1	3000mm
16010+4338	ES 1556	9.5,11.2	235.3	11.05	2022.487	3	
16042+5923	ES 2650	8.56,10.0	209.1	10.83	2022.505	3	
16051+5426	ES 743	9.71,12.8	11.9	5.45	2022.507	1	
16090+5756	ES 2651	6.33,12.14	139.4	12.38	2022.501	1	
16126+5748	ES 1793	8.74,11.52	56.8	5.62	2022.501	1	
16186+5120	ES 627	9.88,10.98	287.2	11.86	2022.501	1	
16232+6017	ES 1827	10.2,12.1	36.4	4.92	2022.501	1	
16356+5633	ES 2652	11.00,11.12	180.8	13.34	2022.501	1	
16362+5255	STF2078AB	5.38,6.42	103.5	2.99	2022.539	1	
16379+5608	A 1140	8.61,11.7	117.8	3.29	2022.501	1	
16408+5014	ES 632	11.27,11.70	107.9	1.64	2022.537	1	
16426+2340	STF2087AB	8.84,8.90	287.7	5.24	2022.539	1	3000mm
16440+5036	ES 76AB	10.77,11.27	43.0	2.20	2022.519	2	
16440+5036	ES 76AC	10.77,11.07	204.6	44.28	2022.519	2	
16442+2331	STF2094AB	7.48,7.87	75.0	1.03	2022.539	1	3000mm
16454+5027	ES 2653	10.48,12.0	289.5	10.85	2022.501	1	
16461+5012	ES 969	11.01,11.45	237.5	2.57	2022.537	1	
16465+4759	ES 1089AB	10.66,11.7	150.5	12.55	2022.522	2	
16465+4759	ES 1089AC	10.66,12.73	29.8	32.63	2022.522	2	
16465+4759	CTT 20DE	10.75,12.49	126.3	27.40	2022.507	1	
16465+4759	CTT 20EF	12.49,12.72	33.9	34.65	2022.507	1	
16518+5103	ES 971AB	10.53,12.21	43.42	46.31	2022.522	2	
16555+5141	ES 972	11.64,11.93	104.1	2.08	2022.537	1	
16566+5127	ES 2654	9.21,9.83	282.5	37.03	2022.537	1	
16566+4505	ES 2655	9.72,9.92	67.2	47.70	2022.543	2	
17053+5428	STF2130AB	5.66,5.69	356.9	2.68	2022.539	1	3000mm
17131+5408	STF2146AB	8.71,10.56	223.5	2.50	2022.539	1	3000mm
17146+1423	STF2140AB	3.48,5.40	103.5	4.86	2022.602	1	a Her
17161+5854	ES 1794	11.00,11.22	139.4	4.02	2022.543	2	
17195+5832	KR 46	9.34,9.60	63.5	1.58	2022.537	1	3000mm
17220+5638	ES 2657AB	8.60,11.2	96.4	27.9	2022.548	1	
17220+5638	ES 2657BC	11.2,11.5	72.9	11.51	2022.548	1	
17245+4327	ES 1413	10.34,12.9	240.5	7.70	2022.548	1	
17270+5718	ES 2658	9.98,12.1	15.7	9.83	2022.548	1	
17319+5655	ES 2659	8.63,11.15	215.0	11.69	2022.561	1	
17374+5040	ES 2661AB	8.46,9.84	102.6	58.52	2022.561	1	

17374+5040	ES 2661BC	9.84,12.8	17.5	14.94	2022.561	1	
17386+5546	STF2199	8.03,8.60	52.3	2.02	2022.539	1	3000mm
17444+4027	ES 9004	8.10,12.7	248.2	13.29	2022.561	1	
17467+2759	ES 469AB	9.03,11.79	267.3	47.14	2022.548	1	
17467+2759	ES 469BC	11.79,14.8	149.0	3.72	2022.548	1	
17464+2757	NEW	12.15,12.7	341.4	6.80	2022.548	1	See section 3.2
17484+4941	ES 1092	11.40,11.8	21.9	3.65	2022.561	1	
17496+3649	ES 2169	11.40,11.7	337.4	8.54	2022.548	1	
17536+6103	ES 1833	7.95,12.6	261.4	8.14	2022.561	1	
17555+4108	ES 1557AB	9.08,12.4	12.8	11.75	2022.548	1	
17555+4108	ES 1557AC	9.08,12.29	216.0	27.00	2022.548	1	
17555+4108	ES 1557AD	9.08,13.35	313.7	40.22	2022.548	1	
17566+3110	ES 343	9.74,12.4	284.6	8.28	2022.548	1	
17573+3351	ES 344	9.7,10.2	31.6	9.06	2022.548	1	
17574+5111	ES 78AB	9.44,12.38	130.3	7.88	2022.548	1	
18003+4548	ES 1260	10.63,11.7	201.6	2.77	2022.561	2	
18011+4521	STF3129	7.59,10.64	167.7	30.82	2022.561	1	
18015+4517	STF2270	10.95,11.1	211.7	6.26	2022.561	1	
18025+3643	ES 2479	10.65,12.7	232.0	9.92	2022.561	1	
18033+2751	ES 470	9.45,10.7	209.7	8.11	2022.600	1	
18047+2750	SLE 109	10.72,13.7	79.6	9.76	2022.600	1	
18047+2707	ES 471AC	7.21,10.2	44.9	23.92	2022.600	1	
18047+2707	SLE 106AD	7.21,11.03	244.9	88.83	2022.600	1	
18047+2707	SLE 106AE	7.21,10.84	43.1	183.62	2022.600	1	
18048+5435	ES 641	11.0,11.2	65.4	1.94	2022.600	1	3000mm
18069+4647	ES 1157AB	8.42,11.29	179.6	30.6	2022.600	1	
18069+4647	ES 1157AD	8.36,11.65	237.2	50.43	2022.600	1	
18069+4647	ES 1157BC	11.29,12.0	11.7	2.55	2022.600	1	
18077+3904	ES 2018	10.13,11.15	235.1	5.76	2022.600	1	
18080+3642	ES 183	9.36,12.7	168.6	8.33	2022.600	1	
18089+3254	ES 184AB	9.7,11.9	160.4	4.96	2022.600	1	
18107+3903	ES 2569	9.5,10.0	275.3	9.97	2022.602	1	
18111+3258	ES 185	9.89,10.99	283.6	12.79	2022.600	1	
18127+5557	ES 643	10.71,12.9	49.3	3.53	2022.613	1	
18138+6235	ES 1836	10.65,12.5	151.9	3.89	2022.602	1	
18138+5341	ES 645	8.94,12.7	84.7	2.96	2022.613	1	
18147+5635	BU 1274A,BC	6.37,10.91	237.2	93.98	2022.613	1	
18147+5635	BU 1274BD	9.8,10.4	4.9	5.41	2022.613	1	
181554+6410	NEW	8.93,11.44	263.8	32.36	2022.600	1	See section 3.3
18156+4417	ES 1420AB	10.22,11.4	67.2	8.38	2022.613	1	
18156+4417	ES 1420AC	10.22,14.5	10.6	14.42	2022.613	1	
18157+3723	ES 2664	10.57,10.78	84.0	9.23	2022.655	2	
18162+6404	ES 186	8.23,12.0	329.0	7.95	2022.600	2	
18162+4423	ES 1421	8.70,11.86	344.7	12.12	2022.655	2	
18197+4453	ES 2665AB	8.76,11.27	21.8	10.07	2022.698	1	
18210+3630	ES 2110	9.3,10.8	95.2	6.40	2022.698	1	
18218+6358	ES 1837	9.83,11.6	212.3	16.20	2022.698	1	

18259+6029	ES 2666	8.45,9.92	268.5	45.28	2022.698	1	
18269+4031	ES 1653	11.2,11.4	191.0	10.16	2022.698	1	
18280+2708	ES 475	9.74,10.7	221.6	10.20	2022.698	1	
18306+2805	ES 476AB	11.0,11.6	348.4	2.62	2022.723	1	
18306+2805	ES 476AC	11.0,12.0	324.3	28.34	2022.6723	1	
18325+4513	ES 1262	10.90,11.15	256.1	1.53	2022.747	1	3000 mm
18329+6343	STF2357	9.32,9.89	270.0	4.62	2022.735	2	
18337+3726	MLB 937	11.53,13.9	117.4	2.887	2022.723	1	
18339+3208	SLE 209	8.22,12.	29.1	10.31	2022.723	1	
18340+5058	ES 785AB	9.56,10.0	97.6	9.43	2022.723	1	
18340+5045	ES 786	11.33,11.6	322.0	5.82	2022.723	1	
18349+2701	ES 477	9.30,11.9	226.7	10.40	2022.747	1	
18347+2700	NEW	10.34,10.69	252.4	27.84	2022.735	2	See section 3.4
18369+3846	H 5 39AB	0.09,9.5	184.7	84.81	2022.582	2	Vega
18369+3846	STFB 9AE	0.09,9.5	38.5	84.21	2022.592	2	
18375+3112	A 250	9.39,10.61	115.2	2.39	2022.723	1	
18386+4700	ES 1159AB	9.8,11.5	252.0	3.75	2022.723	2	
18386+4700	ES 1159AC	9.8,11.1	346.2	19.70	2022.723	2	
18393+6348	ES 126AB	8.36,11.47	50.9	72.63	2022.723	1	
18393+6348	ES 126BC	11.47,12.34	22.4	4.78	2022.723	1	
18413+6311	ES 1839	10.5,12.5	12.8	4.21	2022.747	1	
18439+6039	ES 189AB	10.2,12.2	107.3	3.18	2022.747	1	
18443+3940	STF2382AB	5.15,6.10	341.1	2.05	2022.602	1	Eps Lyr,
18443+3940	STF2383CD	5.25,5.38	72.2	2.39	2022.602	1	
18466+3853	ES 2021AB	11.26,12.2	254.7	20.24	2022.747	1	
18466+3853	ES 2021BC	12.2,13.4	293.2	4.14	2022.747	1	
18473+6254	ES 127	11.12,11.30	143.8	4.94	2022.747	1	
18501+3322	STFA 39AB	3.63,6.69	147.5	45.79	2022.602	1	b Lyr
18501+3322	BU 293AE	3.63,10.14	316.5	67.38	2022.602	1	
18501+3322	BU 293AF	3.63,10.62	17.4	86.20	2022.602	1	
18508+4543	ES 1264	10.37,11.5	114.0	3.29	2022.764	1	
18516+3739	ES 2025AB	10.98,11.46	354.6	25.81	2022.764	1	
18516+3739	FYM 39AE	10.98,13.4	300.2	63.18	2022.764	1	
18516+3739	FYM 39AG	10.98,12.8	114.6	55.53	2022.764	1	
18516+3739	ES 2025BC	11.46,14.2	78.1	6.36	2022.764	1	
18516+3739	ES 2025BD	11.46,12.2	10.9	5.32	2022.764	1	
18520+3731	ES 2026AB	7.34,12.8	110.5	20.42	2022.764	1	
18520+3731	ES 2026BC	12.8,13.3	328.5	4.25	2022.764	1	
18523+3321	ES 2233AB	8.65,11.9	246.5	44.60	2022.764	1	
18523+3321	ES 2233BC	11.9,12.1	89.0	2.38	2022.764	1	
18545+3719	HO 90	8.72,12.7	226.9	3.69	2022.764	1	
18551+3645	ES 2485	11.0,11.5	164.0	5.20	2022.764	1	
18569+5723	ES 1747	10.26,10.58	350.3	1.59	2022.764	1	
18569+3112	ES 2422	8.96,12.0	179.8	5.66	2022.764	1	
18569+3112	ES 2422 AC	8.96,13	249.6	23.67	2022.764	1	see section 3.5
18569+3112	ES 2422 AD	8.96,12.5	317.2	31.85	2022.764	1	see section 3.5
18569+3112	ES 2422 AE	8.96,12	321.2	13.40	2022.764	1	see section 3.5

18580+6159	ES 1843	11.00,12.3	168.1	4.93	2022.764	1	
18593+6347	ES 1844AB	9.6,10.5	18.8	2.63	2022.764	1	
18598+5543	ES 1748	9.45,10.8	53.5	6.59	2022.764	1	
21069+3845	STF2758AB	5.20,6.05	153.9	32.04	2022.723	1	
21069+3845	STF2758AH	5.35,9.97	261.8	139.04	2022.723	1	
21069+3845	SMR 1AI	5.35,10.74	235.4	54.54	2022.723	1	
21069+3845	SMR 40AO	5.35,12.65	274.2	181.10	2022.723	1	
21069+3845	SMR 40AP	5.35,12.84	282.1	170.61	2022.723	1	
21069+3845	SMR 40AQ	5.35,13.19	291.9	78.86	2022.723	1	
23007+3105	STF2968	6.69,9.48	97.7	3.08	2022.947	1	
23045+3123	ES 396	10.84,10.91	303.6	37.66	2022.947	1	
23058+5006	ES 107AB	9.40,12.3	221.6	6.47	2022.947	1	
23058+5006	FOX9019AC	9.40,12.5	57.3	11.26	2022.947	1	
23105+5454	ES 1037	10.83,11.92	339.2	2.91	2022.947	1	
23153+5500	HJ 1861AB	10.12,12.0	258.7	18.44	2022.947	1	
23153+5500	HJ 1861BC	12.0,12.5	110.8	5.49	2022.947	1	
23154+5516	STI2963	12.06,12.8	183.2	9.10	2022.947	1	
23155+5516	NEW	12,13	345.8	7.87	2022.947	1	see section 3.6
23155+5516	NEW	12,14	303.4	18.79	2022.947	1	see section 3.6
23185+5409	ES 695AB	10.00,10.98	312.4	3.82	2022.947	1	
23187+5244	ES 1042	10.20,10.78	312.6	2.81	2022.947	1	
23192+5408	ES 696	9.78,12.4	232.5	2.90	2022.947	2	
23204+5530	ES 697AB	9.10,9.89	344.5	67.79	2022.947	1	
23204+5530	ES 697BC	9.89,13.4	71.0	4.59	2022.947	1	
23242+3753	ES 2002	10.6,11.1	101.1	4.02	2022.958	1	
23249+5430	ES 2728	9.79,10.17	247.3	10.11	2022.947	1	
23253+3528	ES 2136	10.3,12.0	355.6	3.64	2022.958	1	
23257+4800	ES 857	10.5,11.8	166.4	2.63	2022.958	1	
23266+5458	ES 1043AB	9.30,11.60	27.2	28.53	2022.947	1	
23266+5458	ES 1043AD	9.30,12.14	15.5	43.27	2022.947	1	
23266+5458	ES 1043BC	11.1,11.3	116.0	-	2022.947	1	
23271+5302	ES 1044	10.4,12.4	270.6	2.66	2022.953	1	
23273+5204	New	10.23,12.2	164.5	12.25	2022.953	1	see section 3.7
23293+2949	ES 400	10.83,11.4	210.5	6.01	2022.958	1	
23370+3456	ES 2208	10.8,11.0	86.5	2.61	2022.947	1	
23380+5249	ES 2729	8.08,9.53	142.0	19.80	2022.958	1	
23354+5212	NEW	11.4,12.3	14.4	3.95	2022.958	1	see section 3.8
23432+5455	ES 1048AB	10.87,12.57	249.4	14.61	2022.958	1	
23432+5455	ES 1048AC	10.87,11.57	283.0	16.42	2022.958	1	
23432+5455	ES 1048AD	10.87,10.84	14.8	70.42	2022.958	1	
23432+5455	ES 1048DE	10.84,10.9	322.9	4.60	2022.958	1	
23460+6013	ES 1767	10.85,12.9	38.3	5.56	2022.947	1	
23461+6028	STF3037AB	7.35,9.20	214.1	2.26	2022.947	1	
23465+5443	STI3032	11.94,12.9	220.7	10.62	2022.958	1	
23481+5947	ES 2733	9.89,11.1	84.6	9.05	2022.947	1	
23481+4106	ES 2734	8.35,10.08	222.8	28.67	2022.947	1	
23503+5114	ES 1124	10.38,10.87	247.5	2.75	2022.958	1	

23537+5453	ES 1050AB	9.73,12.6	228.2	3.60	2022.958	1
23537+5453	ES 1050AC	9.73,10.46	309.6	39.95	2022.958	1
23544+5139	ES 1125	10.87,11.14	331.6	4.44	2022.958	1
23546+5141	DAM 257	11.4,15.	325.3	8.33	2022.958	1
23583+5002	ES 927	10.42,12.9	190	6.10	2022.958	1
23596+5359	ES 703AB	8.40,12.0	269.8	7.35	2022.958	2
23596+5359	ES 703AC	8.40,11.32	265.2	50.75	2022.958	2

Acknowledgements:

This research has made use of the Washington Double Star Catalog maintained at the U.S. Naval Observatory.

This research has made use of the SIMBAD database, operated at CDS, Strasbourg, France

References:

Burnham, A.W., A General catalogue of 1290 double stars discovered from 1871 to 1899 by S.W. Burnham, reprint by Amazon

Losse, Florent (2016), Reduc Software, http://www.astrosurf.com/hfosaf/uk/tdownload.htm#reduc#

Schlimmer, S. Joerg (2022), Double Star Measurements with a 12-inch Newtonian Telescope, Annual Report of 2021, Journal of Double Star Observations Vol. 18, No. 3, p. 322-335

New Measurements of the WDS 15232+3017 (STF 1937)

Zsolt Szamosvári
Hungarian Astronomical Association Double Star Section
H-2500 Esztergom, Hungary
szamos.photo@gmail.com

Abstract

The quintuple system WDS 15232+3017 was observed using the iTelescope network's T19 telescope to make new measurements of the system's angular separation and position. WDS 15232+3017 AB,C has an average angular separation and position angle of 76.84" and 357.14°, AB,D 218.06" and 39.77°, AB,E 213.73" and 130.20°. These measurements, combined with parallax and proper motion data from Gaia DR3 and SIMBAD, suggest that the stars are physically relationship. It was not possible to measure AB, it is outside the resolution limit of the telescope used.

1. Introduction

The goal of this research was to provide additional measurements of angular separation and position angle to determine whether the components of WDS 15232+3017 form a binary system. Furthermore, to provide new measurement data for the WDS on the components AB,C, for AB,D and AB,E. WDS 15232+3017 is registered as a quintuple system with components A, B, C, D, E. There are 8 observations of stars C and D each, and 1 observation of star E in the WDS. The number of observations of the AB components is over 1 000, and the orbit elements are also known for this. In this paper, the various orbit solutions are illustrated, and the calculated angular separation and position angle for the year 2023 are also given.

2. Brief History

WDS 15232+3017 was discovered by Sir William Herschel in 1781. The first successful measurement of AB was made by Friedrich von Struve in 1827. The first successful measurement of component C was made in 1856, and component D in 1879. The star marked E was added to the system in 2000. In the WDS, the last observation for stars C and D was in 2006, for star E in 2000.

3. General Description

WDS 15232+3017 (STF 1937) is in the constellation Corona Borealis, Bayer's name is Eta CrB, Flamsteed's is 2 CrB. It is listed in the SIMBAD database as HD 137107, SAO 64673, GL584A, Tyc 256-01366-1. Its celestial coordinates are 15h 23m 12.23s +30° 17' 17.7". The distance of the primary star from Earth is between 17.86 and 16.72 parsecs (SIMBAD, Wenger et al, 2000).

There are a very close double stars here, which we consider to be the main star. It has two similar type companions further afield, as well as a brown dwarf.

4. Equipment and Methods

The images were acquired by the T19 telescope, located in Beryl Junction, Utah, USA, at an elevation of 1 570 meters. The CCD camera for T19 is an FLI-PL 16803 with a resolution of 0.63" per pixel, housing an array 4096 by 4096, with a FOV of 43,2 by 43,2 arcminutes. The CCD camera is mounted on a Planewave 17 Corrected Dirk-Kirkham (CDK) OTA, with a focal length of 2 912 mm with an aperture of 431 mm and a focal ratio of f/6.8.

First, 10 images taken on July 4, 2023 (2023,512) with 60s exposure time and luminance filter. Second, on July 12, 2023 (2023,526), 10 images were taken with an exposure time of 120s and luminance filter. Figure 1 shows the instrument. Source: iTelescope.net.

Figure 1: The T19 Telescope

For measurements, was used AstroImageJ (Collins et al, 2017) software. The FITS files were calibrated using my astronomy.net key within the software. At this point, the program shows the images with the correct skyline, and allows for accurate separation and position angle measurement. Was adjusted the brightness and aperture sizes individually to get the best results.

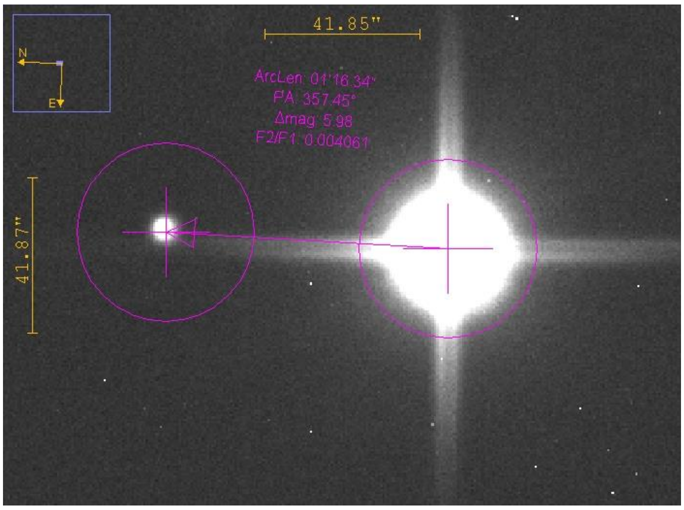

Figure 2: AstroimageJ during measurement.

All images were measured as shown in Figure 2. Was obtained astrometric data of the stars from the online databases of GAIA DR3 and SIMBAD (Gaia Collaboration, 2022 and Wenger et al, 2000). Was analyzed these with Plot tool Excel spreadsheets (Harshaw, 2020) and Rowe-Harshaw (RHS) Excel spreadsheet (Harshaw, 2018). Was rounded the values obtained by measurements and calculations to 2 decimal places.

Was also used the interactive sky atlas ALADIN (Bonnarel et al, 2000), the Stellarium software (Zotti et al, 2021) for the research. Was received the WDS data on the Stelle Doppie (Sordiglioni) website, and the detailed data sets were requested from the USNO.

The latest DR3 release database of the ESA Gaia space observatory only contains data on components C and D. The satellite only measured the G,B,R magnitudes and exact position of component A. No data is available for component B. The SIMBAD database operated by the University of Strasbourg, on the other hand, contains more data than this, although they are not the most recent, but they provide a good starting point for performing the calculations. The Kirkpatrick et al study published in 2000 provides more information about the brown dwarf. Since there are no T-eff data for the AB pair, average surface temperatures corresponding to their spectrum type (G2V) were used. There is no exact surface temperature for the brown dwarf either, the mentioned study only puts it between 1300 and 1600 K°. It was calculated using the average of these two values.

The parallax data for star A is 1995, but the Hipparcos satellite provided a new parallax value for the two stars (A and B) in 2007. It was assumed that there is no great distance between them, since they appear very close, so the error-corrected parallax was given to component B as well. The data appearing in different sources and at different times cannot provide a sufficiently certain result, but this state reflects our current knowledge of the stars of the system. If there will be more accurate measurements of the stars in the future, the following findings may of course change.

5. Data

Figure 3 shows an image of WDS 15232+3017 with the components marked. Unfortunately, the E component is difficult to notice because it is more visible in the IR spectrum. This caused difficulties during the measurement, so the result is uncertain.

The AB components do not separate in the picture, they look like one star. However, the other components were well measurable. Component E is only noticeable as a faint speck of a few pixels.

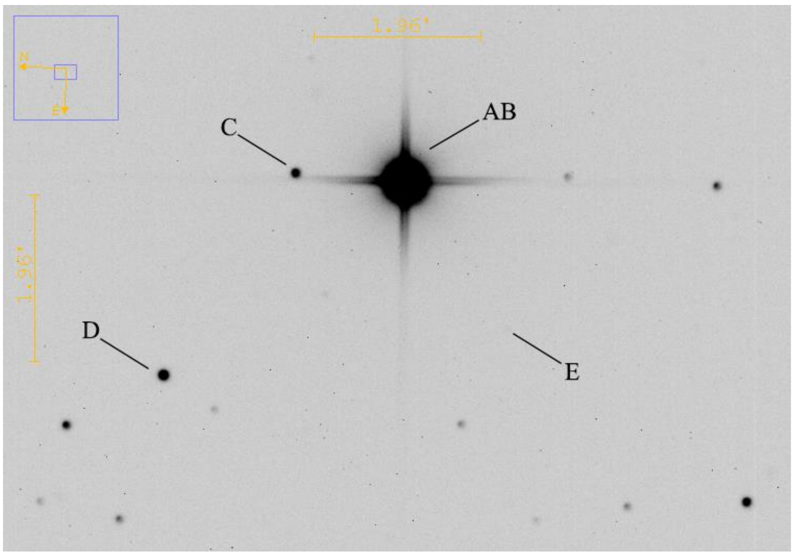

Figure 3: The WDS 15232+3017 system

The following table (Table 1) summarizes the results of measurements made in the images. The average (Mean), standard error (STE) and standard deviation (STD) of the measurements are given individually. The angular separation and position angle calculated from the coordinates from the Gaia and SIMBAD databases are also indicated with the 2016 epoch. (Gaia). The difference between the brightness of the two stars was also calculated from data in databases.

Table 1: Summary of results

	AB,C			AB,D			AB,E		
	Sep"	PA°	Δ mag	Sep"	PA°	Δ mag	Sep"	PA°	Δ mag
Mean	76.84	357.14	6.02	218.06	39.77	5.46	213.73	130.20	10.37
STE	0.04	0.04	0.04	0.06	0.01	0.04	2.07	0.80	0.48
STD	0.05	0.05	0.05	0.07	0.02	0.05	2.82	1.08	0.61
Gaia	75.11	357.70	7.89	217.82	40.32	7.01	189.96	136.33	10.55

The recent measurements have been compared with the latest observations at WDS. The differences are shown in the following table.

Table 2: Deviations from WDS

Comp	Epoch	Δ Sep"	Δ PA°
AB,C	2006	3.10	98.54
AB,D	2006	0.40	1.13
AB,E	2000	20.23	6.20

6. Discussion

First, based on the collected data, the astrophysical properties of the components were determined using the Plot tool in the Excel spreadsheet. These are summarized in Table 3.

Table 3: Astrophysical properties

Comp	Rad (ʘ)	Mass (ʘ)	Lum (ʘ)	Spect	T_{eff} K°	Abs Mag
A	1.30	1.14	1.72	G2V	5 830	4.25
B	0.99	1.00	1.00	G2V	5 830	4.83
C	1.27	1.12	1.59	G	5 656	4.33
D	6.94	2.75	48.53	G	5 820	0.63
E	0.02	0.04	0.00	L8V	1 450	14.71

The mass values were estimated with the Plot tool, this Excel spreadsheet also estimated the spectrum type of components D and C in the "Spect" column. With the help of this data, the components could also be placed on the HRD (Figure 4).

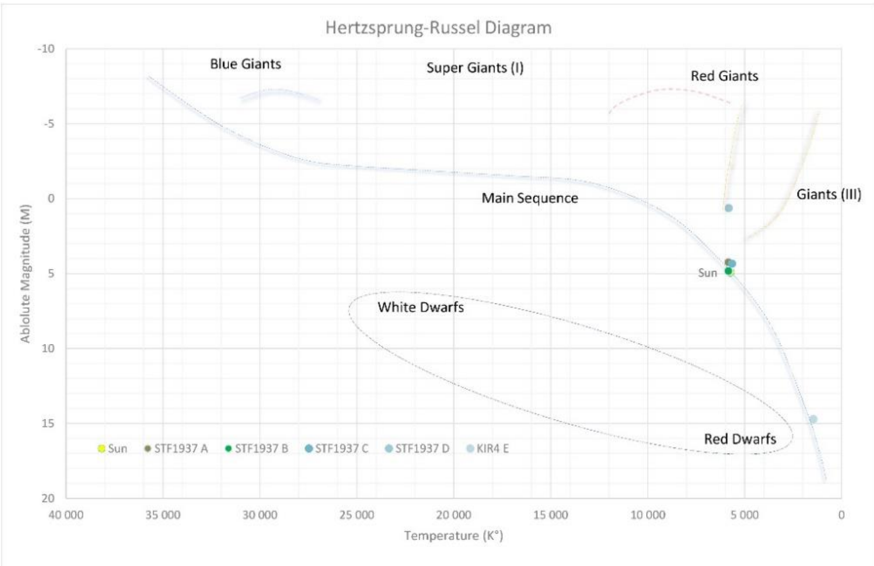

Figure 4: Components on the HRD.

The stars in the system WDS 15232+3017 are in the main sequence and are solar-like. The exception is star D, which is a giant star. The component E is also on the main sequence, but at the bottom of it.

The results of the detailed examination of the relationship of the components to each other are summarized in Table 4. First, some explanation for the table.

- The "Overlap" column shows the correlation between the distance between the two stars. Parallax errors must also be considered. In this way, it can be determined whether there is an overlap in the distance of the stars from the Earth.
- The "Wtd Sep" column shows the projected distance between the members as seen from Earth. The value is given in astronomical units (AU).
- The next two columns are a theoretical limit. They show how large the gravitational limit calculated from the mass of the stars can be. The first column shows the gravitational limit of the primary star, and the second the gravitational limit resulting from the mass of the two stars. In practice, we do not know where such a border between the stars might lie, but some theoretical value must be taken into account in order to establish the physical relationships. If the values of the "Wtd Sep" column do not exceed those of the two columns, the interaction between the two stars is likely. The value is given in astronomical units (AU).
- The column "V_{esc}" shows the escape velocity of the system, and the next column shows the difference in radial velocities. The values are in km/s. If the latter is smaller than the former, then a physical connection between the stars is possible.
- The "V_{orb}" and "V_{obs}" columns contain the values of the maximum orbital velocity and the observed orbital velocity calculated from the historical data of the observations. The values are in km/s. If the observed velocity does not exceed the orbital one, then a physical connection is possible.
- The column "∑ Prob" shows the aggregated possibility of gravitational interaction in percentage. Here you can see that there is a gravitational interaction between each member of the system.

Table 4: Relationships of components

Comp	Overlap	Wtd Sep	M_A Limit	$\sum M_{tot}$ Limit	V_{esc}	ΔRV	V_{orb}	V_{obs}	∑ Prob
AB	15%	40	3 061	11 587	9.71	1.36	7.54	0.04	95.05%
AB,C	-98%	2 619	3 061	12 253	1.24	26.63	0.96	20.77	86.96%
AB,D	-95%	7 687	3 061	21 073	0.95	138.04	0.74	1.66	89.90%
AB,E	-6%	3 464	3 061	6 380	0.78	No RV	0.60	0.94	88.82%

In the case of AB components, the gravitational bond exists since it is a very close pair. Even the E component has an overlap, but it is much less than the former. While there is no overlap in the case of members C and D.

The projected separation does not exceed the aggregate limit for any component. But the D and E components are already beyond the gravitational binding limit of the A star. Their weighted value is a maximum of 2.5 %.

Only for the AB components, the possibility of gravitational bound is shown by the difference between the escape velocities and the radial velocities. Unfortunately, radial velocity is not available for component E.

This is also the case for the relationship between the maximum orbital velocity and the orbital velocity calculated from historical observational data. Thus, the different velocities do not show the possibility of gravitational bound, except for the AB component. The maximum weighted value of the speed correlation is 5%.

The appendix of the RHS Excel spreadsheet gives a binarity probability from the distance and proper motion values of the components. The weighted value of the various indicators indicating the existence of a gravitational bond was added to this probability (see above). An additional maximum of 2.5% was assigned to the R^2 value indicating the fitting of the trendline. This is how the aggregated probability was formed.

From the historical data received from the USNO, the Plot tool drew the diagrams shown in Figure 5 per pair. For the AB components, the more than 1000 observations nicely show the orbit of the B component. Here the gravitational bound is clear. The fit of the trend line to the data points is also very high for the other components also. Furthermore, the length and direction of the resulting motion vectors are the same, with only component E showing a difference in direction and length. These very well indicate the possibility of a physical relationship between the stars.

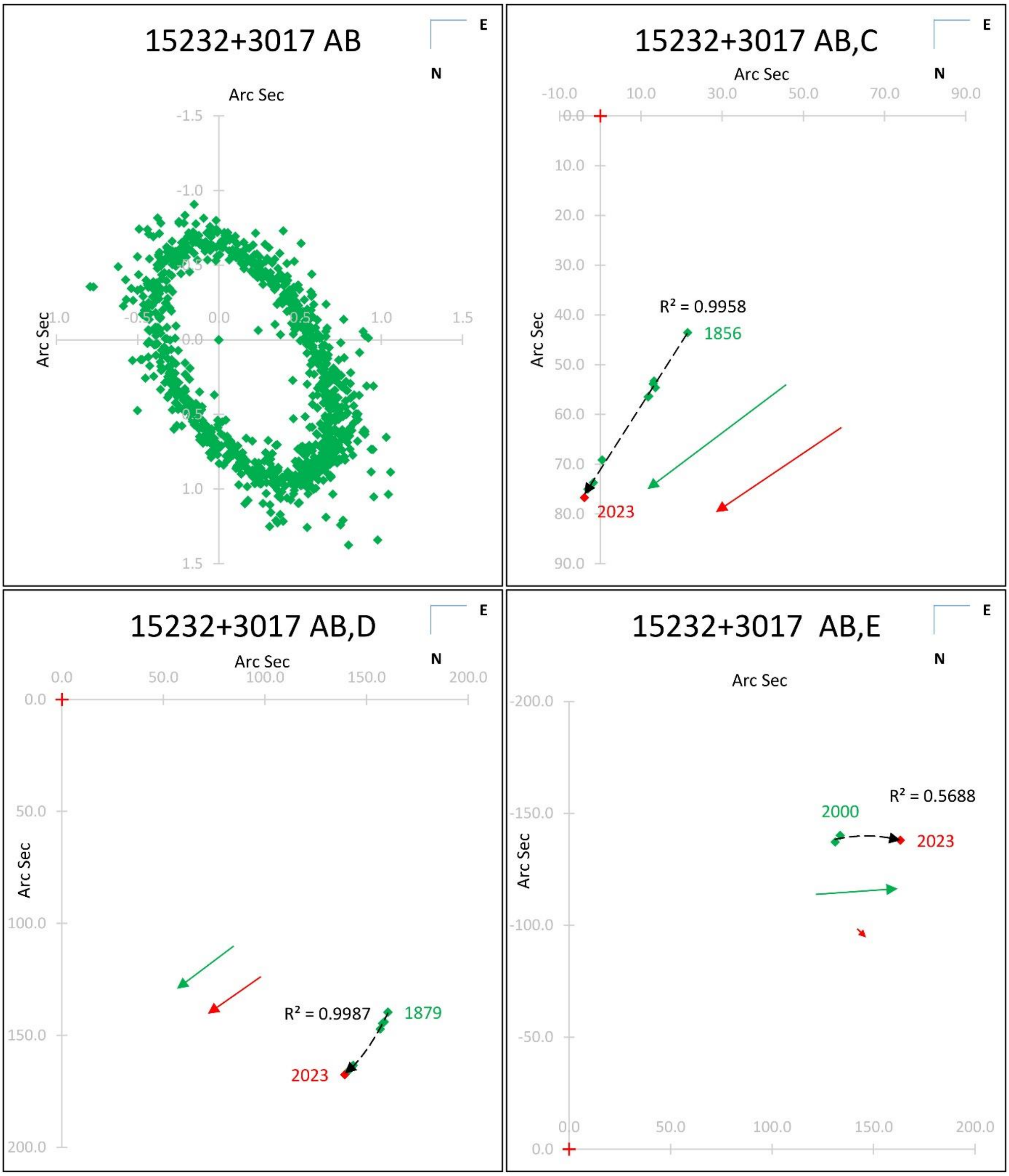

Figure 5: Historical observations of components.

Among the data points, the new observation was marked in red. The date of the first observation was also indicated. The red vector is predicted based on the proper motions, and the green one is the vector calculated based on the measurements. An orbit calculation was also performed for the AB component. This was compared with the orbit shape received from the USNO. Figure 6 shows that the two orbits have the same shape.

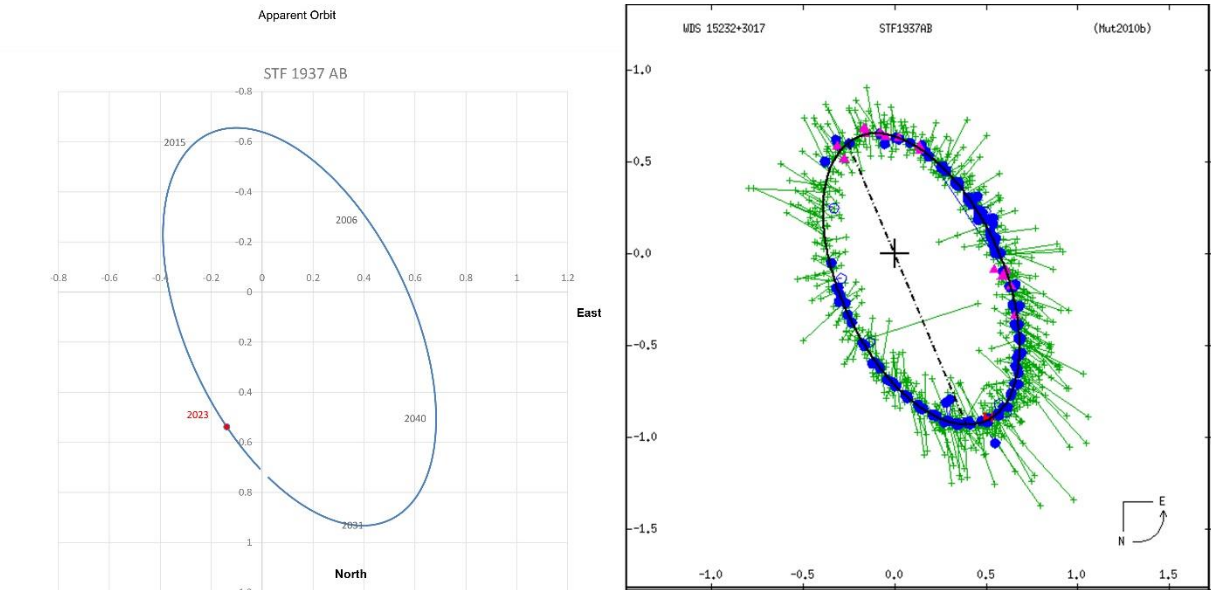

Figure 6: Orbit solutions.

During the orbit calculation, for the position of component B in 2023, an angular separation of 0.52" and a position angle of 340.81° results were obtained.

Plotting the angular separation relative to the year of observation gives a good impression of the uniformly receding motion of the secondary stars.

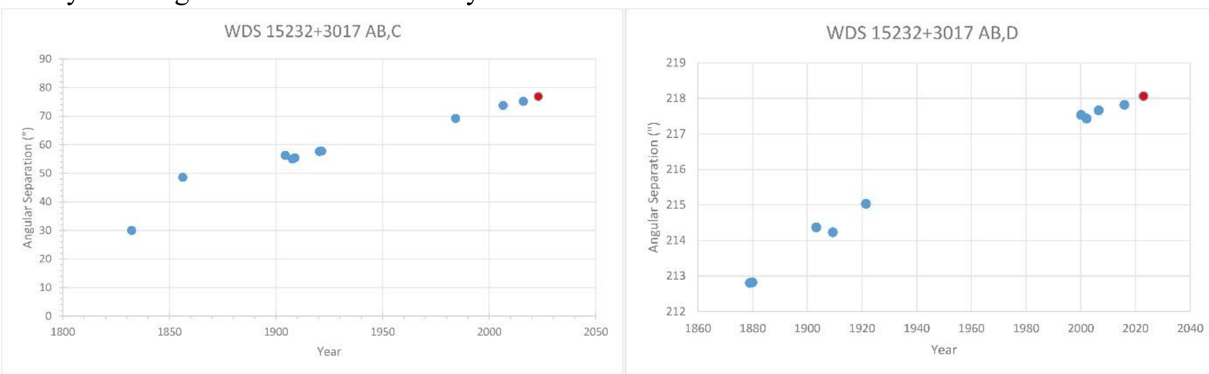

Figure 7: The motion of the secondary stars in WDS 15232+3017 relative to the primary stars. Historical data is shown in blue and current test results in red.

7. Conclusion

During the research, the latest angular separation and position angle of the components of the WDS 15232+3017 quintuple system were determined. It has been established that the stars of this system are gravitationally bound.

8. Acknowledgements

I would like to thank Rachel Matson of the USNO for providing the historical data for this work. I also acknowledge that this work uses the Washington Double Star Catalog maintained at the US Naval Observatory, the SIMBAD database, and the ALADIN sky atlas. This work also used data from the European Space Agency (ESA) Gaia mission (https://www.cosmos.esa.int/gaia) processed by the Gaia Data Processing and Analysis Consortium (https://www.cosmos.esa.int/web/gaia/dpac/consortium). The financing of DPAC was provided by national institutions, especially those participating in the Gaia Multilateral Agreement. Thanks to Richard Harshaw for the Plot tool.

9. References

The Washington Double Star Catalog, 2023: http://www.usno.navy.mil/ USNO/astrometry/optical-IR-prod/wds/WDS.

Collins, K. A., Kielkopf, J. F., Stassun, K. G., and Hessman, F. V. (2017). AstroImageJ: Image Processing and Photometric Extraction for Ultra-Precise Astronomical Light Curves. Astronomical Journal, 153(77).

Harshaw, R. (2018). Gaia DR2 and the Washington Double Star Catalog: A tale of two databases. Journal of Double Star Observations, Vol. 14 No. 4. Page 734-740. October 1, 2018.

Harshaw, R. (2020) Using Plot Tool 3.19 to Generate Graphical Representations of the Historical Measurement Data. Journal of Double Star Observations Vol. 16 No. 4. Page 386-400 September 1, 2020.

Kirkpatrick J.D., Dahn C.C., Monet D.G., Reid I.N., Gizis J.F., Liebert J., Burgasser A.J. (2001). Brown Dwarf Companions to G-type Stars. I. Gliese 417B and Gliese 584C. Astronomical Journal, 121:3235-3253, 2001 June.

Rica, F. M., 2012, “Determining the Nature of a Double Star: The Law of Conservation of Energy and the Orbital Velocity”, JDSO, Vol. 7, No. 4; 254-259.

Knapp, Wilfried, 2019, “The ‘True’ Movement of Double Stars in Space”, JDSO, Vol. 15, No. 3; 464-488.

Sinachopoulos&Mouzourakis, 1992, “Searching for Optical Visual Double Stars”, Complementary Approaches to Double and Multiple Star Research, IAU Colloquium 135., ASP Conference Series, Vol. 32, 1992 Harold A. McAllister and William I. Hartkopf (eds).

Zotti, G., Hoffmann, S. M., Wolf, A., Chéreau, F., & Chéreau, G. (2021). The Simulated Sky: Stellarium for Cultural Astronomy Research. Journal of Skyscape Archaeology, 6(2), 221–258.

Bonnarel, F. et al. (2000) The ALADIN interactive sky atlas. A reference tool for identification of astronomical sources. Astronomy and Astrophysics Supplement, v.143, p.33-40.

Wenger, M. et al. (2000) The SIMBAD astronomical database. The CDS reference database for astronomical objects. Astronomy and Astrophysics Supplement, v.143, p.9-22.

Gianluca Sordiglioni's (SDG) StelleDoppie: https://www.stelledoppie.it/

Measurements of 50 Double Stars with 25 and 30-cm Refractors

Roger C. Ceragioli
University of Arizona, Tucson, AZ; lensbender@msn.com

Abstract

The present article forms a continuation of the author's first report, published in the April 2023 issue of the *Journal of Double Star Observations*.[1] Since those observations were concluded, the author has continued taking measurements, initially using the same 254-mm apochromatic refractor described there, but later employing a newly completed 310-mm achromatic refractor, folded into a compact 1.5-meter long configuration. This new instrument has proven excellent, as the images included in the present report will show. Since May 2023, the author has used this larger refractor exclusively, both for visual observation and for double-star measurements. It gradually became clear that by careful technique, this telescope could successfully image close doubles in the southern sky, down to a declination of about -30°. This has opened the possibility of examining some neglected van den Bos and Rossiter pairs. The present report discusses the techniques employed to achieve this, and lists measures of 50 doubles and triples made by the author from January through early July 2023. Appended is an "atlas" or table of images for all the stars measured.

1. Introduction

The author designed and built a 310-mm f/15 achromatic refractor in 2022-23. Ordinarily, such a classic type of instrument would have required an enormous tube and mounting, as was customary in the 19th c. Instead, the author "folded" the light path using flat mirrors, allowing a much abbreviated tube. Figure 1 shows the ray-path of the system, with the achromatic doublet objective depicted at lower left, and three folding flats in succession. The focus falls at upper right where the rays (blue lines) converge to a point. The author built the lenses, mirrors, and complete tube assembly.

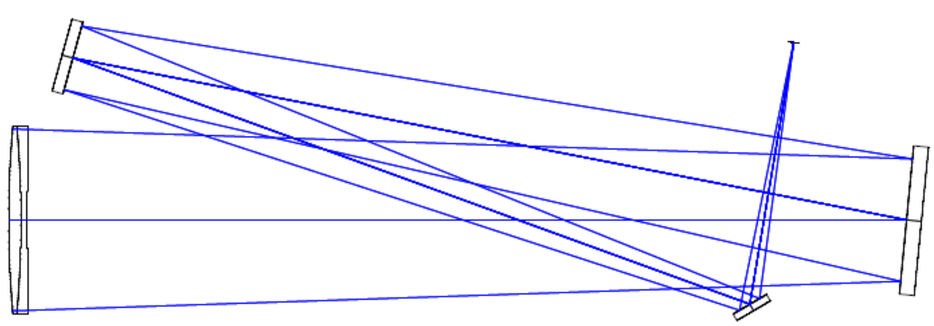

Figure 1: Ray-path of 310-mm f/15 folded refractor

1. Ceragioli, R.C., "Measurements of 26 Double Stars with a 254-mm Refractor," *JDSO*, 19.2 (2023), pp. 150-158.

The completed tube assembly is shown in Figure 2. It easily fits on an Astro-Physics™ 1100GTO telescope mounting, and can be set up and taken down nightly, as needed.

Figure 2: Completed tube assembly of 310-mm f/15 folded refractor on AP-1100 mounting

To image stars with this telescope, a ZWO ASI290 monochrome CMOS camera (depicted in Figure 2) has been used exclusively, together with a yellow filter (Wratten #12). The latter removes unfocused light (secondary spectrum), as found in all achromatic refractors, and eliminates the need for an atmospheric dispersion corrector (ADC) when observing at a low altitude. In the course of using the earlier 254-mm apochromatic refractor, the author discovered how sensitive it was to such dispersion, which visibly elongated star images. This can be detected in the first five stellar systems (STF296AB to HO511AC) illustrated in the "atlas" of images, placed at the end of the present report (see Section 6 below), all of which were taken with the 254-mm apochromatic refractor. The rest of the systems were imaged with the 310-mm achromat. With both of these telescopes, a hexagonal mask was placed over the aperture to reshape the diffraction pattern and divert light from its rings, making faint companions near brighter primaries more easily visible.[2]

2 *Cf.* Argyle, R., (2012), "The Resolution of a Telescope," in *Observing and Measuring Visual Double Stars*, p. 110.

2. Calibration and Method of Data Collection for this Report

A critical parameter in CCD metrology is the image scale (in arcseconds/pixel). This was evaluated as discussed in the author's first report, by applying a diffraction mask to the 310-mm objective, consisting of a grating with alternating dark-and-light bars. The same grating was employed on the 254-mm refractor, and was illustrated in the author's earlier report. With the 310-mm objective, the constant *E* was found to be 0.1292 arcsec/pixel when using the ZWO ASI290 camera (with 2.9-micron pixels), which implies an effective focal length of 4630 mm for the 310-mm achromat, giving an adequate image scale without the need for a Barlow lens.

The general method of proceeding in the present research was identical to what the author described in his first report, except that here, all image grading, stacking, and other processing was carried out with F. Losse's program *REDUC*. "FITS Cubes" of *ca*. 2000 frames each were taken via *FireCapture*, and opened directly into *REDUC*. After finding a subframe that showed both stars to be measured (sometimes after utilizing the "BestOf (Vis)" function) clearly enough, search boxes of suitable size were placed around them and the "ELI" or "Easy Lucky Imaging" tool was invoked. This automatically grades the frames, rejects some, and ultimately stacks those accepted with a view to reinforcing the stars and sharpening them. In the end, ELI allows different percentages of accepted frames to be stacked, which smooths but may also dilute the image cores. The user selects the stacking percentage that seems best for the given FITS Cube, and saves the result as a small FITS file.

Once all the Cubes have been processed, the user opens the reduced FITS files and measures them in the usual way, either by manually pointing and clicking on the sharpened star images or allowing *REDUC* to measure them automatically via the "AutoReduc" function (as explained in the online user's manual). The user can also perform speckle interferometry on the FITS Cubes and save separate files for measurement. Both methods were employed in the present research, in varying amounts, on a case-by-case basis. The "means" thus produced are what one finds in Tables 2 and 3 below.

Over the course of months and after trying other methods of image processing, the author found empirically that *REDUC*'s "ELI" function, performed on FITS Cubes appeared to give the best (that is, sharpest and cleanest) star images, allowing the clearest separation of close doubles with his equipment.

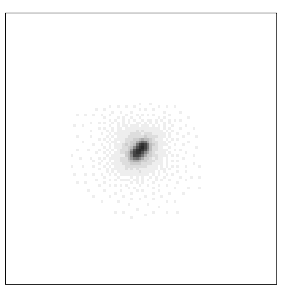

Figure 3: STT208 (Phi UMa)

An example is given in Figure 3 above, showing the close, nearly equal pair STT208 (Phi UMa). This pair of 5th magnitude stars is currently separated by 0.45 arcsec, and lies near the Dawes' limit (0.37 arcsec) of the 310 mm aperture. STT208 is rather clearly split in the above figure, and was even more so by visual inspection on the night of May 24, 2023, when the above image was made. That image is the result of collecting and processing ten FITS Cubes of ca. 2000 frames each, reducing them with ELI, and then further stacking the resultant smaller FITS files. When measured in *REDUC* (and by working from the individual FITS files), the separation of the components was found to be on average 0.44 arcsec, closely matching the Washington Double Star Catalog's (WDS) ephemeris for the star (*cf.* Tables 2 and 4 below).

3. Data Acquired

The following tables summarize the data, and their probable errors. In Table 1, we have numbers derived from the WDS for comparison. From left to right, we find in the first column the WDS 9-digit identifier. In column two appears the discoverer's code and catalog number. The third and fourth columns present the WDS-listed magnitudes of the primary and secondary stars. The fifth column gives the magnitude difference. The sixth and seventh columns list the position angles (θ) in degrees, and separations (ρ) in arcseconds of the stars, according to the latest observation contained in the WDS, measured in the year specified in the eighth and final column.

Table 1. WDS data on the doubles measured for the present report

WDS ID	Name	M1	M2	ΔM	WDS θ	WDS ρ	Year
02442+4914	STF296AB	4.16	10	5.84	306.1	21.15	2020
05003+3924	STT92AB	6.02	9.50	3.48	285.0	4.08	2017
05013+5015	STF619	9.51	9.88	0.37	161.7	4.23	2021
05172+3246	COU1088	10.16	11.54	1.38	233.0	1.67	1991
06012+3516	HU826AB	10.13	10.26	0.13	303.6	0.48	1992
06012+3516	HO511AC	10.13	11.8	1.67	173.4	4.01	2016
09521+5404	STT208	5.28	5.39	0.11	316.9	0.48	2022
12115+5325	STF1608AB	8.11	8.27	0.16	220.5	13.60	2021
12272+2701	STF1643AB	9.03	9.45	0.42	3.10	2.76	2020
12412-0127	BU607	9.7	11.9	2.2	307.7	0.89	1982
12533+2115	STF1687AB	5.15	7.08	1.93	202.8	1.20	2020
12533+2115	STF1687AC	5.15	9.76	4.61	127.1	28.50	2016
13026+2318	COU95	9.7	11.3	1.6	286.1	0.70	2013
13076-1415	RST3820	10.5	11.2	0.7	253.1	0.81	1943
13120+3205	STT261	7.4	7.64	0.24	337.4	2.53	2020
13152-1004	A2781	10.4	12.3	1.9	358.5	0.91	1989
13166+5034	STT263	9.53	9.74	0.21	137.5	1.75	2019
13169+1701	BU800AB	6.66	9.50	2.84	104.1	7.65	2020
13181-1820	RST2839AB	9.7	11.3	1.6	47.5	0.50	1960
13199-2748	B247	9.56	12.7	3.14	316.6	2.54	1960
13284+1543	STT266	7.97	8.42	0.45	355.3	1.92	2020
13298-2634	B250	8.5	9.5	1.0	46.9	0.53	1990
13375+3618	STF1768AB	4.98	6.95	1.97	94.5	1.62	2020

13400-1914	RST2858	10.4	11.2	0.8	235.9	0.66	1940
13403-1913	RST2859	10.45	10.70	0.25	123.3	2.34	2016
13491+2659	STF1785	7.36	8.15	0.79	192.6	2.72	2021
14095-2205	RST2891	10.4	12.7	2.3	141.0	0.93	2016
14165+2007	STF1825	6.47	8.42	1.95	153.9	4.22	2019
14247-1140	STF1837	6.87	7.94	1.07	270.0	1.27	2016
14271-1505	RST3879	10.4	12.6	2.2	110.1	0.71	1943
14314+8257	MLR337	9.90	11.62	1.72	167.2	2.17	2022
14381-0841	BU804	8.69	11.10	2.41	134.6	1.29	2016
14447-0712	RST3893	10.28	11.44	1.16	179.0	0.64	1991
14493-1409	BU106AB	5.61	6.62	1.01	7.3	1.94	2019
14579-2834	B283	10.3	10.7	0.4	247.4	0.47	1962
15023-0858	RST3903	10.31	12.3	1.99	122.5	1.25	2016
15055+5707	A1113	9.6	12.3	2.7	317.3	0.72	2016
15055-0701	BU119AB	8.09	8.76	0.67	273.9	2.33	2019
15199+6701	HU1161AB	8.05	10.87	2.82	224.8	1.67	1991
15304-2717	B292AB	9.11	12.3	3.19	103.6	1.82	1965
15304-2717	B292AC	9.11	12.83	3.72	97.7	15.33	2016
15484-2210	B2370	10.3	11.7	1.4	92.8	0.50	1959
16006-2027	HLD126	9.66	11.72	2.06	34.2	2.29	1991
16009+1918	A2081AB	9.08	12.4	3.32	321.0	2.42	1987
16011+6531	HU1170	9.73	11.27	1.54	147.1	1.13	1991
16044-1122	STF1998AB	4.84	4.86	0.02	11.9	1.15	2020
16044-1122	STF1998AC	4.84	7.30	2.46	44.6	7.15	2019
16044-1122	STF1998BC	4.86	7.30	2.44	37.5	8.77	2019
16096-2037	HU660	8.6	11.8	3.2	67.3	2.57	1965
16359-2510	RST3033	9.3	11.5	2.2	145.7	0.58	1940

Table 2 presents the author's measured data. Column one and two reprise the WDS ID and discoverer codes. Columns three and four present the author's measured position angles and separations. These are averages of all the ELI and speckle images. Column five lists the Julian epoch (JE) of observation. And columns six and seven give the number of ELI and speckle images, and the number of nights on which the star was observed. When more than one night is indicated, the θ, ρ, and JE are averages of the individual nights.

Table 2. Author's measurements.

WDS ID	Name	Obs. θ	Obs. ρ	JE	#Ims	#Nts
02442+4914	STF296AB	305.3°	21.19″	2023.02	11	1
05003+3924	STT92AB	284.9°	4.20″	2023.17	9	1
05013+5015	STF619	162.6°	4.24″	2023.17	10	1
05172+3246	COU1088	223.5°	1.47″	2023.10	30	3
06012+3516	HU826AB	312.4°	0.80″	2023.14	13	2

06012+3516	HO511AC	173.6°	4.03″	2023.14	13	2
09521+5404	STT208	315.8°	0.44″	2023.39	10	1
12115+5325	STF1608AB	220.5°	13.57″	2023.38	5	1
12272+2701	STF1643AB	2.0°	2.80″	2023.40	14	2
12412-0127	BU607	300.7°	0.86″	2038.40	12	1
12533+2115	STF1687AB	204.6°	1.16″	2023.42	32	3
12533+2115	STF1687AC	126.7°	28.63″	2023.44	10	1
13026+2318	COU95	278.9°	0.70″	2023.39	15	2
13076-1415	RST3820	249.9°	0.81″	2023.45	6	1
13120+3205	STT261	338.8°	2.66″	2023.39	11	1
13152-1004	A2781	7.3°	0.72″	2023.44	6	1
13166+5034	STT263	136.6°	1.72″	2023.42	11	1
13169+1701	BU800AB	104.4°	7.73″	2023.39	10	1
13181-1820	RST2839AB	30.4°	0.60″	2023.42	6	1
13199-2748	B247	308.8°	4.26″	2023.45	5	1
13284+1543	STT266	358.8°	1.97″	2023.42	11	1
13298-2634	B250	43.3°	0.52″	2023.46	14	2
13375+3618	STF1768AB	93.9°	1.67″	2023.40	12	1
13400-1914	RST2858	224.8°	0.55″	2023.42	6	1
13403-1913	RST2859	123.2°	2.35″	2023.42	5	1
13491+2659	STF1785	194.1°	2.62″	2023.41	12	1
14095-2205	RST2891	142.4°	0.82″	2023.45	5	1
14165+2007	STF1825	151.8°	4.35″	2023.41	12	1
14247-1140	STF1837	268.1°	1.10″	2023.49	12	1
14271-1505	RST3879	111.3°	0.77″	2023.45	5	1
14314+8257	MLR337	167.1°	2.14″	2023.40	5	1
14381-0841	BU804	134.0°	1.23″	2023.40	7	1
14447-0712	RST3893	174.8°	0.54″	2023.41	5	1
14493-1409	BU106AB	8.4°	1.89″	2023.48	21	2
14579-2834	B283	234.9°	0.52″	2023.48	20	2
15023-0858	RST3903	125.2°	1.12″	2023.46	11	2
15055+5707	A1113	317.6°	0.66″	2023.48	8	1
15055-0701	BU119AB	273.8°	2.34″	2023.51	12	1
15199+6701	HU1161AB	227.0°	1.40″	2023.51	11	1
15304-2717	B292AB	106.2°	1.87″	2023.45	5	1
15304-2717	B292AC	97.1°	15.55″	2023.45	5	1
15484-2210	B2370	89.6°	0.55″	2023.47	8	1
16006-2027	HLD126	39.5°	2.07″	2023.51	4	1
16009+1918	A2081AB	324.5°	2.44″	2023.48	10	1
16011+6531	HU1170	147.8°	0.86″	2023.51	6	1
16044-1122	STF1998AB	16.5°	1.03″	2023.51	10	1
16044-1122	STF1998AC	41.5°	8.02″	2023.51	11	1
16044-1122	STF1998BC	45.0°	7.11″	2023.51	10	1

16096-2037	HU660	59.4°	3.94″	2023.47	12	1
16359-2510	RST3033	139.6°	0.73″	2023.51	9	1

Table 3 indicates the statistical errors, specifying the standard deviations (SD) of position angle (θ) and separation (ρ), together with the standard errors of the mean (SEM), derived from the author's measures. The standard deviations come directly from *REDUC*. The standard errors were computed by the author. Where the double star in question was observed on more than one night, these are averages of the individual nights. As usual in such measurements, the largest SDs occur with the position angles of close doubles, as for example B250, whose separation is about 0.5 arcsec.

Table 3. Measurement errors.

WDS ID	Name	θ SD	θ SEM	ρ SD	ρ SEM
02442+4914	STF296AB	0.31	0.093	0.11	0.033
05003+3924	STT92AB	0.17	0.057	0.02	0.005
05013+5015	STF619	0.15	0.046	0.01	0.003
05172+3246	COU1088	0.74	0.135	0.03	0.005
06012+3516	HU826AB	1.95	0.541	0.05	0.013
06012+3516	HO511AC	0.31	0.086	0.02	0.006
09521+5404	STT208	1.48	0.466	0.04	0.011
12115+5325	STF1608AB	0.09	0.040	0.05	0.021
12272+2701	STF1643AB	0.22	0.059	0.02	0.005
12412-0127	BU607	0.66	0.189	0.01	0.004
12533+2115	STF1687AB	0.87	0.154	0.04	0.007
12533+2115	STF1687AC	0.08	0.025	0.04	0.014
13026+2318	COU95	1.39	0.065	0.03	0.008
13076-1415	RST3820	1.41	0.574	0.03	0.013
13120+3205	STT261	0.21	0.063	0.02	0.005
13152-1004	A2781	2.92	1.192	0.05	0.019
13166+5034	STT263	0.59	0.176	0.02	0.005
13169+1701	BU800AB	0.14	0.044	0.03	0.009
13181-1820	RST2839AB	3.30	1.347	0.05	0.021
13199-2748	B247	1.04	0.465	0.13	0.057
13284+1543	STT266	0.15	0.045	0.01	0.003
13298-2634	B250	4.15	1.109	0.05	0.013
13375+3618	STF1768AB	0.43	0.123	0.01	0.003
13400-1914	RST2858	1.26	0.512	0.03	0.014
13403-1913	RST2859	0.68	0.302	0.04	0.018
13491+2659	STF1785	0.32	0.091	0.02	0.005
14095-2205	RST2891	1.70	0.758	0.03	0.015
14165+2007	STF1825	0.25	0.072	0.02	0.007
14247-1140	STF1837	1.21	0.349	0.03	0.009
14271-1505	RST3879	1.74	0.778	0.01	0.006

14314+8257	MLR337	0.66	0.295	0.05	0.022
14381-0841	BU804	2.19	0.828	0.05	0.017
14447-0712	RST3893	0.76	0.340	0.01	0.006
14493-1409	BU106AB	0.33	0.071	0.03	0.005
14579-2834	B283	3.38	0.755	0.04	0.009
15023-0858	RST3903	1.62	0.487	0.05	0.015
15055+5707	A1113	4.08	1.441	0.06	0.020
15055-0701	BU119AB	0.48	0.137	0.02	0.005
15199+6701	HU1161AB	1.75	0.528	0.07	0.021
15304-2717	B292AB	1.00	0.449	0.08	0.036
15304-2717	B292AC	0.26	0.116	0.09	0.040
15484-2210	B2370	1.79	0.631	0.02	0.007
16006-2027	HLD126	0.42	0.210	0.03	0.016
16009+1918	A2081AB	0.74	0.232	0.05	0.015
16011+6531	HU1170	1.10	0.447	0.03	0.012
16044-1122	STF1998AB	0.34	0.108	0.02	0.006
16044-1122	STF1998AC	0.15	0.045	0.03	0.009
16044-1122	STF1998BC	0.16	0.051	0.04	0.012
16096-2037	HU660	0.58	0.166	0.05	0.014
16359-2510	RST3033	2.42	0.807	0.09	0.030

4. Discussion and Notes

Table 4 shows the residuals of the author's measurements from the last WDS published data, as well as from the orbital ephemeris (if one exists). The first and second columns are as in the previous tables. The third and fourth give the residuals, showing the author's observations minus the most recent WDS data, and the author's work minus the current (2023) ephemeris position, respectively. The ephemerides come from Matson, *et al.*, *Sixth Catalog of Orbits of Visual Binary Stars*, on the WDS website. The fifth column references the published orbit that generated the ephemeris in question. Notes on residuals of special interest follow the table.

Table 4. Residuals from WDS and 2023 Ephemerides.

WDS ID	Name	Δ from WDS (θ, ρ)	Δ from 2023 Ephemeris	Orbital Ref.
02442+4914	STF296AB	-0.8°, 0.04″	0.2°, 0.73″	KSC2017
05003+3924	STT92AB	-0.1°, 0.12″	1.1°, -0.04″	Cve2006e
05013+5015	STF619	0.9°, 0.01″	0.3°, 0.13″	Kis2009
05172+3246	COU1088	-9.5°, -0.20″	N/A	N/A
06012+3516	HU826AB	8.8°, 0.32″	N/A	N/A
06012+3516	HO511AC	0.2°, 0.02″	N/A	N/A
09521+5404	STT208	-1.1°, -0.04″	-2.0°, -0.01″	Msn2021c
12115+5325	STF1608AB	0.0°, -0.03″	0.0°, -0.02″	Izm2019

12272+2701	STF1643AB	-1.1°, 0.04″	-0.1°, 0.05″	Ole2003b
12412-0127	BU607	-7.0°, -0.03″	N/A	N/A
12533+2115	STF1687AB	1.8°, -0.04″	1.7°, -0.05″	Izm2019
12533+2115	STF1687AC	-0.4°, 0.13″	N/A	N/A
13026+2318	COU95	-7.2°, 0.00″	N/A	N/A
13076-1415	RST3820	-3.2°, 0.00″	N/A	N/A
13120+3205	STT261	1.4°, 0.13″	0.6°, 0.01″	Izm2019
13152-1004	A2781	8.8°, -0.19″	N/A	N/A
13166+5034	STT263	-0.9°, -0.03″	-1.2°, 0.01″	Izm2019
13169+1701	BU800AB	0.3°, 0.08″	0.0°, 0.00″	Izm2019
13181-1820	RST2839AB	-17.1°, 0.10″	N/A	N/A
13199-2748	B247	-7.8°, 1.72″	N/A	N/A
13284+1543	STT266	3.5°, 0.05″	0.2°, 0.00″	Izm2019
13298-2634	B250	-3.6°, -0.01″	N/A	N/A
13375+3618	STF1768AB	-0.6°, 0.05″	0.4°, -0.04″	Izm2019
13400-1914	RST2858	-11.1°, -0.11″	N/A	N/A
13403-1913	RST2859	-0.1°, 0.01″	N/A	N/A
13491+2659	STF1785	1.5°, -0.10″	0.5°, -0.02″	Izm2019
14095-2205	RST2891	1.4°, -0.11″	N/A	N/A
14165+2007	STF1825	-2.1°, 0.13″	-0.6°, -0.03″	Izm2019
14247-1140	STF1837	-1.9°, -0.17″	-1.2°, -0.09″	Izm2019
14271-1505	RST3879	1.2°, 0.06″	N/A	N/A
14314+8257	MLR337	-0.1°, -0.03″	N/A	N/A
14381-0841	BU804	-0.6°, -0.06″	N/A	N/A
14447-0712	RST3893	-4.2°, -0.10″	N/A	N/A
14493-1409	BU106AB	1.1°, -0.05″	1.0°, -0.07″	Zir2015a
14579-2834	B283	-12.5°, 0.05″	N/A	N/A
15023-0858	RST3903	2.7°, -0.13″	N/A	N/A
15055+5707	A1113	0.3°, -0.06″	N/A	N/A
15055-0701	BU119AB	-0.1°, 0.01″	0.7°, -0.01″	Kiy2017
15199+6701	HU1161AB	2.2°, -0.27″	N/A	N/A
15304-2717	B292AB	2.6°, 0.05″	N/A	N/A
15304-2717	B292AC	-0.6°, 0.22″	N/A	N/A
15484-2210	B2370	-3.2°, 0.05″	N/A	N/A
16006-2027	HLD126	5.3°, -0.22″	N/A	N/A
16009+1918	A2081AB	3.5°, 0.02″	N/A	N/A
16011+6531	HU1170	0.7°, -0.27″	N/A	N/A
16044-1122	STF1998AB	4.6°, -0.12″	0.7°, -0.09″	Doc2009g
16044-1122	STF1998AC	-3.1°, 0.87″	-0.9°, 0.50″	Zir2008
16044-1122	STF1998BC	7.5°, -1.66″	N/A	N/A
16096-2037	HU660	-7.9°, 1.37″	N/A	N/A
16359-2510	RST3033	-6.1°, 0.15″	N/A	N/A

Notes:

05172+3246 COU1088: 3 WDS measures. The first two (from Couteau in 1974 & and Heintz in 1988) agree with one another in PA to within 0.6°, while the third (from TYCHO in 1991) differs from these by *ca.* +5.8°. The author's measures are closer to Couteau's in PA and Sep.

06012+3516 HU826AB: 6 WDS measures, from 1904 to 1981 which seem to show an increase in PA (300° to 308°) over 77 years (*i.e.* 0.1°/year). The author's measure would show a further increase to 312° in 42 years (also 0.1°/year). TYCHO measurements (1992) would decrease PA by 4.5° with respect to Heintz's (1981) at a rate of 0.4°/year. The author's Sep. increase is perhaps not real since there was no clear change in separation from 1904 to 1981. The companion double (HO511AC) shows good agreement with last published WDS measures made in 2015-16.

12412-0127 BU607: 18 WDS measures from 1867 to 1982. PA and Sep. show gradual decrease from 320° to 308°, and from 1.4 to 0.9 arcsec over the interval. The author's measures show no further clear decrease in Sep., but a continued decrease in PA. Long term PA decrease over 115 years was by about 0.1°/year; decrease since 1982 would be by 0.17°/year.

13026+2318 COU95: 12 WDS measures from 1966 to 2013, suggesting rapid decrease in PA (from 298° to 286° or 283°), and some increase in Sep. which may now have ceased (from 0.5 to 0.7 arcsec). Author's measures suggest continued rapid decrease in PA (to 279°), and no change in Sep.

13076-1415 RST3820: 2 WDS measures from 1937 and 1940. Author's measurement found no change in Sep., and modest 3° decrease in PA. "Relfix" over 85 years.

13152-1004 A2781: 9 WDS measures from 1914 to 1989, showing an increase of 17° in PA (0.23°/yr); and 0.2 to perhaps 0.4 arcsec in Sep. Author's measures show further increase of 9° in PA at roughly the same rate (0.26°/yr). Sep. is more in line with early measures than that of 1989. Possibly no real change in Sep. since 1914.

13181-1820 RST2839AB: 4 WDS measures from 1935 to 1960, with PA ranging from 32° to 48°, and Sep. from 0.3 to 0.5 arcsec, without clear temporal direction (*i.e.* there is scatter in the data). Author's present measurement, after an interval of 63 additional years, may show a real decrease in PA and increase in Sep. Further long term, high precision measurements could clarify the matter.

13199-2748 B247: 3 WDS measures from 1926 to 1960, showing PA decrease from 328° to 317°, and increase in Sep. from 1.8 to 2.5 arcsec. Author's recent measures show further PA decrease to 309° and Sep. increase to 4.3 arcsec, suggesting an optical pair with (perhaps) a linear solution.

13298-2634 B250: 8 WDS measures from 1926 to 1990. These show PAs from 41° to 49°, and Seps of 0.43 to 0.55 arcsec, without clear temporal direction. Author's measurements on two nights fall within this range at 42° and 0.54 arcsec. No clear movement after nearly 100 years.

13400-1914 RST2858: 2 WDS measures from 1935 and 1940, with PAs of 235° and 236°, and Sep. of 0.7 arcsec. Author's measures after 83 years show PA decrease of 11° and Sep. decrease of 0.1 arcsec. The nearby star RST2859, last measured in 2016, shows close agreement with the author's measures.

14095-2205 RST2891: 4 WDS measures from 1935 to 2016, perhaps showing an increase in PA from 136° to 141°, and Sep. from 0.6 to 0.9 arcsec. Author's measurement might show a slight further increase in PA to 142°.

14271-1505 RST3879: 2 WDS measures from 1937 and 1943, showing PA of 110° and Sep. of 0.7 arcsec. Author's measures show PA of 111° and Sep. of 0.8 arcsec, suggesting no clear movement after about 85 years.

14447-0712 RST3893: 4 WDS measures from 1938 to 1991. The first two are by Rossiter, the third by W. Heintz, and the last by HIPPARCOS, with PA decrease from 190° to 179°, and Sep. increase from 0.41 to 0.64 arcsec. The PA change would be at about 0.21°/yr. The author found a further decrease of 4° over 32 years giving a rate of 0.13°/yr, and a possible decrease in Sep. of 0.1 arcsec.

14579-2834 B283: 4 WDS measures from 1926 to 1962, showing a decrease in PA from 251° to 247° (0.09°/yr), and no clear change in Sep. Author's measures after an interval of 61 years show further decrease in PA to 235° (0.2°/yr) and no clear change in Sep.

15023-0858 RST3903: 3 WDS measures from 1938 to 2016, giving possible decreasing PA from 128° to 123°, and Seps steady at 1.2 arcsec. Author's measure would imply slight increase in PA and decrease in Sep. Perhaps, then, no real change since 1938. "Relfix."

15199+6701 HU1161AB: 7 WDS measures from 1905 to 1991, with a possible slight increase in PA from 222° to 225°, and Sep. from 1.5 to 1.7 arcsec. Author's measurements after 32 additional years suggest a further increase in PA to 227°, and possible decrease in Sep. to 1.4 arcsec.

15304-2717 B292AB: 3 WDS measures from 1926 to 1965, with PAs from 109° to 104°, and Sep. steady at 1.8 arcsec. Author's recent measurement closely accords, suggesting no clear movement in about 100 years.

15484-2210 B2370: 3 WDS measures from 1929 to 1959, possibly showing a slight decrease in PA by 2° (0.07°/yr), and no clear change in Sep. Author's measure after an interval of 64 years may show a further decrease in PA by 3° (0.05°/yr), but no clear change in Sep.

16006-2027 HLD126: 11 WDS measures from 1882 to 1991, showing no clear change in PA or Sep. Author's measures fall within the range of prior observations, also showing no clear movement of the pair after 140 years. "Relfix."

16009+1918 A2081AB: 8 WDS measures from 1909 to 1987, showing a gradual increase in PA from about 309° to 321° (0.15°/yr), and no clear change in Sep. over an interval of 78 years. Author's measures show a further increase in PA to 325° (0.11°/yr since 1987), but no clear change in Sep.

16096-2037 HU660: 10 WDS measures from 1902 to 1965, showing decrease in PA from 88° to 67°, and increase in Sep. from 1.8 to 2.6 arcsec. Author's measures show further decrease in PA to 59°, and increase in Sep. to 3.9 arcsec, suggesting an optical pair with (perhaps) a linear solution.

16359-2510 RST3033: 2 WDS measures from 1935 and 1940, with possible decrease of PA (from 150° to 146°), and increase of Sep. (from 0.5 to 0.6 arcsec). Author's measures would continue the trend (to 140° and 0.7 arcsec).

5. Non-detections

Table 5 lists fifteen systems in which the secondary was not detected by the author, although probably being within range of his 310-mm telescope.

Table 5. Non-Detection of Reported Secondaries

WDS ID	Name	JE	#Ims	#Nts
13137+2949	HO55AB	2023.42	5	1
13513-3315	RST2875	2023.45	3	1
14420-3249	SEE210AB	2023.45	6	1

14471-2729	B280	2023.47	5	1
14489-1247	RST3895	2023.42	5	1
14491-2228	B1765	2023.42	4	1
14506-2221	B1766	2023.48	5	1
15055-0501	HDS2125AB	2023.51	6	1
15139-2612	B288	2023.44	6	1
15195-2609	B289	2023.45	3	1
15343-1613	RST3923	2023.45	2	1
15475+7357	MLR194	2023.44	6	2
16152-0048	DOO62	2023.48	3	1
16164-2417	RST3010	2023.49	3	1
16500-2327	RST3045	2023.48	5	1

5. Acknowledgments

This research has made use of the Washington Double Star Catalog maintained at the U.S. Naval Observatory. The author wishes to thank the USNO, and Drs Brian Mason and Rachel Matson for their prompt and kind assistance. Also, F. Losse for the use of *REDUC*; T. Edelmann for *FireCapture*; and G. Sordiglioni for *Stelle Doppie*. The author also acknowledges and thanks *Stellarium*, and the SIMBAD database.

6. Images of Systems Measured

Below are images of double and triple systems taken through the author's 254-mm (first five images) and 310-mm (all remaining images) telescopes, demonstrating resolution of the stars.

(North toward bottom/east toward right)

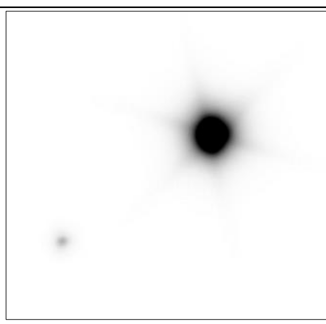
STF296AB

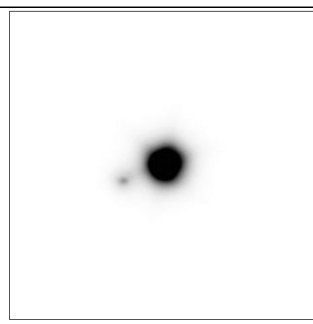
STT92AB

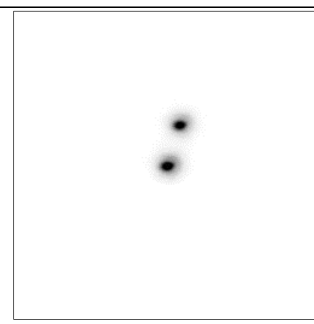
STF619

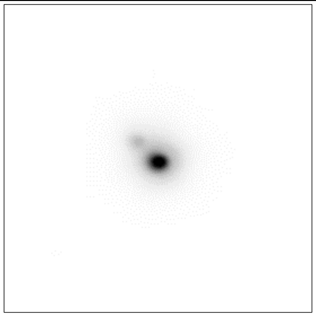
COU1088

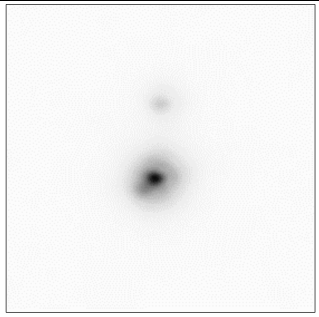
HU826AB + HO511AC

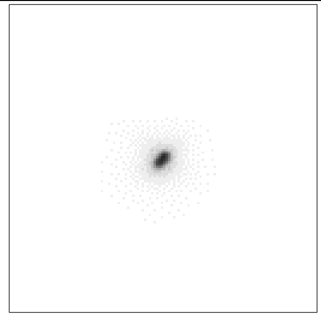
STT208

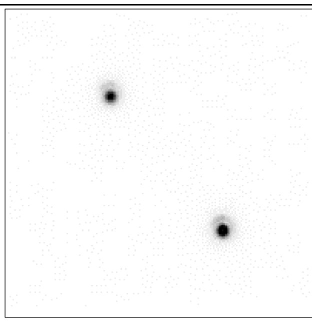
STF1608AB

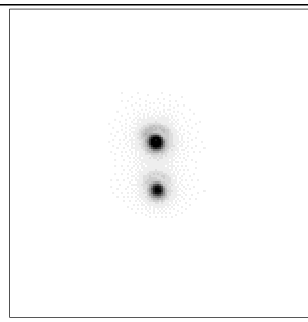
STF1643AB

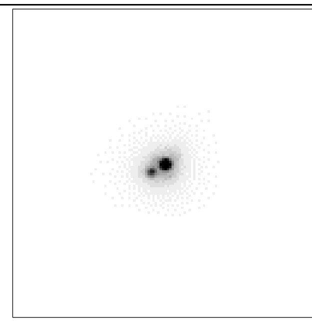
BU607

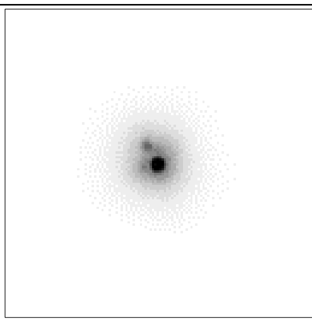
STF1687AB

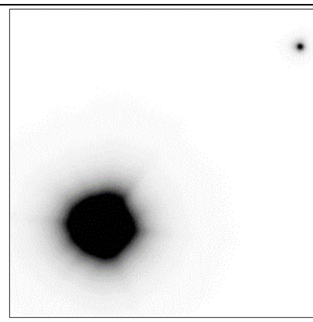
STF1687AC

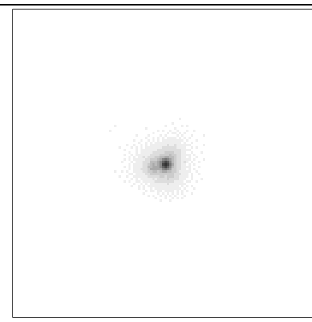
COU95

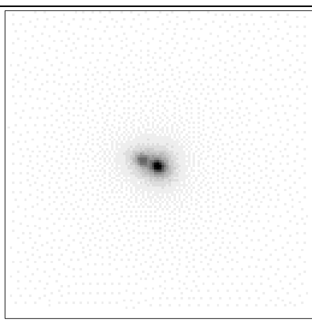
RST3820

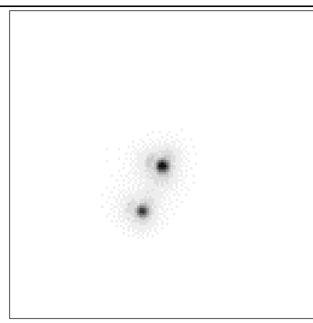
STT261

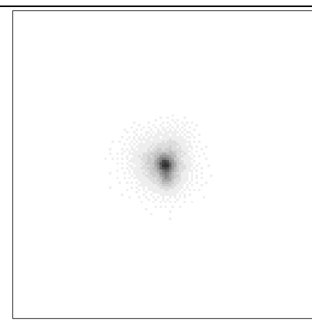
A2781

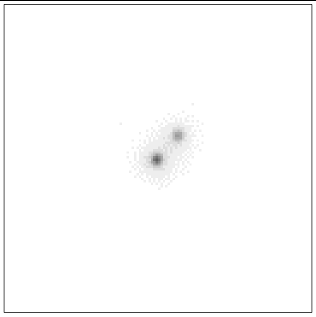
STT263

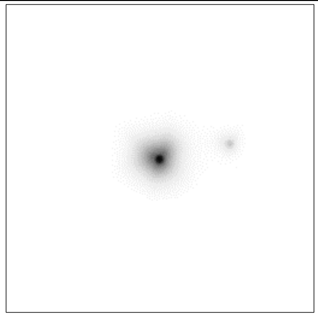
BU800AB

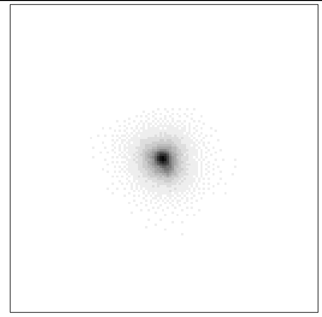
RST2839AB

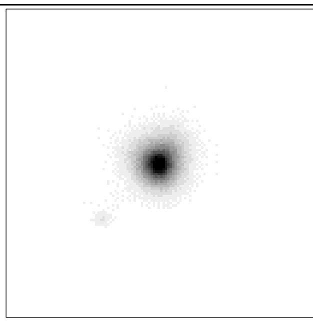
B247

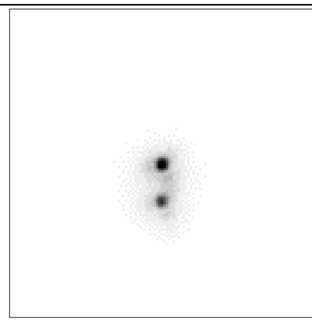
STT266

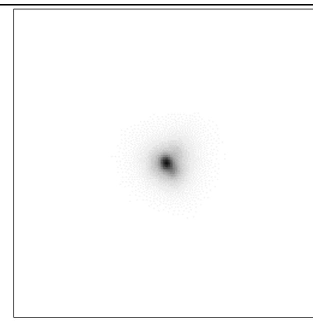
B250

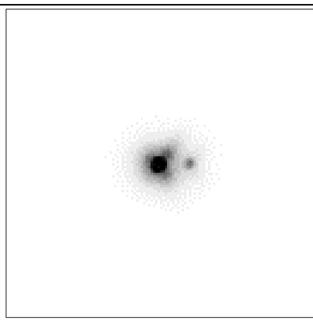
STF1768AB

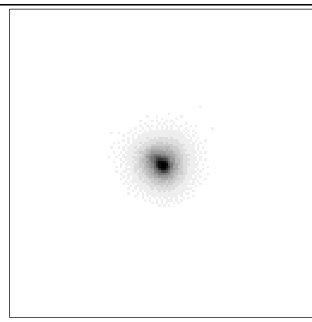
RST2858

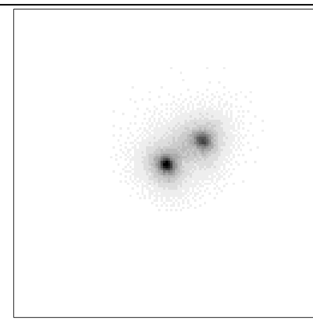
RST2859

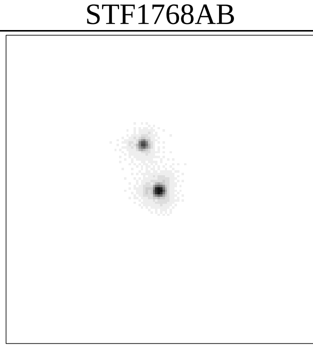
STF1785

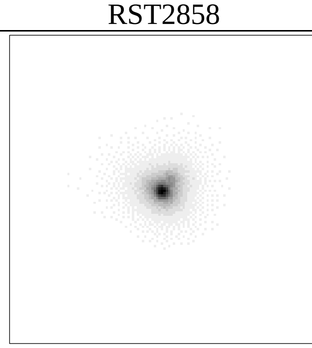
RST2891

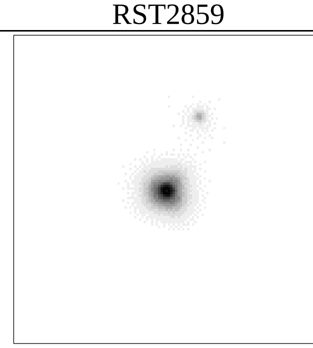
STF1825

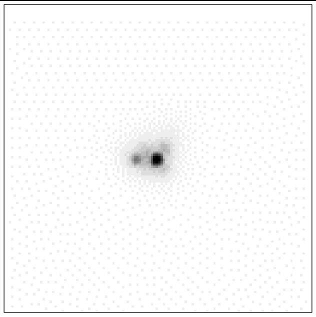

STF1837

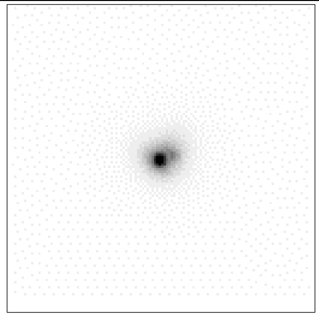

RST3879

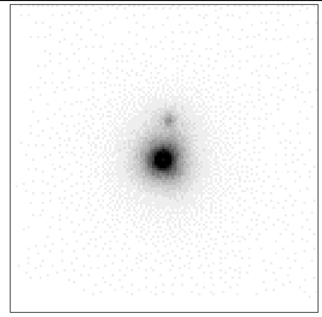

MLR337

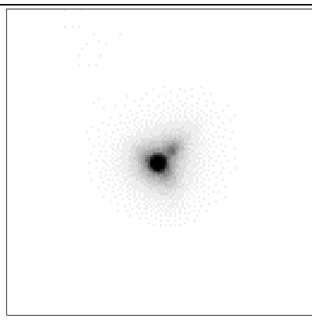

BU804

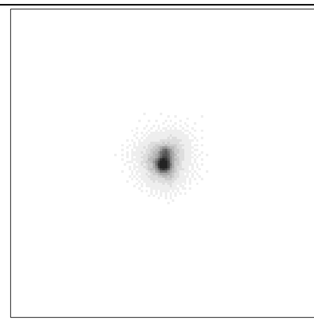

RST3893

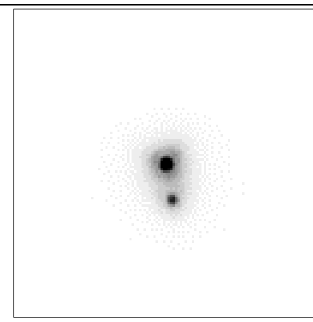

BU106AB

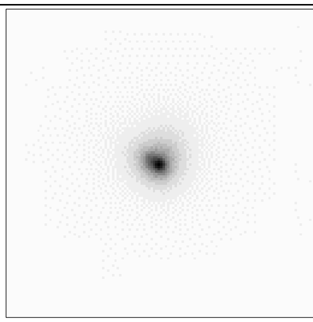

B283

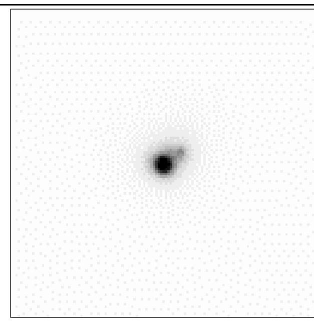

RST3903

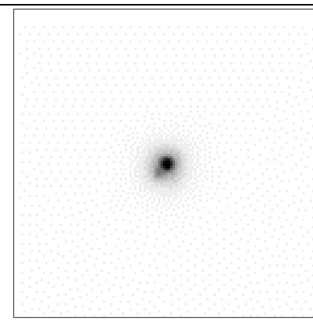

A1113

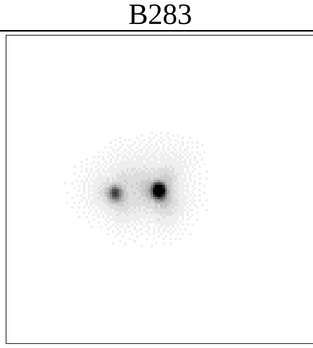

BU119AB

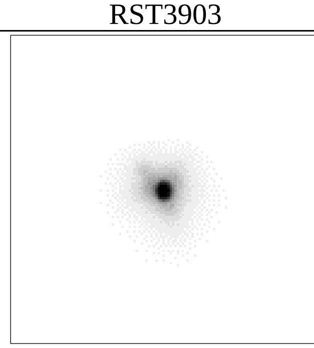

HU1161AB

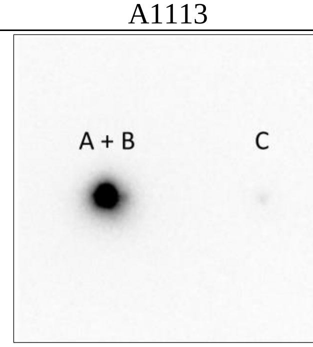

B292AB + C

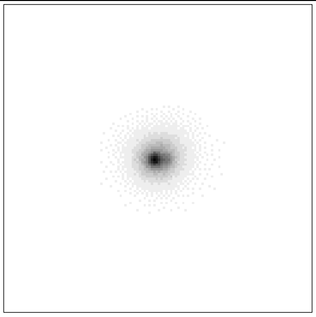
B2370

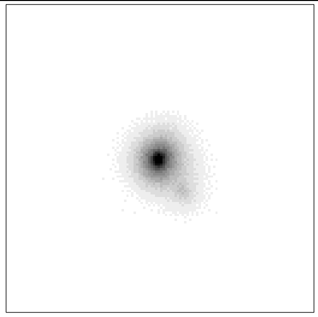
HLD126

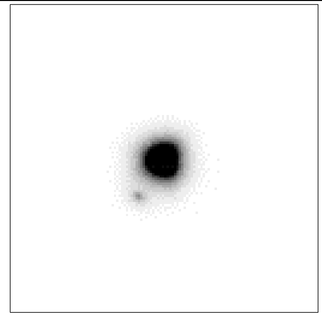
A2081AB

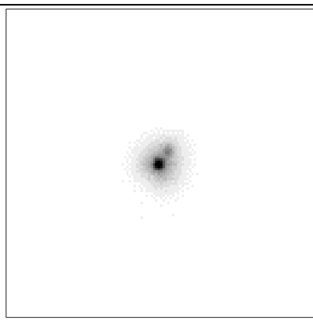
HU1170

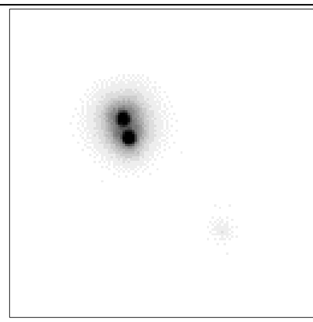
STF1998AB + C

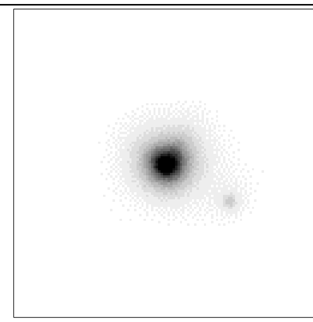
HU660

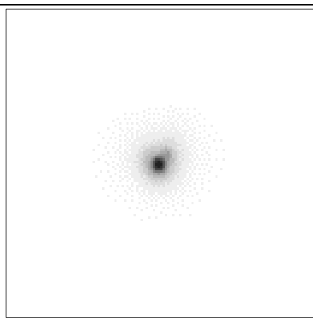
RST3033

Systems where reported secondary was not detected

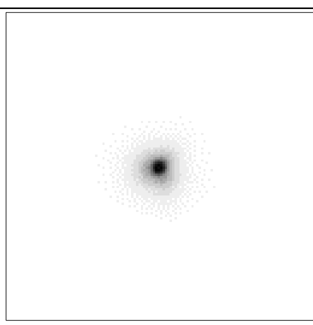
HO55AB

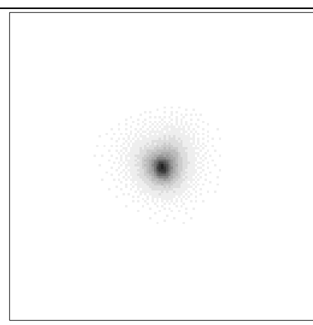
RST2875

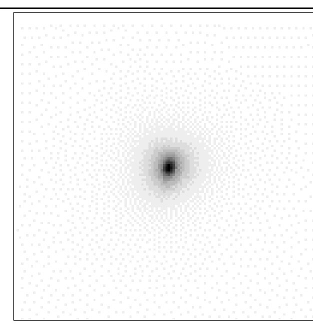
SEE210AB

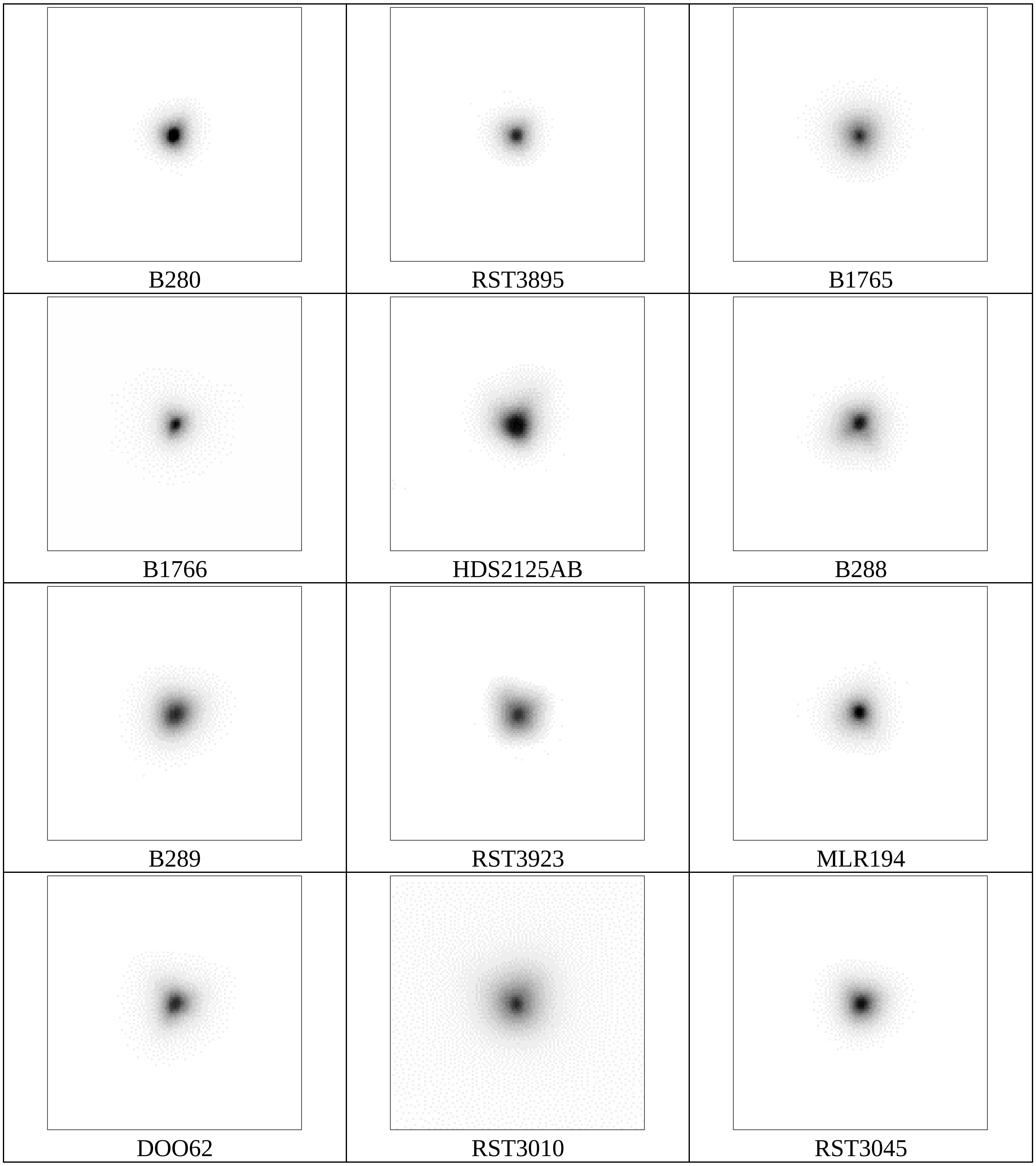

References

Cotterell, J.D. (2015). "Calibrating the Plate Scale of a 20 cm Telescope with a Multiple-Slit Diffraction Mask." *Journal of Double Star Observations*, 11(4), 387-389.

Losse, F., "REDUC Tutorial," (V5.34). Retrieved from http://www.astrosurf.com/hfosaf/reduc/tutorial.htm

Mason, B.D. *et al*., “Washington Double Star Catalog.” Retrieved from http://www.astro.gsu.edu/wds/

Matson, R.A., *et al*., *“Sixth Catalog of Orbits of Visual Binary Stars.”* Retrieved from http://www.astro.gsu.edu/wds/orb6.html

Maurer, A. (2012). “The Diffraction Grating Micrometer.” In R.W. Argyle (ed.), *Observing and Measuring Visual Double Stars*, (Springer), 183-193.

……………………………………..

About the author: Roger Ceragioli works as an optical engineer at the Richard F. Caris Mirror Lab, University of Arizona, Tucson, USA. His expertise is in optical fabrication and design, and he is in charge of diamond generating operations on the Giant Magellan Telescope’s primary mirrors. He holds a Ph.D. from Harvard University.

ASTRONOMICAL ASSOCIATION OF QUEENSLAND 2022/23 PROGRAMME

BLUE STAR OBSERVATORY MEASUREMENT OF NEGLECTED SOUTHERN MULTIPLE STARS

Graeme Jenkinson, Des Janke
Astronomical Association of Queensland, Australia.
E-mail - bluestars@iprimus.com.au

ABSTRACT

This paper presents the final results of a 2022/23 programme of photographic measurements of fifteen southern multiple stars. All results were obtained using an Atik 460EX mono CCD camera used in conjunction with an equatorially mounted 400mm F4.5 Newtonian reflector

The mean 95% confidence intervals for the new measures are ± 0.596° in PA and ± 0.074" in separation.

System	Last listed measure			New measure			Comment
	PA º	Sep. ″	Epoch	PA º	Sep. ″	Epoch*	
B247	317	2.5	1960	311.279	4.150	2022.382	Clear movement in both axes over 62 years.
BRT3000	310	2.8	1913	163.3	11.012	2022.382	Large variation in both measurements.
DAM1225	88	13.2	2015	88.224	13.173	2023.061	Confirmation of 2015 measurement. Little probable change.
DAM1389AC	207	19.6	2015	207.963	19.333	2022.918	Confirmation of 2015 measurement. Little probable change.
DAM1636	317	5.6	2015	316.82	5.600	2023.283	Confirmation of 2015 measurement. Little probable change.
I 183	139	3.3	1999	137.907	3.802	2023.053	Little probable movement over 21 years.
I 461	332	3.2	1986	331.286	3.034	2022.382	Possible minor reduction in both axes over 37 years.
I 1062	180	3.3	1980	177.406	3.21	2023.053	Continuing decrease in PA. Separation appears static.

LDS201 A-B	241	46.1	2018	236.697	47.758	2023.053	Both figures similar to original 1911 measure.
LDS201 A-C	256	74.5	2015	254.840	74.02	2023.053	Possible slight decrease in PA.
LDS201 C-D	57	4.0	2015	58.041	3.943	2023.053	Possible slight increase in PA.
MLO63	291	3.2	1895	140.494	3.529	2022.382	Large difference in PA.
RSS205	312	10.4	2015	312.988	10.188	2023.176	Possible slight increase in PA.
SKF415	255	33.7	2015	255.366	33.467	2023.053	Possible very small decrease in PA.
TDS7065	175	2.6	1991	178.022	11.174	2023.283	Considerable increase in separation over 32 years.

* Epochs of new measures given in Besselian years as the average of the observations making up the measure.

Also included in a separate table below are the details of three possible new pairs found while studying the fifteen known pairs. These new pairs were located usually within or near the instrument field of view while searching for/imaging the known pairs.

System	R.A.	Dec.	Mag.	PA º	Sep. ″	Epoch*
Possible new pair near TDS7065 Vela	10 08.16	-56 55 48	14.55 & 14.56	155.964	4.974	2023.387
Possible new pair near DAM1389 (Beta Fornax)	02 48.50	-32 28	12.09 & 14.77	215.341	6.673	2022.916
Possible new pair near DAM1636 Antlia	09 30.25	-39 28 20	14.68 & 16.38	351.423	5.596	2023.285

* Epochs of new measures given in Besselian years as the average of the observations making up the measure.

INTRODUCTION

These latest results are part of an ongoing programme commenced in 2008 by the Double Star Section of the Astronomical Association of Queensland. The target stars were selected from the Washington Double Star Catalogue (WDSC) and were observed in Queensland, Australia from a latitude of approximately 27° S.

METHOD

Nightly sets of one hundred images were obtained with the equipment described above, after which the images were stacked using Atik DAWN software and then analyzed using the astrometric double star program REDUC (Losse, 2008). Approximately ten stacked images of each target were taken per night for seven nights and the results averaged to obtain measures of separation and position angle with sufficient confidence.

Full details of the method are given in Napier-Munn and Jenkinson (2009). Subsequent work on the errors inherent in the method is described in Napier-Munn and Jenkinson (2014). As proficiency has grown in the use of this equipment with the 400mm reflector, close doubles with considerable magnitude difference between the components have been successfully measured.

Fellow AAQ member Des Janke provided invaluable assistance processing the original FITS image files into JPEG photographs, along with his use of Vizie-R to gather details of the possible new pairs.

RESULTS

For all of the systems shown below the WDSC information is first reproduced, showing the epoch 2000 position, magnitudes, separation, PA, and the last recorded measurement. The new measurements are then given in tabular form, including the mean and standard deviation and 95% confidence limits. Any uncertainties between the images and the last recorded measurements are discussed. Finally a conclusion is given as to whether any movement of the component stars has occurred in PA or separation, based on the P-value for the t-test comparing the new mean values with the catalogued value ($P < 0.05$ is considered as evidence of change).

Results as detailed in the tabulated results above, along with the fifteen known/neglected pairs:

- Three possible new pairs recorded in the constellations of Antlia, Fornax & Vela.
- Confirmation checks were carried out on a number of pairs recently measured in 2015 & 2018. These pairs were located in the same field of view as the nearby target pairs and were measured as part of the programme.
- Large variation in position of BRT3000 secondary compared to the original measure. Images appear to show a possible close companion to the secondary. Reference to Gaia DR2 Catalog data represented in Cartes du Ciel as reproduced below shows the following data suggesting this is a double star system:

Gaia DR2 6188321238085200384 (primary)
Visual magnitude: 11.07
Proper motion in right ascension: -8.150 [mas/y]
Proper motion in declination: -28.878 [mas/y]
Distance: 907.2 light years

Gaia DR2 6188321027631669376 (original secondary)
Visual magnitude: 17.28
Proper motion in right ascension: -8.521 [mas/y]
Proper motion in declination: -28.394 [mas/y]
Distance: 1112.7 light years

Gaia DR2 6188320928846317184 (possible triple companion)
Magnitude BP: 18.138
Proper motion in right ascension: -8.741 [mas/y]
Proper motion in declination: -29.220 [mas/y]
Distance: 918.6 light years

Image shows secondary in quite a different position angle. Looking at Gaia DR2 data it appears the secondary is a double, and forms a triple system, with primary due to similar proper motion.

Please note that all attached images are aligned with North to the bottom and East to the right.

B247	RA. 13 19.9	DEC. -27 48	Last Measure 1960
Hydra	MAG. 9.56 & 12.70	PA. 317°	SEP. 2.5"
Date	**No. images**	**PA°**	**Sep"**
12 Apr 2022	10	311.82	4.235
14 Apr 2022	10	313.15	3.901
15 Apr 2022	10	311.04	4.412
18 Apr 2022	10	310.94	4.110
04 May 2022	10	310.99	4.090
06 Jun 2022	10	310.89	4.204
07 Jun 2022	10	310.12	4.099
Mean		**311.279**	**4.150**
Standard deviation		0.961	0.157
95% CI +/-		0.889	0.146
P(t) movement		0.000	0.000

COMMENTS

Movement in both axes over 62 years.

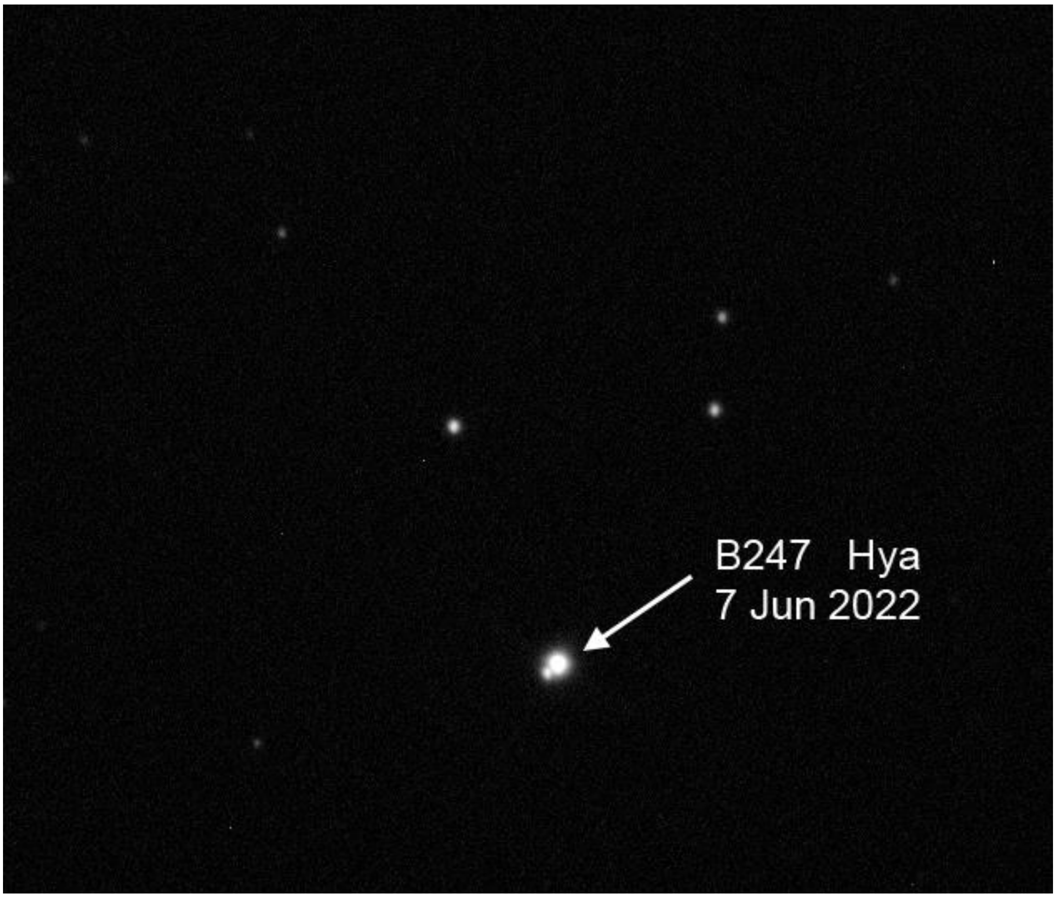

BRT3000	RA. 13 24.5	DEC. -28 37	Last Measure 1913
Hydra	MAG. 12.53 & 12.62	PA. 310°	SEP. 2.8"
Date	**No. images**	**PA°**	**Sep"**
12 April 2022	10	162.70	11.116
14 April 2022	10	163.41	11.130
15 April 2022	10	163.88	10.927
18 April 2022	10	162.84	10.829
04 May 2022	10	162.65	11.098
06 June 2022	10	164.14	10.978
07 June 2022	10	163.48	11.008
Mean		**163.300**	**11.012**
Standard deviation		0.589	0.111
95% CI +/-		0.545	0.103
P(t) movement		0.000	0.000

COMMENTS

Large unexplained variations in both PA and separation measurements. The secondary also appears to show a barely resolved very close & faint companion.

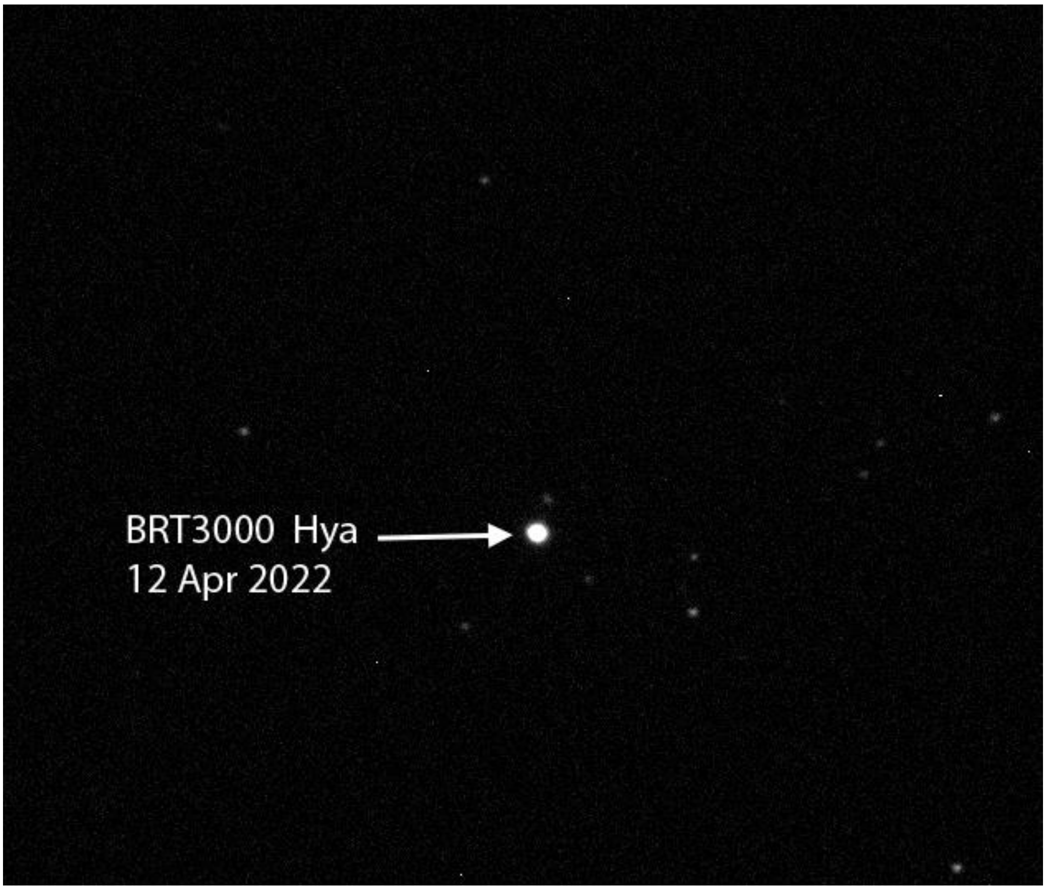

DAM1225	RA. 08 01.7	DEC. -14 12	Last Measure 2015
Puppis	MAG. 10.8 & 11.9	PA. 88.0°	SEP. 13.2"
Date	**No. images**	**PA°**	**Sep"**
20 December 2022	10	88.26	13.175
17 January 2023	10	88.19	13.152
18 January 2023	10	88.30	13.171
21 February 2023	10	88.20	13.164
24 February 2023	10	88.22	13.185
25 February 2023	10	88.11	13.199
27 February 2023	10	88.29	13.168
Mean		**88.224**	**13.173**
Standard deviation		0.066	0.015
95% CI +/-		0.061	0.014
P(t) movement		0.000	0.000

COMMENTS

Little probable movement since previous measure.

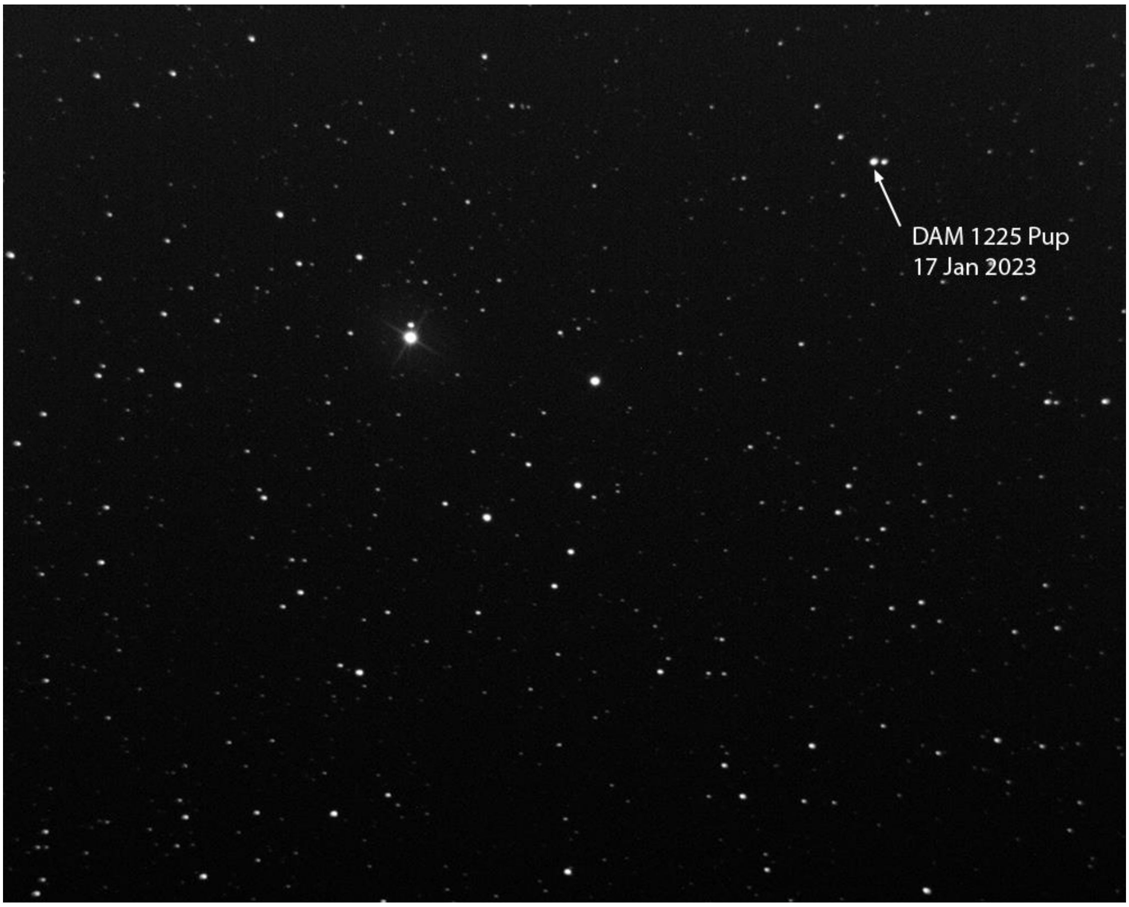

DAM 1389AC	RA. 02 49.1	DEC. -32 24	Last Measure 2015
Fornax	MAG. 4.46 & 13.2	PA. 207°	SEP. 19.6"
Date	**No. images**	**PA°**	**Sep"**
17 November 2022	10	207.93	19.468
18 November 2022	10	208.05	19.226
19 November 2022	10	207.94	19.370
25 November 2022	10	207.49	19.321
26 November 2022	10	207.81	19.372
14 December 2022	10	208.50	19.266
16 December 2022	10	208.02	19.310
Mean		**207.963**	**19.333**
Standard deviation		0.302	0.079
95% CI +/-		0.279	0.073
P(t) movement		0.000	0.000

COMMENTS

Possible slight increase in PA over seven years.

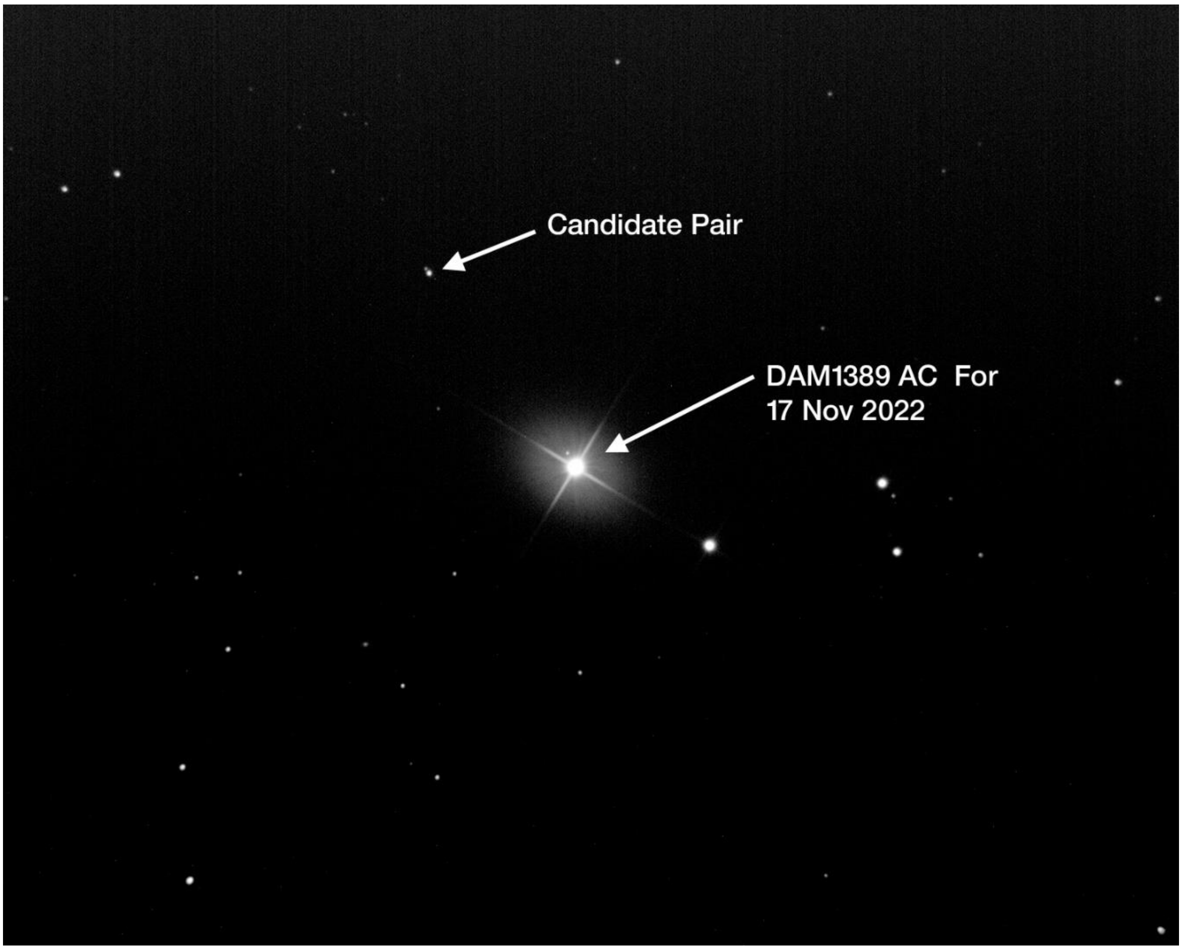

DAM1636	RA. 09 30.5	DEC. -39 26	Last Measure 2015
Antlia	MAG. 11.5 & 13.00	PA. 317°	SEP. 5.6"
Date	**No. images**	**PA°**	**Sep"**
11 April 2023	10	316.71	5.595
12 April 2023	10	316.70	5.609
13 April 2023	10	316.92	5.597
17 April 2023	10	316.95	5.598
Mean		**316.820**	**5.600**
Standard deviation		0.133	0.006
95% CI +/-		0.212	0.010
P(t) movement		0.074	0.942

COMMENTS

Four nights imaging only due to inclement weather.
Little probable movement since previous 2015 measure.

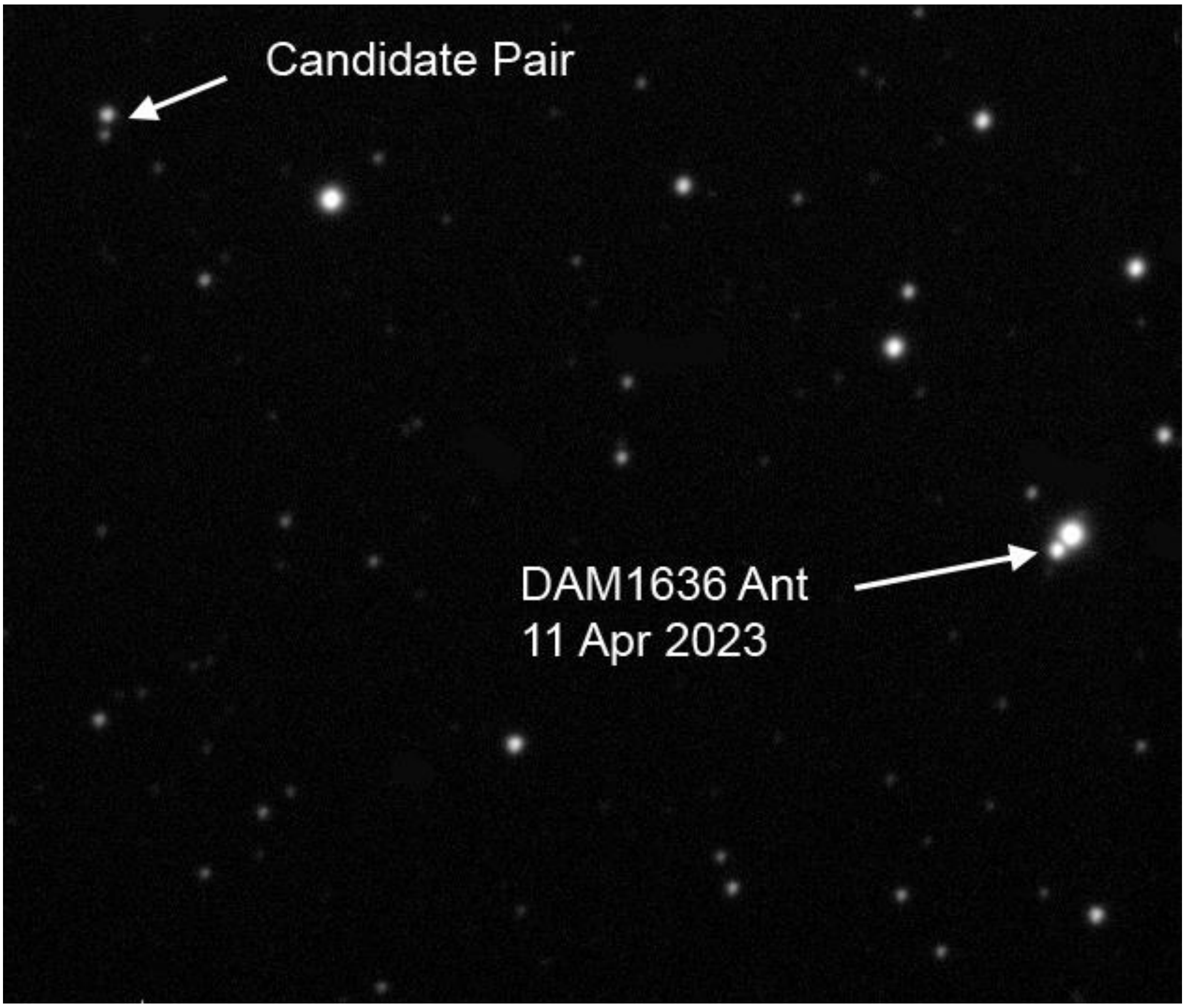

I 183	RA. 07 00.8	DEC. -25 39	Last Measure 1999
Canis Major	MAG. 7.41 & 9.93	PA.139 °	SEP. 3.3"
Date	**No. images**	**PA°**	**Sep"**
20 December 2022	10	140.15	3.606
21 December 2022	10	137.11	3.848
22 December 2022	10	135.17	3.923
17 January 2023	10	138.44	3.723
22 January 2023	10	136.80	3.940
18 February 2023	10	139.77	3.770
Mean		**137.907**	**3.802**
Standard deviation		1.905	0.128
95% CI +/-		1.999	0.134
P(t) movement		0.219	0.118

COMMENTS

Six nights imaging only due to inclement weather.
Little if any probable movement over 21 years.

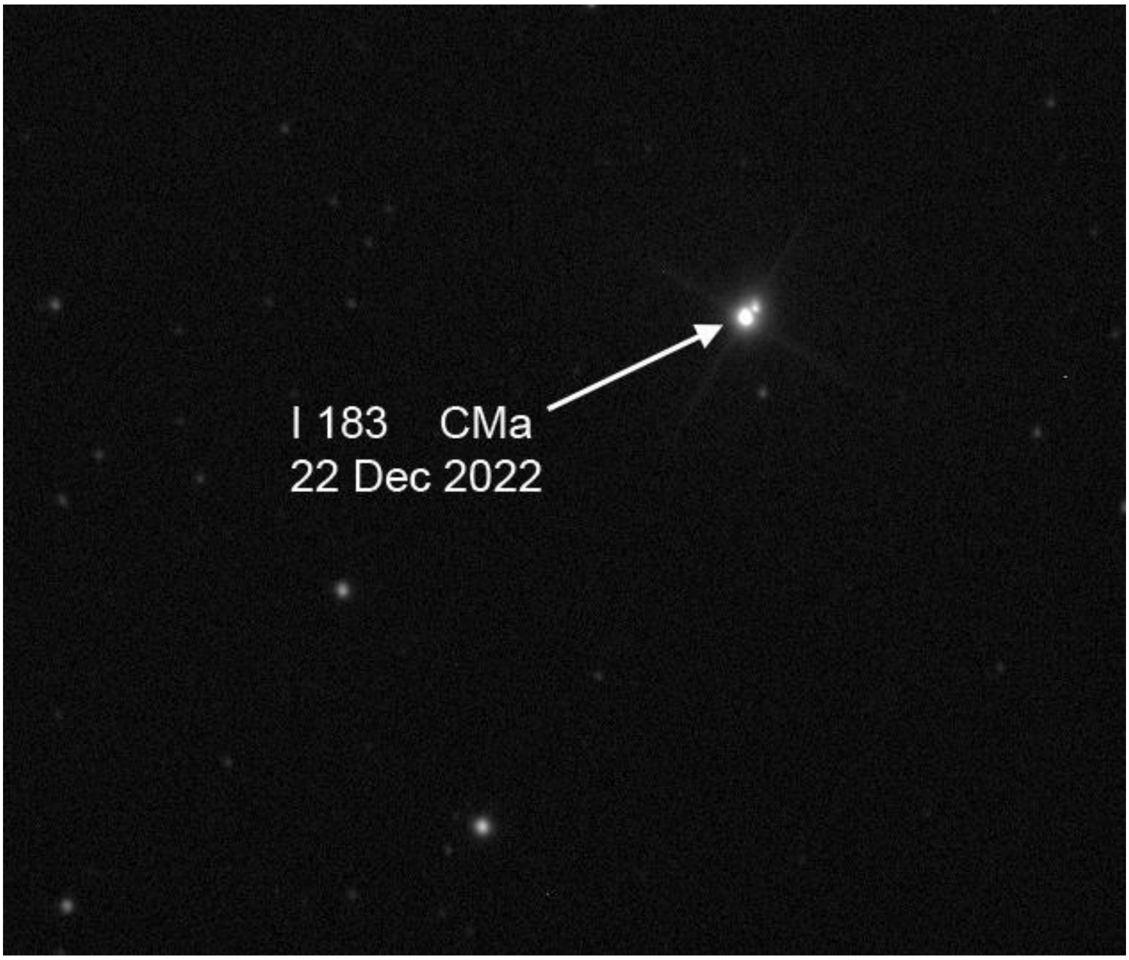

I 461	RA. 02 51.2	DEC. -21 25	Last Measure 1986
Eridanus	MAG. 9.04 & 10.6	PA. 332°	SEP. 3.2"
Date	**No. images**	**PA°**	**Sep"**
17 November 2022	10	332.79	3.091
18 November 2022	10	332.01	2.737
19 November 2022	10	331.78	3.027
25 November 2022	10	331.23	3.050
26 November 2022	10	331.29	3.124
14 December 2022	10	329.75	3.223
16 December 2022	10	330.15	2.986
Mean		**331.286**	**3.034**
Standard deviation		1.055	0.152
95% CI +/-		0.976	0.140
P(t) movement		0.124	0.027

COMMENTS
Possible minor reduction of both axes over 37 years.

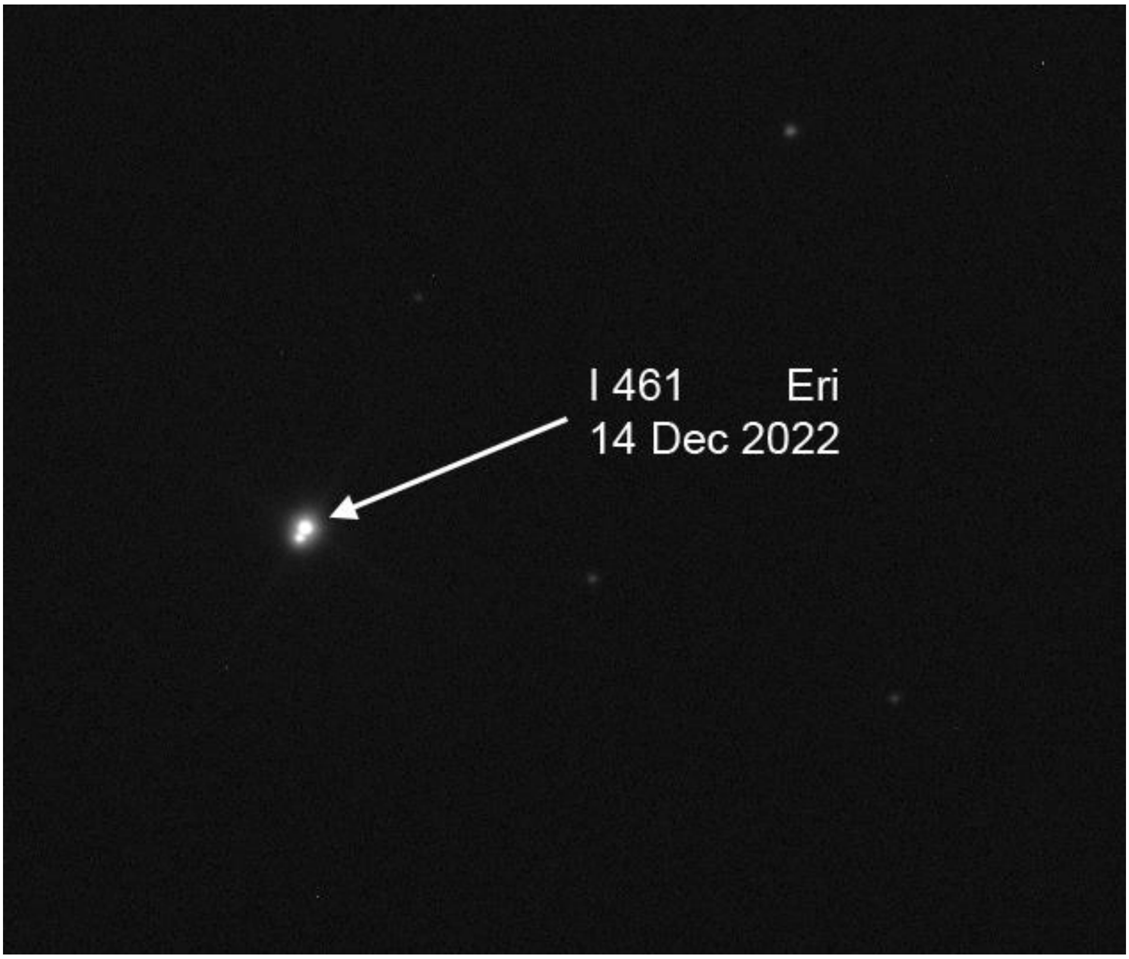

I 1062	RA. 08 04.3	DEC. -31 24	Last Measure 1980
Puppis	MAG. 9.23 & 11.70	PA. 180°	SEP. 3.3"
Date	**No. images**	**PA°**	**Sep"**
21 December 2022	10	177.30	3.249
22 December 2022	10	176.55	3.240
26 December 2022	10	177.64	3.112
17 January 2023	10	177.65	3.234
18 January 2023	10	177.07	3.094
22 January 2023	10	177.75	3.187
18 February 2023	10	177.88	3.354
Mean		**177.406**	**3.210**
Standard deviation		0.468	0.089
95% CI +/-		0.433	0.082
P(t) movement		0.000	0.036

COMMENTS

Continuing decrease in PA since the first 1911 measure of 183°.
Separation would appear static since 1980 measure.

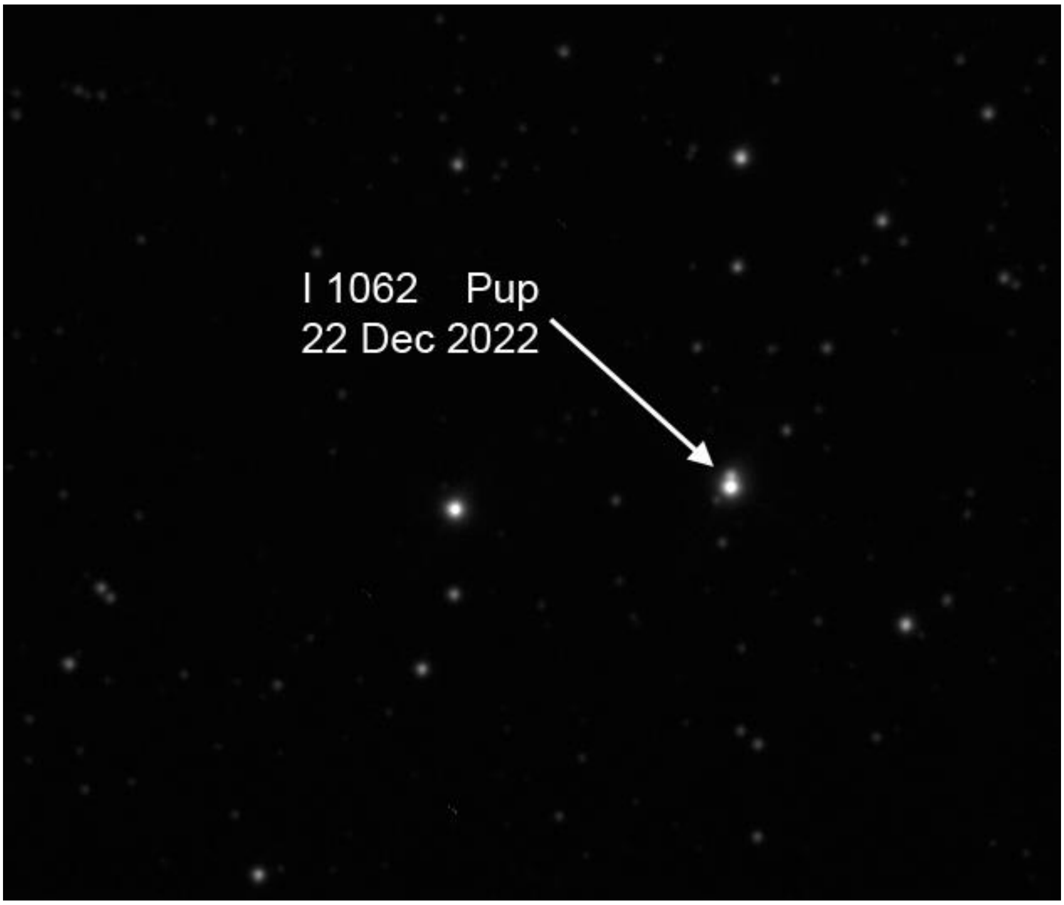

LDS201 A-B	RA. 08 03.9	DEC. -31 33	Last Measure 2018
Puppis	MAG. 8.8 & 9.71	PA. 241°	SEP. 46.1 "
Date	**No. images**	**PA°**	**Sep"**
21 December 2022	10	236.75	47.769
22 December 2022	10	236.66	47.753
26 December 2022	10	236.63	47.642
17 January 2023	10	236.78	47.759
18 January 2023	10	236.68	47.771
22 January 2023	10	236.68	47.813
18 February 2022	10	236.70	47.802
Mean		**236.697**	**47.758**
Standard deviation		0.052	0.056
95% CI +/-		0.048	0.052
P(t) movement		0.000	0.000
COMMENTS Both measures seem to have returned to very similar figures from the first 1911 observation.			

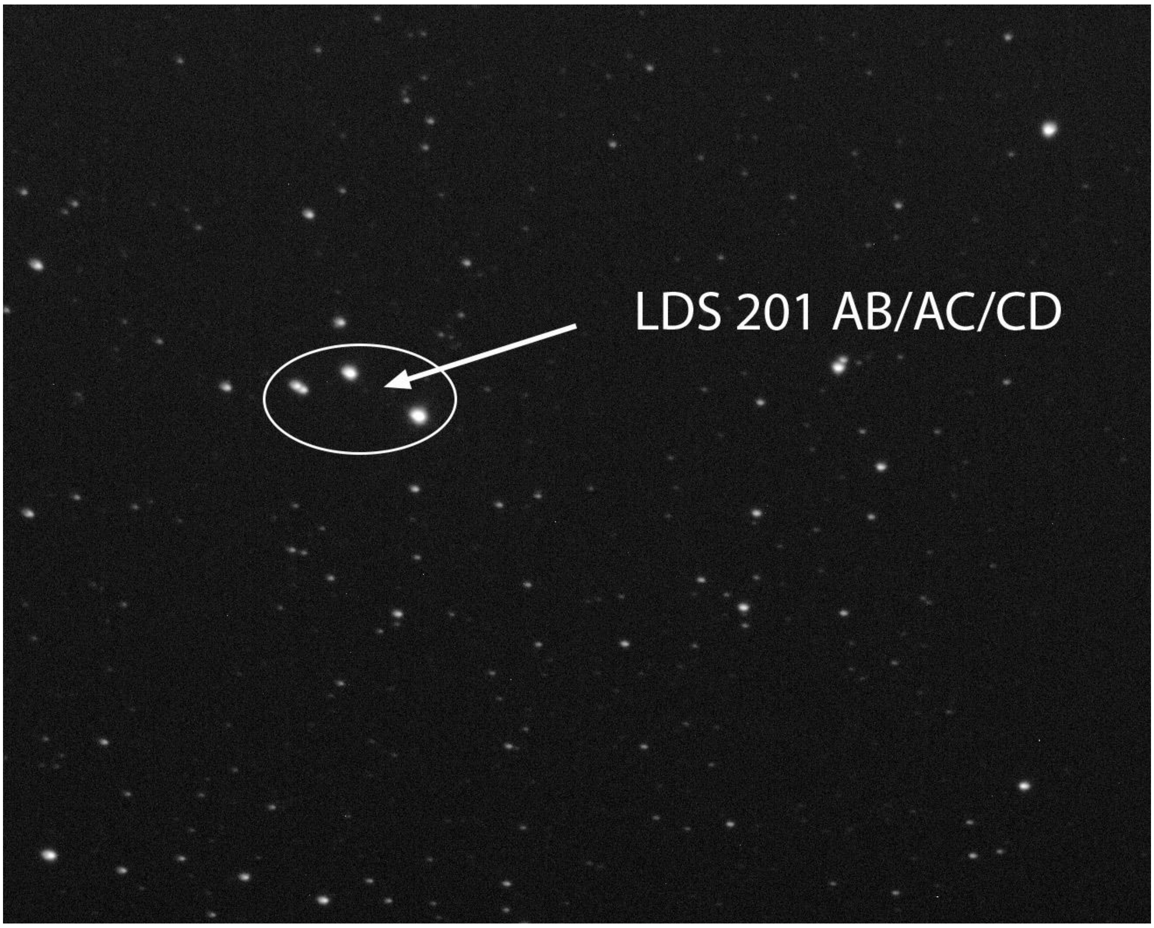

LDS201 A-C	RA. 08 03.5	DEC. -31 33	Last Measure 2015
Puppis	MAG. 8.8 & 10.93	PA. 256°	SEP. 74.5"
Date	**No. images**	**PA°**	**Sep"**
21 December 2022	10	254.88	74.127
22 December 2022	10	254.83	74.036
26 December 2022	10	254.84	73.938
17 January 2023	10	254.92	73.931
18 January 2023	10	254.83	74.043
22 January 2023	10	254.78	74.048
18 February 2023	10	254.80	74.016
Mean		**254.840**	**74.020**
Standard deviation		0.047	0.068
95% CI +/-		0.044	0.063
P(t) movement		0.000	0.000
COMMENTS Possible slight decrease in PA.			

LDS201 C-D	RA. 08 03.5	DEC. -31 33	Last Measure 2015
Puppis	MAG. 10.93 & 11.54	PA. 57°	SEP. 4.0"
Date	**No. images**	**PA°**	**Sep"**
21 December 2022	10	57.59	4.063
22 December 2022	10	58.09	3.846
26 December 2022	10	58.48	3.914
17 January 2023	10	58.25	3.809
18 January 2023	10	58.65	3.97
22 January 2023	10	57.36	3.905
18 February 2023	10	57.87	4.091
Mean		**58.041**	**3.943**
Standard deviation		0.467	0.105
95% CI +/-		0.431	0.097
P(t) movement		0.001	0.200
COMMENTS Possible slight increase in PA.			

MLO63	RA. 15 07.4	DEC. -70 36	Last Measure 1895
Apus	MAG. 9.8 & 11.3	PA. 291°	SEP. 3.2"
Date	**No. images**	**PA°**	**Sep"**
12 Apr 2022	10	141.44	3.602
14 Apr 2022	10	145.93	3.434
15 Apr 2022	10	140.08	3.419
18 Apr 2022	10	138.88	3.303
04 May 2022	10	139.42	3.600
06 Jun 2022	10	140.72	3.627
08 Jun 2022	10	136.99	3.717
Mean		**140.494**	**3.529**
Standard deviation		2.790	0.146
95% CI +/-		2.580	0.135
P(t) movement		0.000	0.001

COMMENTS

Large difference in PA – possible incorrect north-south alignment of original 1895 measurement?

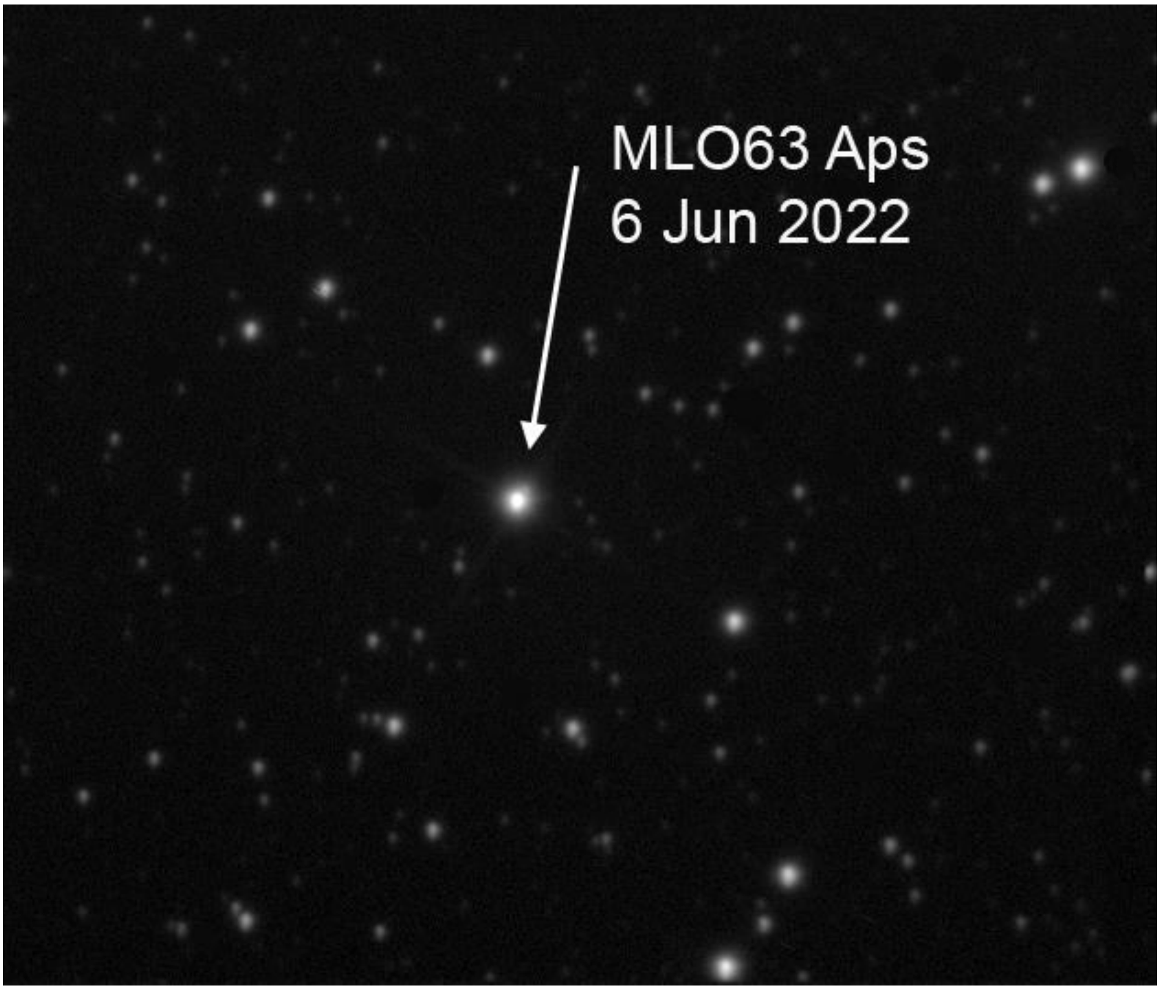

RSS205	RA.09 29.8	DEC. -35 21	Last Measure 2015
Antlia	MAG. 8.56 & 14.5	PA. 312°	SEP. 10.4 "
Date	**No. images**	**PA°**	**Sep"**
21 February 2023	10	313.05	10.204
24 February 2023	10	313.59	10.091
25 February 2023	10	313.31	10.172
27 February 2023	10	312.90	10.203
16 March 2023	10	312.68	10.223
18 March 2023	10	312.40	10.237
Mean		**312.988**	**10.188**
Standard deviation		0.429	0.052
95% CI +/-		0.450	0.055
P(t) movement		0.002	0.000

COMMENTS
Six nights imaging only due to inclement weather.
Possible slight increase in PA over 8 years.

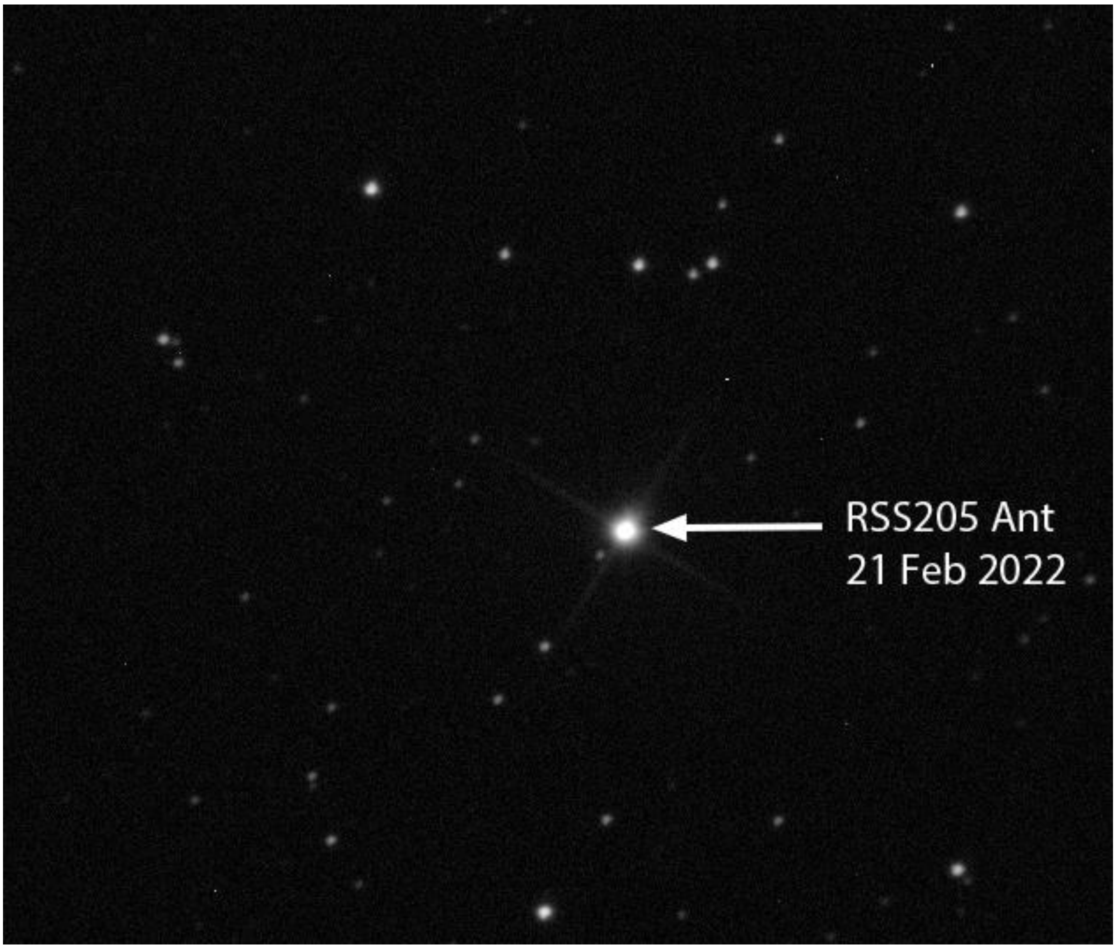

SKF415	RA. 06 50.07	DEC. -44 31	Last Measure 2015
Puppis	MAG. 9.7 & 12.6	PA. 255°	SEP. 33.7"
Date	**No. images**	**PA°**	**Sep"**
20 December 2022	10	255.35	33.463
21 December 2022	10	255.42	33.443
22 December 2022	10	255.43	33.370
26 December 2022	10	255.34	33.408
17 January 2023	10	255.32	33.452
22 January 2023	10	255.32	33.566
18 February 2023	10	255.38	33.566
Mean		**255.366**	**33.467**
Standard deviation		0.045	0.075
95% CI +/-		0.042	0.069
P(t) movement		0.000	0.000

COMMENTS

Possible very small decrease in separation over eight years.

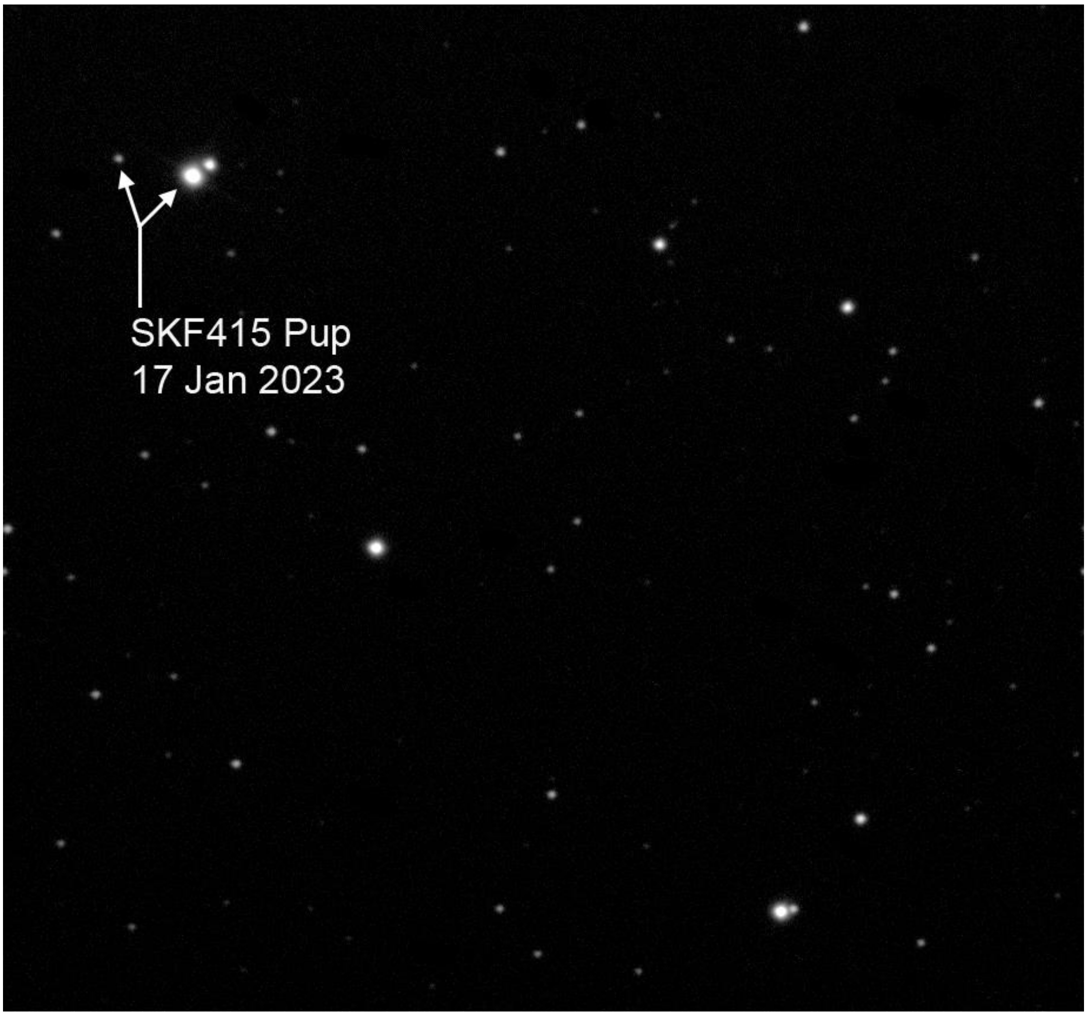

TDS7065	RA. 10 09.1	DEC. -56 51	Last Measure 1991
Vela	MAG. 12.17 & 13.28	PA. 175°	SEP. 2.6"
Date	**No. images**	**PA°**	**Sep"**
11 April 2023	10	177.98	11.18
12 April 2023	10	177.96	11.184
13 April 2023	10	178.05	11.196
14 April 2023	10	178.24	11.132
17 April 2023	10	177.88	11.179
Mean		**178.022**	**11.174**
Standard deviation		0.136	0.025
95% CI +/-		0.169	0.030
P(t) movement		0.000	0.000

COMMENTS
Five night's observations only due to inclement weather.
Considerable increase in separation over thirty two years.

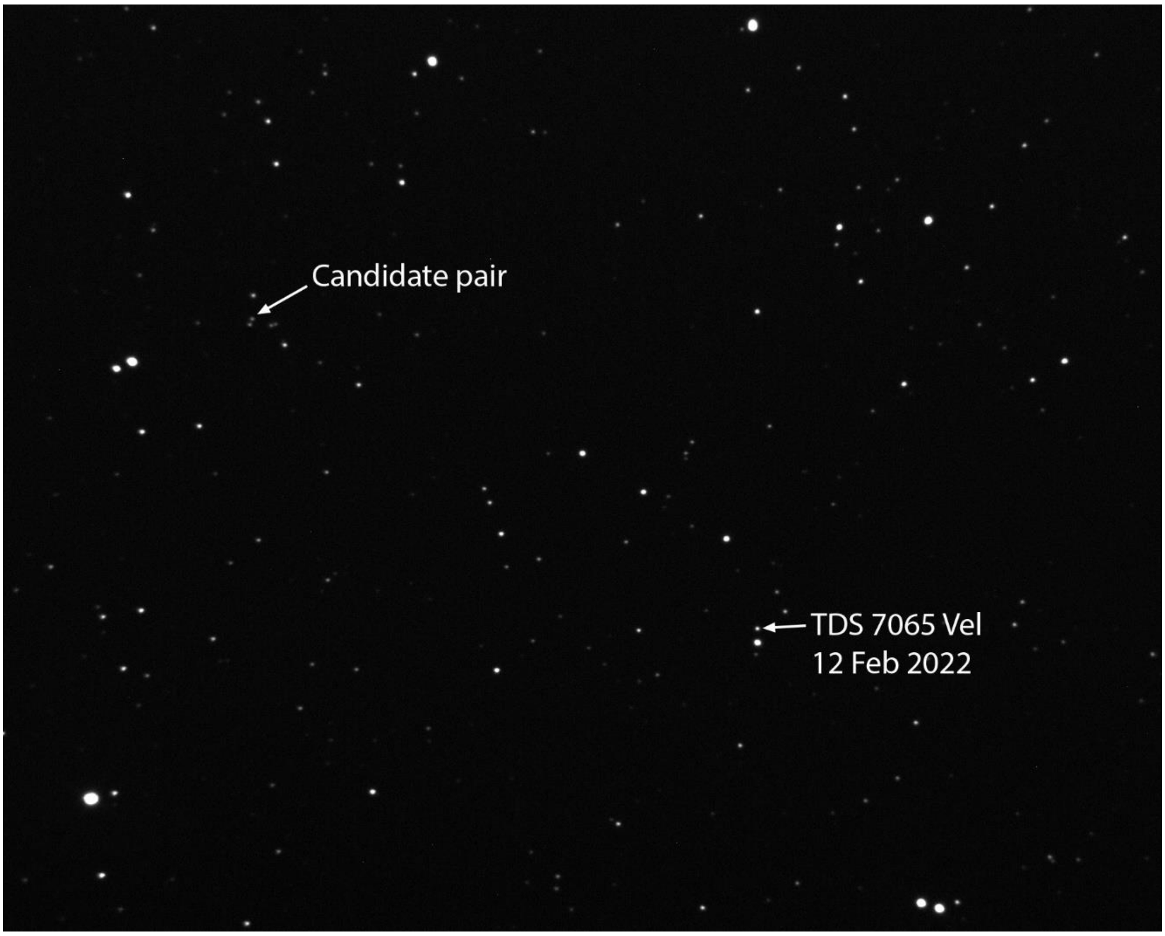

POSSIBLE NEW PAIRS

Possible new pair near DAM1389 (Beta Fornax)	RA.02 48.5	DEC. -32 28	Last Measure n/a
	MAG. 12.09 & 14.77	PA. n/a	SEP. n/a
Date	**No. images**	**PA°**	**Sep"**
17 November 2022	10	215.06	6.689
18 November 2022	10	215.27	6.701
19 November 2022	10	215.73	6.726
25 November 2022	10	214.97	6.533
26 November 2022	10	215.34	6.681
14 December 2022	10	215.3	6.691
16 December 2022	10	215.72	6.692
Mean		**215.341**	**6.673**
Standard deviation		0.294	0.064
95% CI +/-		0.272	0.059
P(t) movement		n/a	n/a

COMMENTS
Possible new pair nearby (S.W.) to Beta Fornax.
Gaia #DR2 5064312147648202496 – brighter component.
Gaia #DR2 5064306272132941696 – fainter component.

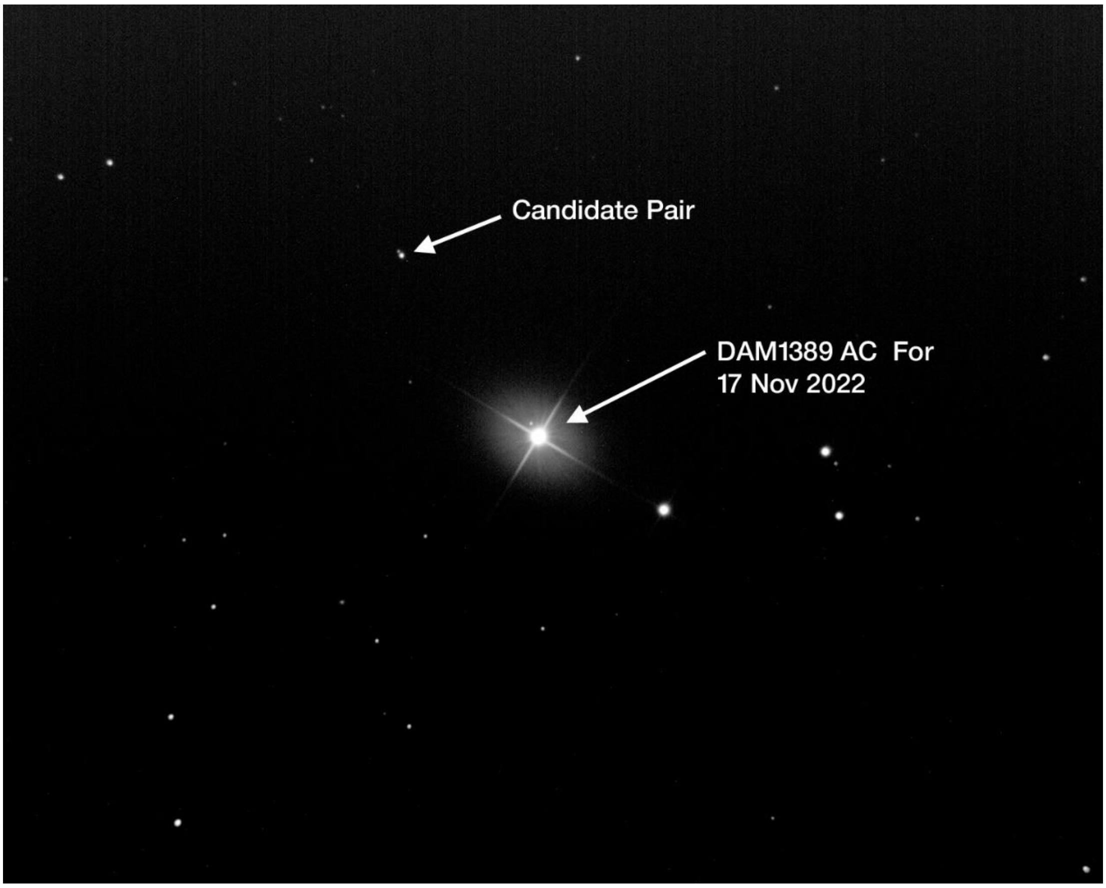

Possible new pair near DAM1636 Antlia	RA. 09 30 25 MAG. 14.68 & 16.38	DEC. -39 28 20 PA. n/a	Last Measure n/a SEP. n/a
Date	**No. images**	**PA°**	**Sep"**
12 April 2023	10	352.03	5.591
13 April 2023	10	351.24	5.597
17 April 2023	10	351.00	5.601
Mean		**351.423**	**5.596**
Standard deviation		0.539	0.005
95% CI +/-		1.339	0.013
P(t) movement		n/a	n/a

COMMENTS

Three nights imaging only due to inclement weather.
Possible new pair SW of DAM1636.
Gaia #DR2 5429699618410021376 – brighter component.
Gaia #DR2 5429699618410021248 – fainter component.

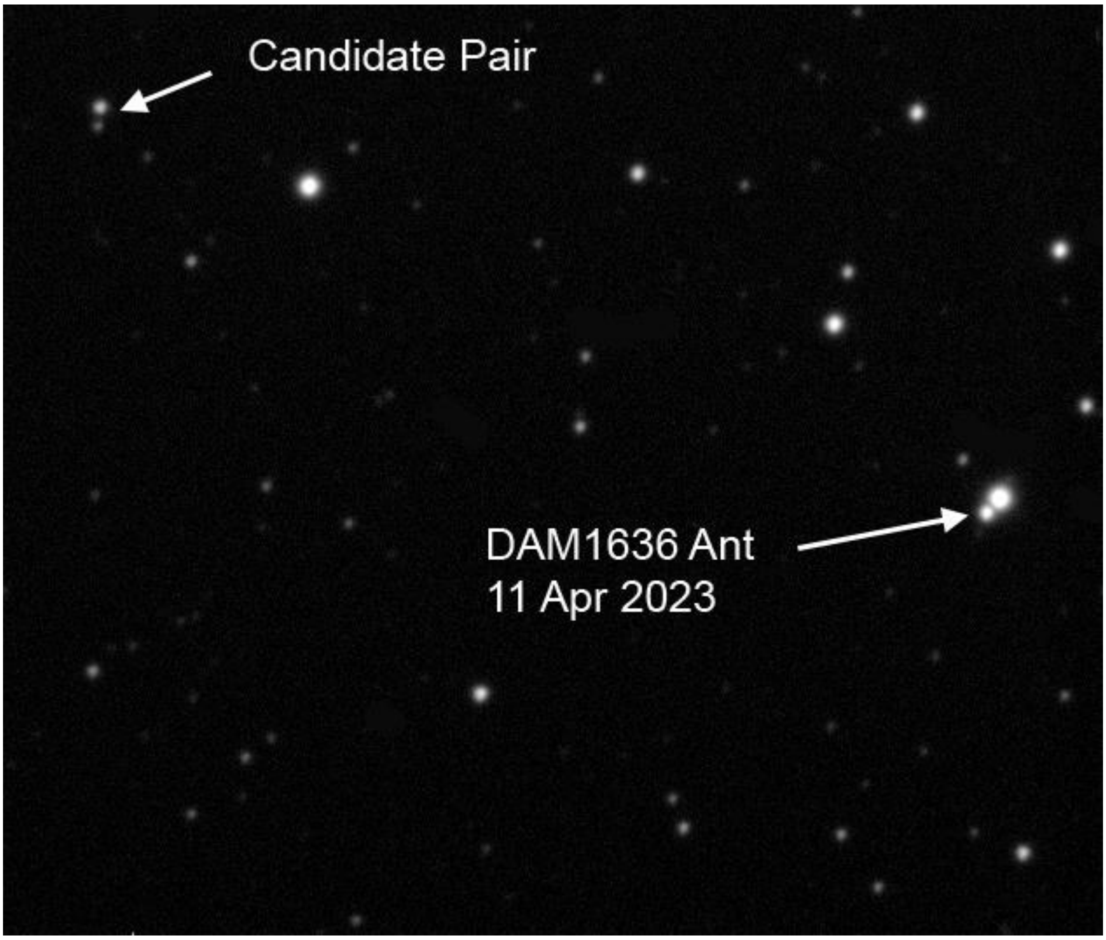

<u>Possible new pair near TDS7065 Vela</u>	RA. 10 08 16	DEC. -56 55 48	Last Measure n/a
	MAG. 14.55 & 14.56	PA. n/a	SEP. n/a
<u>Date</u>	**<u>No. images</u>**	**<u>PA°</u>**	**<u>Sep"</u>**
11 April 2023	10	156.11	4.928
12 April 2023	10	155.72	5.002
13 April 2023	10	156.16	4.984
14 April 2023	10	155.73	4.982
17 April 2023	10	156.1	4.973
Mean		**155.964**	**4.974**
Standard deviation		0.219	0.028
95% CI +/-		0.272	0.034
P(t) movement			

<u>COMMENTS</u>

Five nights imaging only due to inclement weather.
Possible new pair nearby (S.W) of TDS7065.
Gaia #DR2 5258930344338350976 – brighter component.
Gaia #DR2 5258930344338350848 – fainter component.

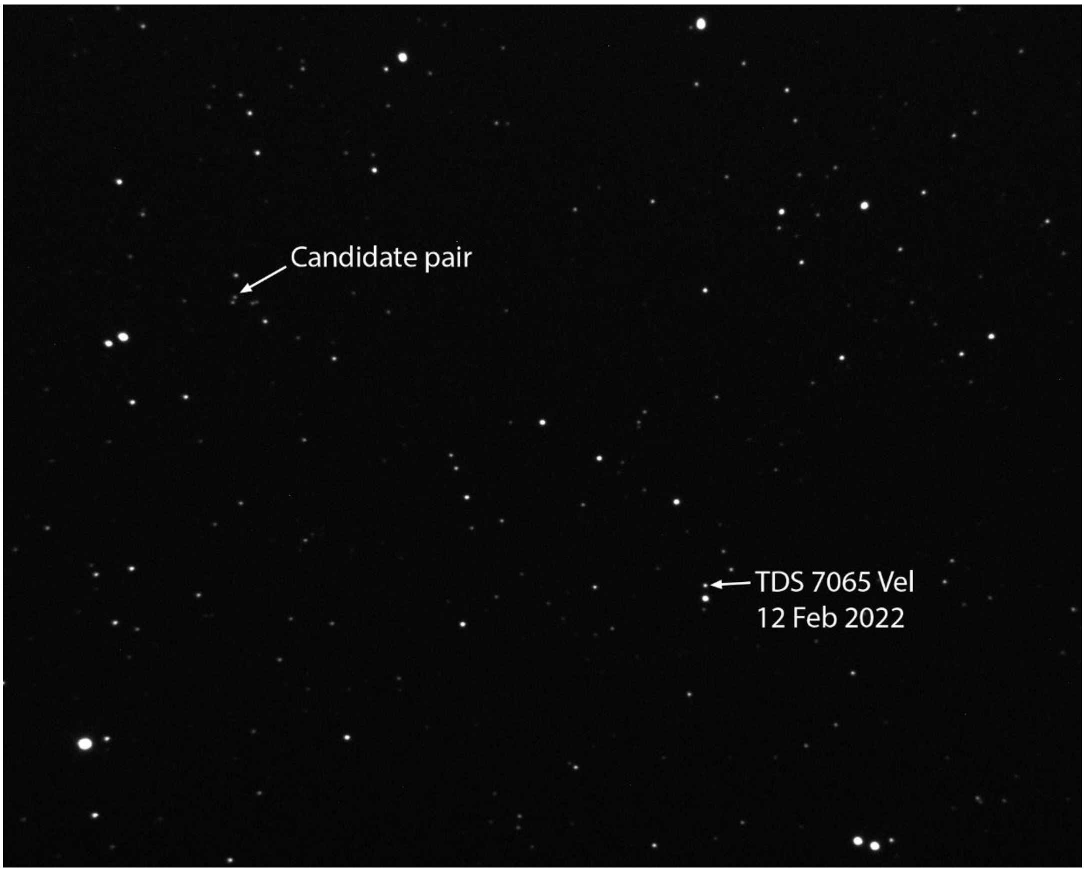

ACKNOWLEDGEMENTS

This research has made use of the Washington Double Star Catalogue maintained at the U.S. Naval Observatory.

The Edward Corbould Research Fund administered by the Astronomical Association of Queensland for granting of funds to upgrade imaging camera and observatory computer to suit.

The assistance of fellow AAQ member Des Janke with processing the original FITS image files into JPEG photographs.

REFERENCES

Argyle, R.W., 2012. Observing and Measuring Visual Double Stars 2nd edition. Springer.

Losse, F. Reduc software, V4.5.1. http://www.astrosurf.com/hfosaf/uk/tdownload.htm

Napier-Munn, T.J. and Jenkinson, G., 2009. Measurement of some neglected southern multiple stars in Pavo. Webb Society Double Star Section Circular 17, 6-12.

Napier-Munn, T.J and Jenkinson G., 2014. Analysis of errors in the measurement of double stars using imaging and the Reduc software. Journal of Double star Observations Vol. 10 No.3.

****

Astrometric Measurements of Double Star ARA 77

Owen Frattini Edwards[1], Kai Lange-Dei[1], Pat Boyce[2], Grady Boyce[2]

1. High Tech High, San Diego, CA
2. Boyce Research Initiatives and Education Foundation

Abstract

We performed our study on WDS 14415-1712 (ARA 77) using the Las Cumbres Observatory telescope network (LCO) to obtain our images. The intention for the candidate was to determine its probability of being a binary pair. Our measured mean Theta and Rho of 110.49° and 10.05" were complementary to prior measurements. Analysis of the system's figures from historical data and test images indicate the candidate cannot be binary.

1. Introduction

WDS 14415-1712 (ARA 77), Figure 1, has 6 recorded measurements in the Washington Double Stars Catalog (WDS) (Mason, 2012). The first of which was made in 1905 upon the system's discovery by S. Aravamudan. Both the Primary and Secondary stars share a low magnitude of 14.4, according to the WDS, thus challenging the ability of our equipment. The candidate was selected to not only evaluate the probability of being a binary pair but also to test the capability of our systems when analyzing dim double stars. Other characteristics of the pair proved interesting, specifically the variation in proper motions of the two stars. Unlike the WDS and GAIA catalogs, SIMBAD provided no information regarding ARA 77.

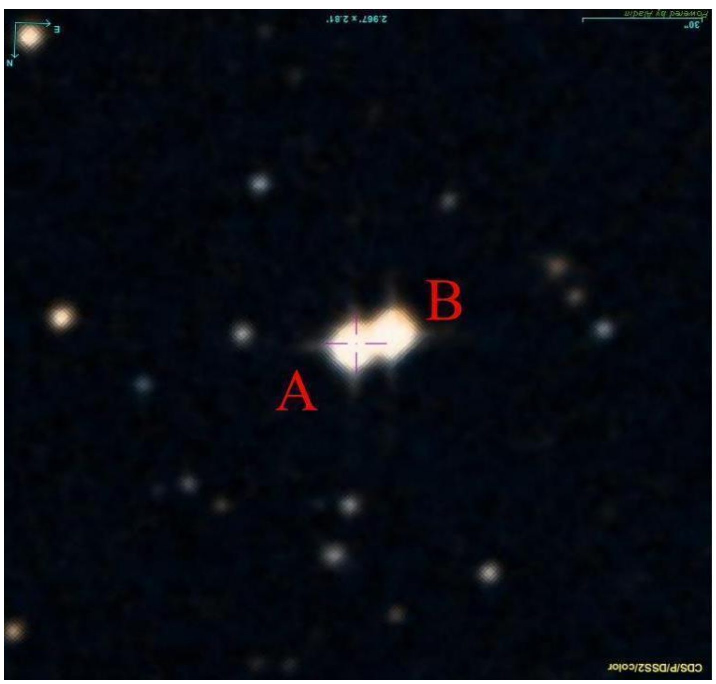

Figure 1: image of Candidate pair taken on Aladdin 10.

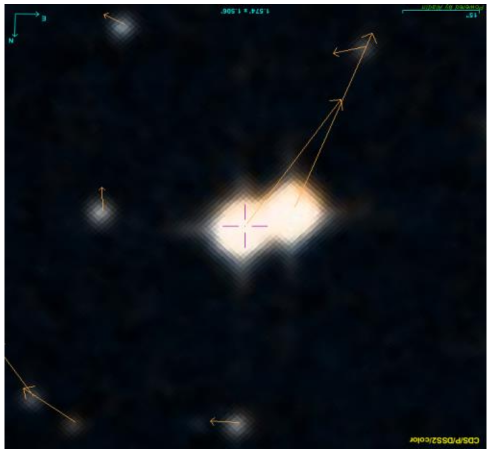

Figure 2: The A and B stars have noticeably different proper motions represented by the yellow arrows in the Aladdin 10 image.

2. Methods and Materials

The images were taken using the Las Cumbres Observatory (LCO) system. The telescope used for observations was located at the Teide observatory in Tenerife, Spain. The telescope used was the 0.4-meter reflector with a SBIG 6303 CCD camera with 8 filter options, and a FOV of 29.2 x 19.5 arcminutes. The LCO 0.4-meter reflector telescopes have been deployed all around the world with ten in total.

Figure 3: AIJ measurements of 14415-1712

3. Observations

A total of 12 images were taken, of which one proved too poor of quality to measure and was therefore excluded from the calculations and measurements. Due to the low magnitude of each star, our exposure times were in the range of 300 to 400 seconds. The Images were calibrated, and plate-solved by the OSS Pipeline (Fitzgerald, 2018). They were measured using AIJ software, Figure 3, and placed in an Excel spreadsheet for statistical calculations.

WDS 14415-1712 ARA 77 Astrometry				
Telescope: (number of images used in each filter)	Epoch 2021.347	Position Angle	Separation	Delta Magnitude
R Sloan (11 used), 12 images total	Mean	110.5°	10.05"	0.05
	standard deviation	0.081°	0.016"	0.006
	standard error of mean	0.02°	0.005"	0.002
Measurement 2015 (Last measurement before this observation)		109.59°	10.041"	0

Table 1: Recorded measurements and accuracy of theta, rho, and delta magnitude for ARA 77.

4. Results

The calculated mean, standard deviation, and standard error of mean for position angle, separation, and delta magnitude of ARA 77 AB are in Table 1. These measurements are nearly identical to that of GAIA's DR2 (Salgado, 2017) and the WDS. With respect to magnitude measurements, GAIA reported a primary magnitude of 12.2 and a secondary magnitude of 12.3, in Sloan g, whereas the WDS reported 14.4 magnitude for both the A and B star.

WDS 14415-1712 ARA 77 Historical Data						
Epoch	1905.35	1916.26	1999.45	2000.48	2010.5	2015
Position Angle	108.4°	103°	108.9°	109.5°	110.2°	109.59°
Separation	10.24"	9.79"	10.06"	10.11"	10.07"	10.04"

Table 2: The measured theta and rho recorded from all prior observations of ARA 77.

5. Discussion

There was minimal change in separation and position angle in the observations, closely following those of previously recorded measurements as seen in Table 2. The Harshaw statistic calculator (Harshaw, 2014), evaluates a pair's likelihood of being binary or optical based on the proper motions, Figure 2. As such, the most recent proper motion and separation measurements for ARA 77, from GAIA, indicates the pair has a vector difference of 0.354. This figure is moderately low suggesting a plausible yet still-uncertain chance of the pair being binary.

The small angle approximation was applied to the parallax measurements of the A and B stars to calculate a minimum possible separation of 4904.02 AU or 0.077 Light years. This falls well within the generally accepted 1 light year maximum separation for a pair to be gravitationally related. However, this measurement only evaluates the pair on a two-dimensional plane. When taking into account the 3rd dimension, that being the pair's radial separation, a vastly different separation is found.

Evaluating each of the star's distances from Earth proves that the small angle approximation is nothing more than a mere illusion and provides a full understanding of the space between Star A and Star B. Star A has a measured parallax of 2.0245 with an error of 0.015 and Star B has a measured parallax of 2.4358 with an error of 0.0152. When applying those values to a parallax calculator to find the radial separation it was discovered that the difference in distance is at least 1330 light years, which is far too great for the stars to be physically bound. The probability of Star A and Star B being within 1 light year was calculated to be 0%. With the distance between Star A and Star B exceeding one light year it makes the chance of the pair having a gravitational relation extremely improbable based on the aforementioned rule of maximum separation. However, keep in mind that parallaxes below 5 mas are an area of great uncertainty in measurements.

6. Conclusion

With all the measurements and calculations conducted on ARA 77, the data provided suggests that the pair is a U code system, as defined by the WDS, meaning, the discrepancy of the two star's proper motions suggest that the pair is non-physical. Additionally, certain characteristics of the pair, namely the variation in radial separation of the stars, seen on GAIA and in historical data received, make the probability of ARA 77 being gravitationally bound highly improbable. These findings among others indicate that the pair can be classified as a U code system and that ARA 77 is non-physical.

Acknowledgements

We would like to thank Pat and Grady Boyce for their assistance and guidance throughout the making of this paper. Additionally, we thank Brian D. Mason at the US Naval Observatory for providing us with crucial data on both of our candidates. The group would also like to thank the Las Cumbres Observatory network for supplying us with equipment and software systems crucial to our research. Also, This work has made use of data from the European Space Agency (ESA) mission Gaia (https:// www.cosmos.esa.int/gaia), processed by the Gaia Data Processing and Analysis Consortium (DPAC, https:// www.cosmos.esa.int/web/gaia/dpac/consortium). Funding for the DPAC has been provided by national institutions, in particular the institutions participating in the Gaia Multilateral Agreement.

We would like to thank our mentor Douglas Frattini Edwards for guiding and helping our group. We would also like to thank Michael Fitzgerald for authorizing our use of the OSS Pipeline. In addition, we would like to thank Richard Harshaw for creating a computing model that significantly added to our research. Furthermore, we would like to thank Bob Buchheim for providing his method of calculating probability, based on radial distance. Finally, we thank the Boyce Research Initiatives and Education Foundation for giving us the opportunity to write this paper.

References

Harshaw, Richard., 2014, "Another Statistical Tool for Evaluating Double Stars". Brilliant Sky , *Journal Of Double Star Observations*

Fitzgerald, M.T., (2018, accepted), "The Our Solar Siblings Pipeline: Tackling the data issues of the scaling problem for robotic telescope based astronomy education projects". *Robotic Tele scopes, Student Research and Education Proceedings.*

Mason, Brian., et al, 2012, "Washington Double Star Catalog, Astronomy Department", United States Naval Observatory, http://ad.usno.navy.mil/proj/ WDS/

Salgado, et al., (2017): Gaia Data Release 2. Gaia achive data access facilities; European Space Agency (ESA) mission Gaia, https://www.cosmos.esa.int/ web/gaia.

Speckle Observation of WDS 15493+6032 HU 912

Joe Smith[1], Bretton Simpson[2], and Pat Boyce[3]

1. Stanford Online High School, Redwood City, California
2. University of California San Diego, La Jolla, California
3. Boyce Research Initiatives and Education Foundation (BRIEF), California

Abstract

The physical system of WDS 15493+6032 HU 912 was observed on June 14, 2022 using the 60-inch telescope at Mount Wilson Observatory. Speckle interferometry was performed on the target system, yielding a mean position angle and standard deviation of 159.4° ± 0.372° with a mean separation and standard deviation of 0.333″ ± 0.008″. Astrometric measurements of this system were calculated using the SpeckleToolBox software [2]. Our measurements of this system return a statistically significant ($p < 0.05$) deviation but also fall along the predicted orbital solution, indicating that the orbital solution for HU 912 does not currently require refinement.

1. Introduction

Our observation of WDS 15493+6032 HU 912 was made on June 14, 2022 at the site of the historic Mount Wilson Observatory. The United States Naval Observatory maintains the Sixth Orbital Catalog for binary stars. In this Sixth Catalog of Orbits of Visual Binary Stars [4], a standardized integer-based grading scale from 1 to 5 is employed for the orbits of known gravitationally bound stars. Grades 3 to 5 are considered in need of some to significant improvement regarding the determination of their orbital solutions. Our target system of WDS 15493+6032 HU 912 has an orbital solution considered Grade 3 [6], suggesting a need for continued observation. HU 912 also fits within an ideal magnitude range between 6 and 9, with a magnitude of 8.60 for the primary stars and a magnitude of 9.01 for the secondary star [5]. Since HU 912 fits the ideal parameters defined above, it was selected to be the target system for observation. As these stars are closely spaced, we needed to employ the measurement method of Speckle Interferometry. Therefore, in addition to observing HU 912, an additional well-understood reference star is necessary to calibrate observations. The nearby target star, WDS 15542+1659 A 2080, was selected as our reference star due to its close proximity, comparable magnitude, and similar air mass. First cataloged in 1905, the target star had been observed a total of 59 times prior to our observation, most recently in 2010. The target star's spectral class is F5.

2. Equipment and Methods

WDS 15493+6032 HU 912 was observed for a duration of one night on the 60" Hale telescope at the Mount Wilson Observatory, Figure 1. The date of the observation was June 14, 2022, or 2022.45. The telescope has a focal ratio of f/16 - a focal length of 24m. The camera used was a ZWO ASI 6200MM (a monochrome CMOS camera) setup with an Astronomik Proplanet-642 BP IR pass filter, with a pixel scale of 3.8 µm and a plate scale of 0.03045 arcseconds per pixel. The field of view for this setup is 5.08′ x 3.38′.

During this observation run for HU 912, a series of a thousand images were taken. An equivalent amount of images were taken for the reference star, necessary to complete the Fourier transform in speckle interferometry [1]. While the reference star is a double star, all other single star systems were either too distant or there was a significant difference is magnitude such that they would not serve as appropriate reference stars, leaving A 2080 as the reference star of choice. As a consequence of the target pair's apparent separation being below 4", speckle interferometry is convenient because it allows for the correction of atmospheric distortion present when observing such a closely-bound double star. Speckle interferometry requires a large amount of images in order to minimize this atmospheric distortion by "freezing" the images over a very short time scale, hence the thousand images taken. The data reduction and bi-spectrum analysis were performed within Speckle Toolbox 1.16 (STB) [2], outputting the then-current astrometric values of the position angle (θ) and separation (ρ).

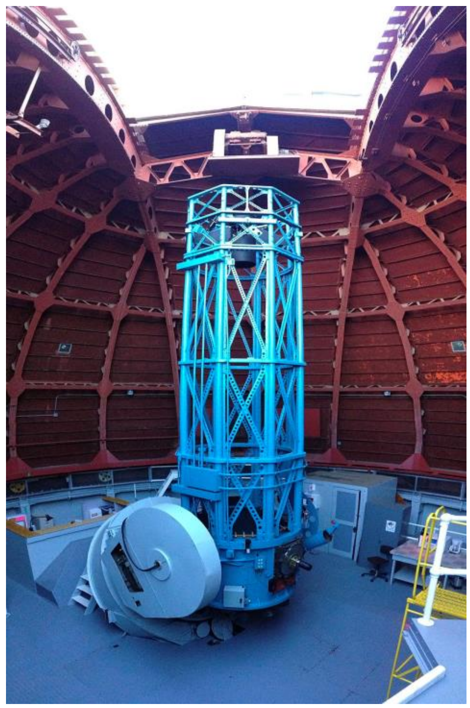

Figure 1: The Mount Wilson Observatory 60" telescope used to image WDS 15493+6032

3. Data

Examples of the specifications for bi-spectrum analysis of HU 912 and astrometry of the autocorrelogram within STB are shown in Figures 2 and 3. The imaged FITS cubes were generated from the same dataset and analyzed independently by three team members, each outputting astrometric measurements, Table 1. These separate calculations allow an average and standard deviation (S.D.) to be calculated. The averages of ρ and θ and the S.D. are shown in Table 2. The ephemeris for the date of observation and the measurements from the last recorded observation are also shown in Table 2.

Table 1. FITS Cube Measurements.

FITS Cubes No.	θ	ρ
No. 1	159.34	0.328
No. 2	159.42	0.329
No. 3	159.15	0.342

Table 2. Measurements of HU 912.

Date	θ	θ S.D.	ρ	ρ S.D.
2010.31	132.1°	-	0.325″	-
2022.45	159.4°	0.372°	0.333″	0.008″
Ephemeris - 2022.45	148.0°	-	0.340″	-

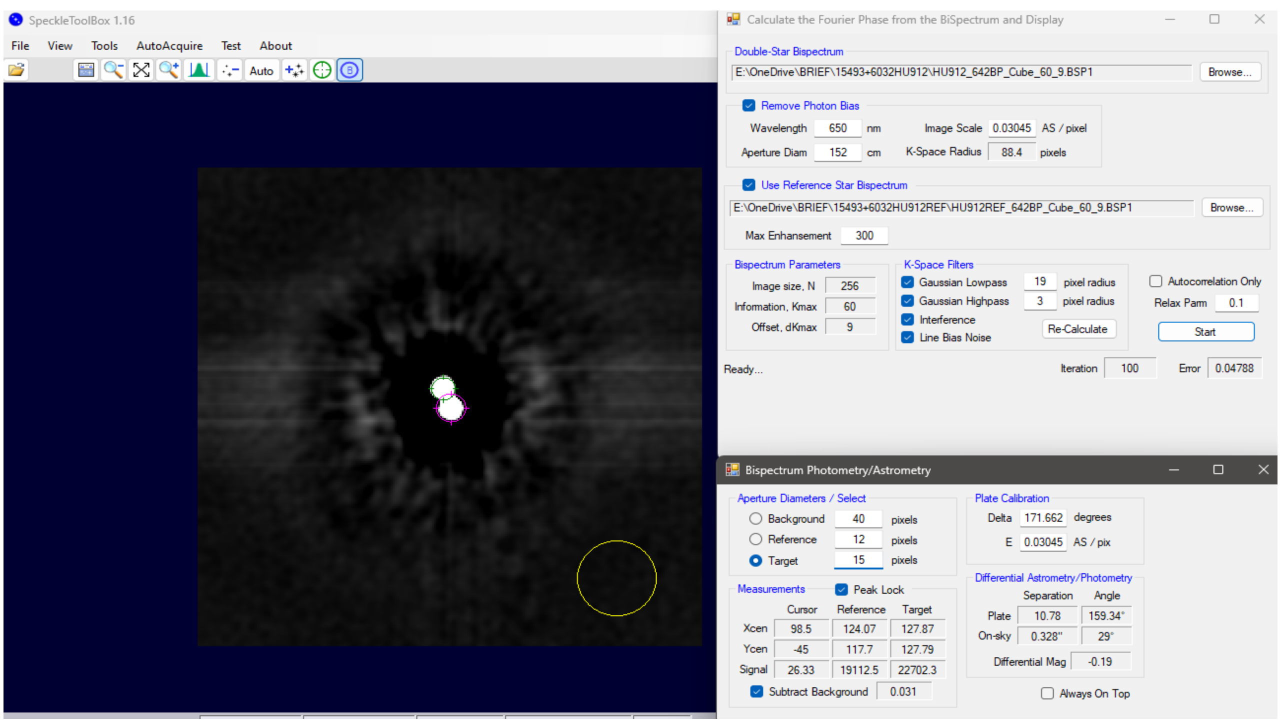

Figure 2: Steps of STB bi-spectrum reconstruction showing panels with specifications for the reconstruction and astrometry.

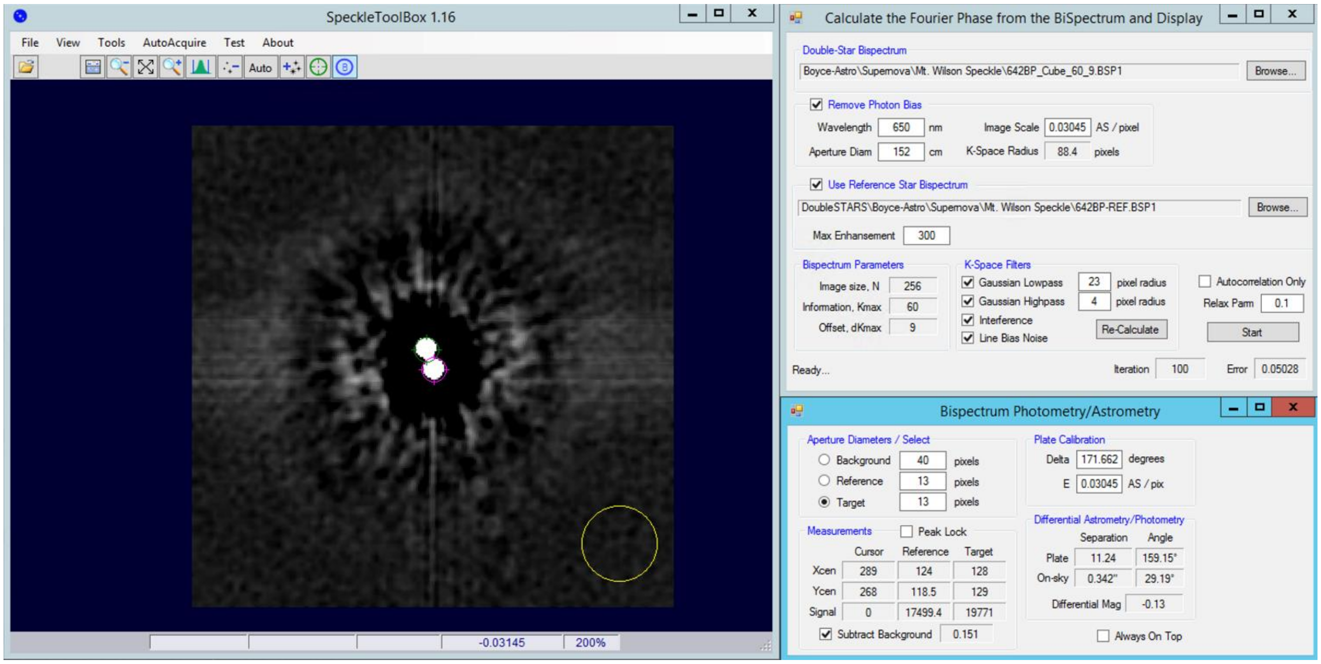

Figure 3: Steps of STB bi-spectrum reconstruction showing panels with specifications for the reconstruction and astrometry.

4. Discussion

We compared the measurements collected in Table 1 to predicted values from an ephemeris for θ and ρ. A linear interpolation was used to find the ephemeris for the given date of the observation [3]:

$$(1)\ y = y_1 + a(y_2 - y_1)$$

where y is the ephemeris for ρ or θ on the given date, y_1 the ephemeride for a given year and y_2 the year after it, and a the decimal value of the date falling between the given years. As an example, the date of this observation was 2022.45. It follows that a is 0.45, and y_1 and y_2 the ephemerides for 2022 and 2023. Upon identifying the values for the ephemerides from the Sixth Catalog of Orbits of Visual Binary Stars, it is found that the ephemeris for this system is 148.0° and 0.34″ for θ and ρ, respectively. The orbital solution from the Sixth Catalog of Orbits of Visual Binary Stars is shown in Fig. 4, where the observed measurement is represented as the red star and the ephemeris the blue star.

The difference between the observed and predicted values for the θ and ρ is 11.40° and 0.007″, respectively, and the S.D. for each is 0.372° and 0.008″, respectively. It follows that there is an approximate 30 σ difference for the θ and a 1 σ difference for the ρ present, indicative of a highly statistically significant measurement. By convention, a measurement must fall, assuming a confidence of 95% ($p < 0.05$), at least 2 σ away from the null (i.e., the mean) to be statistically significant. However, while there may be a discrepancy between the calculated ephemeris for the date of the observation, as can be seen in Figure 4, the observed data fall along the graph of the orbital solution, indicating that the orbital solution and the set of all ephemerides do predict the measurement recorded.

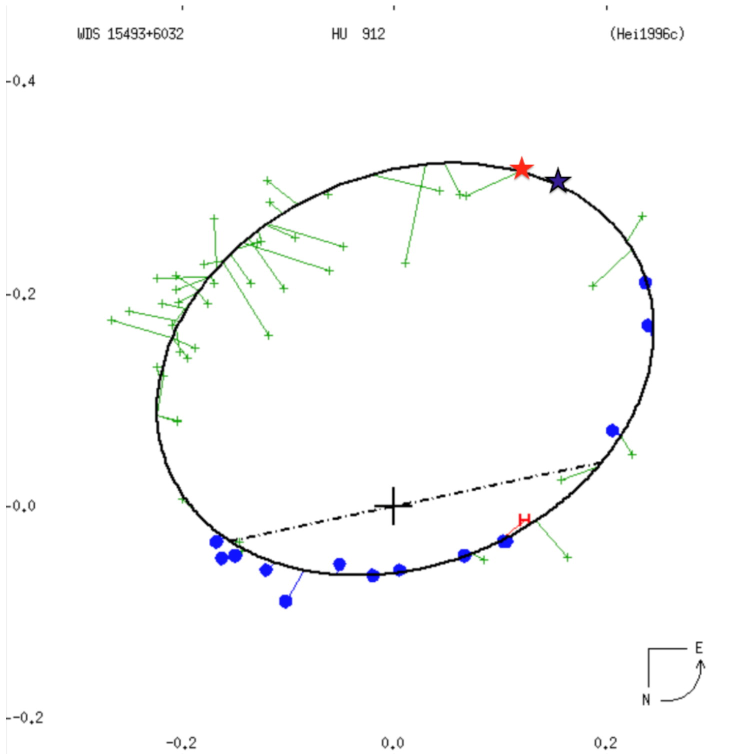

Figure 4: Orbital plot of HU 912 with the measurement denoted by the red star and the ephemeris by the blue star.

5. Conclusion

We report updated measurements of WDS 15493+6032 HU 912 with a position angle of 159.4° ± 0.372° and a separation of 0.333″ ± 0.008″. While there is a significant difference between the predicted ephemeris and the measurement observed, it does not imply that the orbital solution itself requires refinement as the measurement still falls along the orbital solution. Therefore, we conclude that the orbital solution of HU 912 does not require refinement at the present moment.

Acknowledgements

This research has made use of the Washington Double Star Catalog maintained at the U.S. Naval Observatory. The Speckle Toolbox 1.16 software, developed and maintained by Dave Rowe, was also utilized. Additionally, thanks is due to the Mount Wilson Observatory and its faculty's generosity for usage of its telescope, Kalee Tock, Rick Wasson, and Dave Rowe. Gratitude is further extended to Pat Boyce for aid ranging from observation to revision and to Grady Boyce for revision of this paper. We would also like to thank Velne Barud for her contributions to the data reduction and observation process done in this paper.

References

[1] Labeyrie, A. (1970). Attainment of Diffraction Limited Resolution in Large Telescopes by Fourier Analyzing Speckle Patterns in Star Images. Astronomy and Astrophysics, 6, 85.

[2] Harshaw, R., Rowe, D., and Genet, R. (2017). The SpeckleToolBox: A Powerful Data Reduction Tool for CCD Astrometry. Journal of Double Star Observations, 13(1), 16.

[3] Bush, M. (2018). Astrometry Observations of STF 1321AB. Journal of Double Star Observations, 14(1), 38-43.

[4] Mason, B., (2018). The Washington Double Star Catalog, Astrometry Department, U.S. Naval Observatory. http://ad.usno.navy.mil/wds/Webtextfiles/wdsnewframe2.html

[5] Stelle Doppie (2018). 15493+6032 HU 912. https://www.stelledoppie.it/index2.php?iddoppia=64003

[6] Henitz, W.D (1996). Observations of double stars and new pairs XVII. Astrophys. J., Suppl. Ser., 105, 475-480.

Double Star Discovery During an Occultation by the Asteroid (676) Melitta

M. Eleftheriou[1], M. Dogrammatzidis[1], A. Karagiannidis[1], C. Weber[2], F. Casarramona[3]
[1] Amateur Astronomy Club Pegasus, Drama, GR, melefth@gmail.com
[2] International Occultation Timing Association/European Section (IOTA/ES), Berlin, DE
[3] Agrupacio Astronomica de Sabadell (AAS), Las Negras - Nijar, ES

Abstract

On 8 April 2023, an occultation of the star UCAC4 402-083153 (Gaia id: 4155332686530844800) by the asteroid (676) Melitta revealed that this star is a previously unknown double star with a separation of 18.0 mas.

1. Observation

The occultation path from Occult4 [1] (Figure 1) ran over the Greek observatory of Nikiforos Drama (obs1). All the parameters of this occultation event can also be taken from Figure 1. For the observation, a Schmidt-Cassegrain telescope with an aperture of 35.5 cm was used. There were no filters in the optical path. The camera was a QHY174GPS, which operated with an exposure time of 500 ms. The recording from this station led to the discovery of the double star.

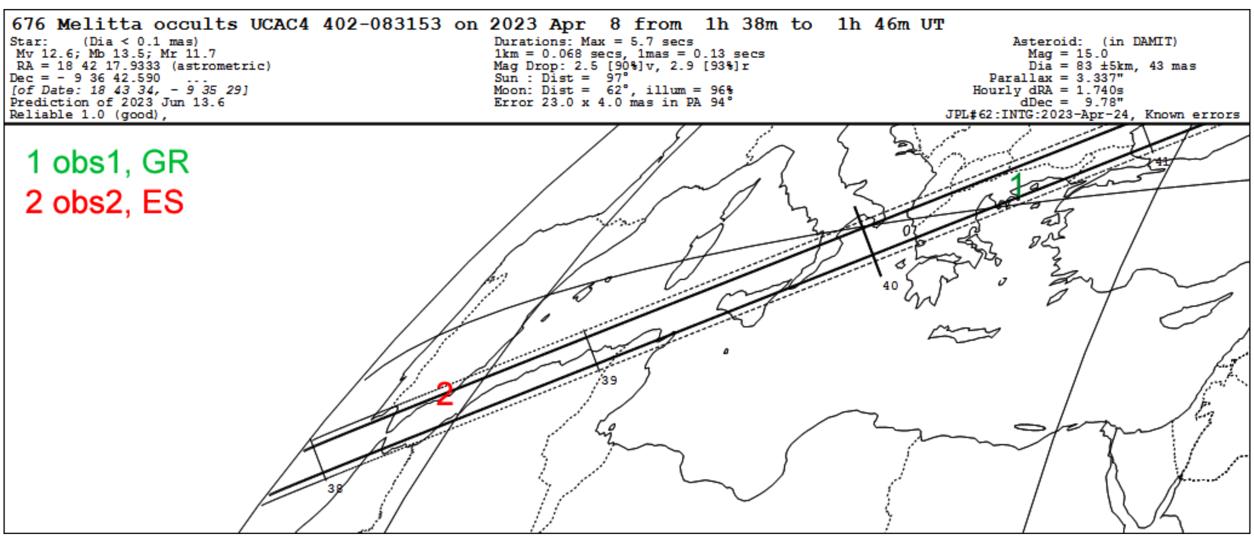

Figure 1: Occult4 prediction of the occultation of UCAC4 402-083153 by Melitta (676)

On the shadow path, there was also a Spanish station (obs2) near Las Negras where a 20 cm Newtonian telescope and a WATEC 910HX-RC camera (exposure time 320 ms, no filters) were used. This station did not register an occultation of the target star; however, with its "near miss" result the ambiguity of the double star solution gotten from the first station's recording could be limited. Both stations used the GPS 1-pps-pulse for precise timing. No other observations of this occultation event are known. The observations of this stellar occultation event took place within the framework of the International Occultation Timing Association/European Section (IOTA/ES) [2] and the results were recorded with its SODIS portal [3].

2. Data reduction

Figure 2 shows the recording from the Spanish station (obs2), prepared with PyMovie/PyOTE [4].

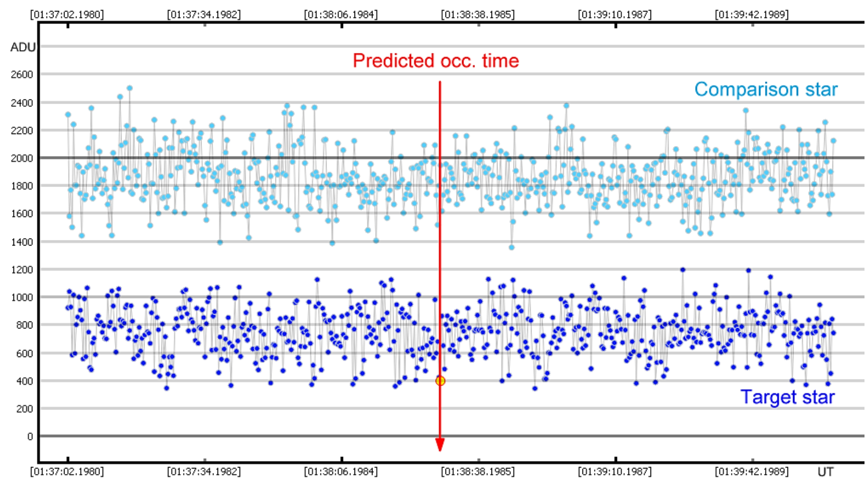

Figure 2: Station obs2 recording - no occultation was detected

For the photometry of the recording of station obs1 (Figure 3), we used the programme Tangra [5].

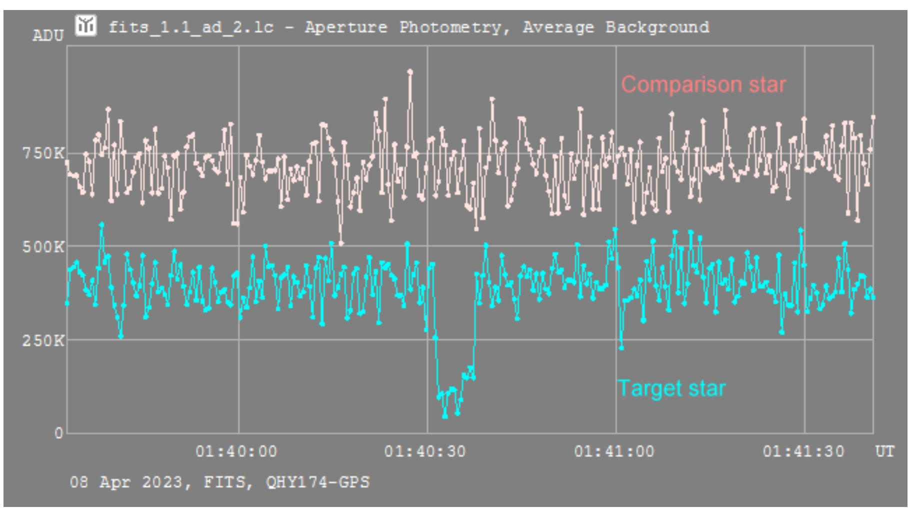

Figure 3: Tangra light curve of the obs1 station recording, showing a clear step on the reappearance from the occultation

In contrast to the station in Spain, this recording shows an occultation with a step-like transition at its end - an indication of the presence of a double star. The star UCAC4 402-083153 is not yet known to be a double star according to the catalogues (WDS, Interferometric Catalog, Gaia). The Occult4 database shows no previous occultations of this star. We used AOTA, part of the Occult4 software package, to extract the obs1 occultation times (Figure 4).

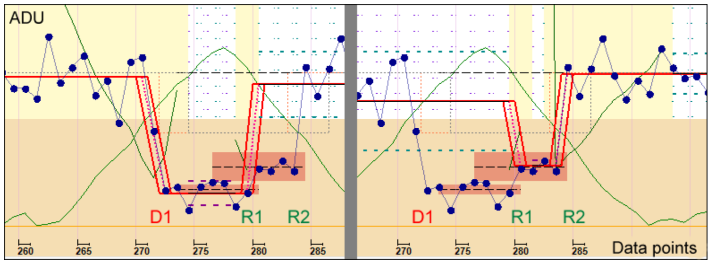

Figure 4: Station obs1 event times extraction with AOTA, for results see Table 1

The derived times are shown in Table 1 as well as the average light levels from the Tangra light curve (Figure 3).

Table 1. Station obs1 event times (AOTA) and average light levels (Tangra).

	D1	R1	R2
Time (UTC)	01:40:31.9 ± 0.3 s	01:40:36.3 ± 0.3 s	01:40:38.2 ± 0.3 s
Average light level (kADU)	404 > 90	90 > 163	163 > 404

3. Analysis

For the analysis, we used the appropriate tools of Occult4 in the standard method described by Herald [6]. Figure 5 and Table 2 show the results.

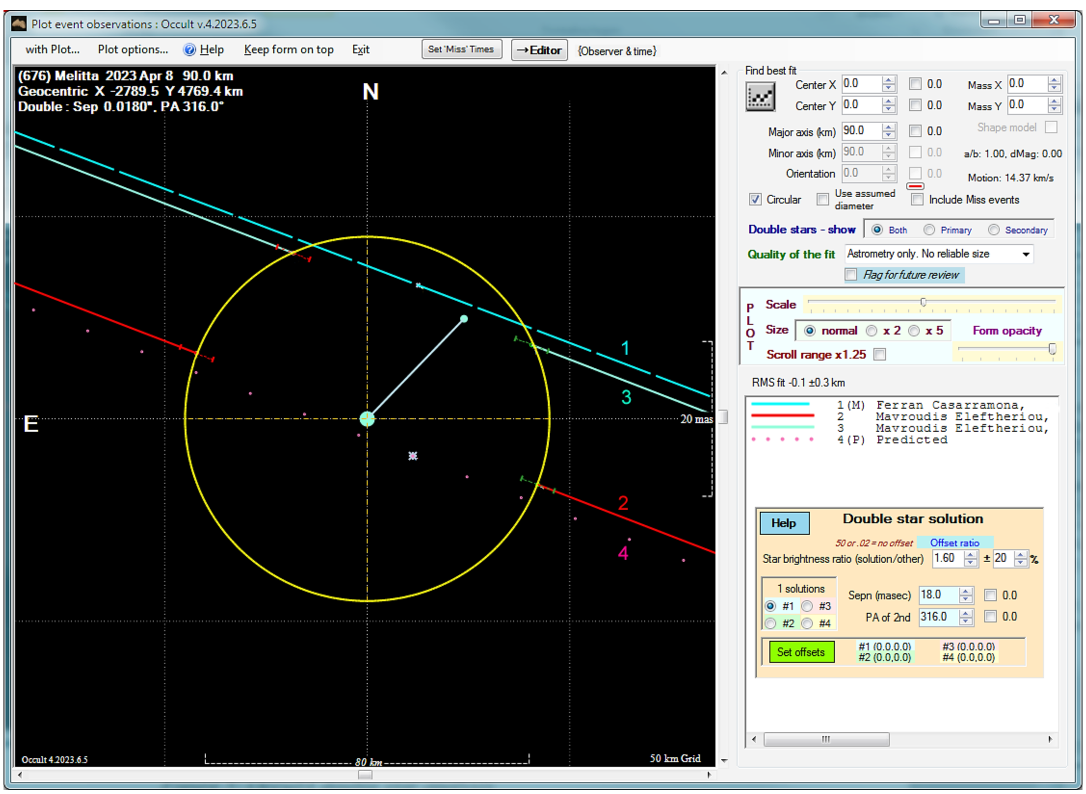

Figure 5: Occult4 double star analysis

The measured chord length of the main event was larger than the predicted diameter of the asteroid (83 ± 5 km). For this reason, we fitted the asteroid with a circle extending over the entire main chord (90 km), see Figure 5. In this way, we could exclude two of the 4 ambiguous double star solutions. Taking the obs2 station non detection recording into account, we can also exclude one of the two remaining solutions (Figure 6).

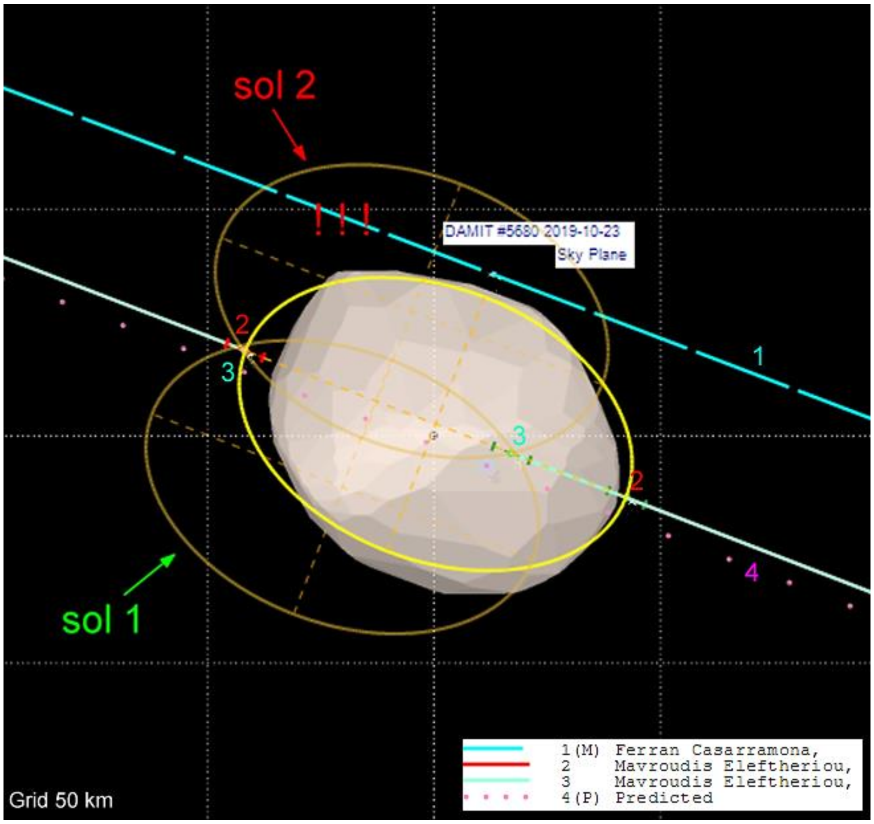

Figure 6: Exclusion of solution sol 2 using Occult4: Station obs2 (chord 1 (M) F. Casarramona) did not record a detection

Assuming a linear camera response of station obs1 recording, we estimated the magnitudes of the double star components using the average light levels given in Table 1. Due to the limited number of data points during the events, the magnitudes given are only rough estimates. Using the Occult4 magnitude calculator, we derived a magnitude of 13.0 for the main component and a magnitude of 13.8 for the fainter component.

4. Results

The derived double star characteristics are shown in Table 2. Further observations are necessary to improve the data.

Table 2. Double star characteristics.

Star	UCAC4	UCAC4 402-083153
	Gaia DR3 ID	4155332686530844800
	GCRS position at epoch 2023.2668	RA 18h 42m 17.933750s, Dec - 9° 36' 42.59475"
	G-mag	12.61
	Estimated diameter (Gaia)	0.04 mas
Double star solution	Separation	18.0 ± 0.1 mas
	Position angle	316.0° ± 0.4°
	Estimated component magnitudes A, B	13.0, 13.8

Acknowledgements

We acknowledge the developers of the software used in this work, especially D. Herald (Occult4), H. Pavlov (Tangra) and B. Anderson (PyMovie, PyOTE). This work has made use of data from the European Space Agency (ESA) mission Gaia (https://www.cosmos.esa.int/gaia), processed by the Gaia Data Processing and Analysis Consortium (DPAC, https://www.cosmos.esa.int/web/gaia/dpac/consortium) Funding for the DPAC has been provided by national institutions, in particular the institutions participating in the Gaia Multilateral Agreement. This research has made use of the Washington Double Star Catalog maintained at the U.S. Naval Observatory.

References

[1] Herald, D., Occult4, http://www.lunar-occultations.com/iota/occult4.htm
[2] International Occultation Timing Association (IOTA)/European Section (IOTA/ES), https://iota-es.de/index.html
[3] IOTA/ES Stellar Occultation Data Input System (SODIS), https://sodis.iota-es.de/
[4] Anderson, B., PyMovie/PyOTE, http://occultations.org/observing/software/pymovie/
[5] Pavlov, H., Tangra, http://www.hristopavlov.net/Tangra3/
[6] Herald, D., et al., 2009, "New double stars from asteroidal occultations, 1971 – 2008", JDSO, 6, 88-96, http://www.jdso.org/volume6/number1/herald.pdf

Speckle Astrometry of WDS 18181-0120

Elias Faughn[1], John Major[2], Paul McCudden[3]
[1] Glenwood Springs High School, Glenwood Springs, CO; faughnelias@gmail.com
[2] Bud Werner Memorial Library, Steamboat Springs, CO
[3] Colorado Mountain College, Steamboat Springs, CO

Abstract

Using data collected from the historic 60" telescope at the Mount Wilson Observatory on 2023.4873 (June 27, 2023), the position angle and separation of the multiple system WDS 18181-0120 were calculated using Speckle Tool Box and compared with previous measurements. The A and B members' mean position angle was found to be 196.46° and the mean separation was 0.1357". The position angle was within 5% of the extrapolated 6th Orbit Catalog estimate, and the separation was within 15%. Previous analysis indicates that the pair are gravitationally bound.

1. Introduction

Antoine Labeyrie first employed speckle methods to reduce the effect of atmospheric distortion and more accurately measure binary stars with separations below what is possible with visual observation (Labeyrie 1970). New techniques and software make it a valuable and accessible field for first-time researchers. The technique uses hundreds of "stacked" images from large aperture telescopes and specialized software to "freeze" atmospheric distortion, making it possible with image processing tools like Speckle ToolBox (Harshaw et al, 2017)) to measure the Position Angle (θ) and Separation (ρ) of close binary stars. This method is an accessible and powerful technique, even when using telescopes of modest aperture.

In June 2023, a team of researchers spent three days observing with the historic 60" telescope on Mount Wilson, using speckle techniques on some 53 targets chosen from a spreadsheet combining the WDS catalog with the 6th Orbit Catalog and Ephemerides (McCudden, et al; 2022). Targets were chosen with separations down to 0.1" separation.

From the resulting target list, WDS18181-0120 (HDS 2587AB, HD 168073, TYC 5098-553-1, SAO 142206, HIP 89680) was chosen for analysis. It is located within the constellation Serpens Cauda (Ser) and was first resolved by Hipparcos in 1991. It has an estimated period of less than 150 years, a distance of 227.79 parsecs (743.05 light years), an apparent magnitude of 7.78, and a spectral class of A0. It is a triple system, but for the purposes of this paper only the AB components were addressed as the C member is outside the parameters for our object selection. A sample speckle image from Mount Wilson Observatory (MWO) is featured in Figure 1. It is a Grade 3 system.

WDS18181-0120 was chosen for observation due to its close ρ (<1.0") separation and was therefore a good test of the techniques and the telescope's limits. The first measurements of the companion's ρ and θ were taken in 1991 by Hipparcos, with six subsequent observations being made, the last in 2019 by Tokovinin (see Table 1).

Our objective was to analyze the object using speckle interferometry and provide another observation, further establishing the orbital path of the companion and informing future estimates of its period.

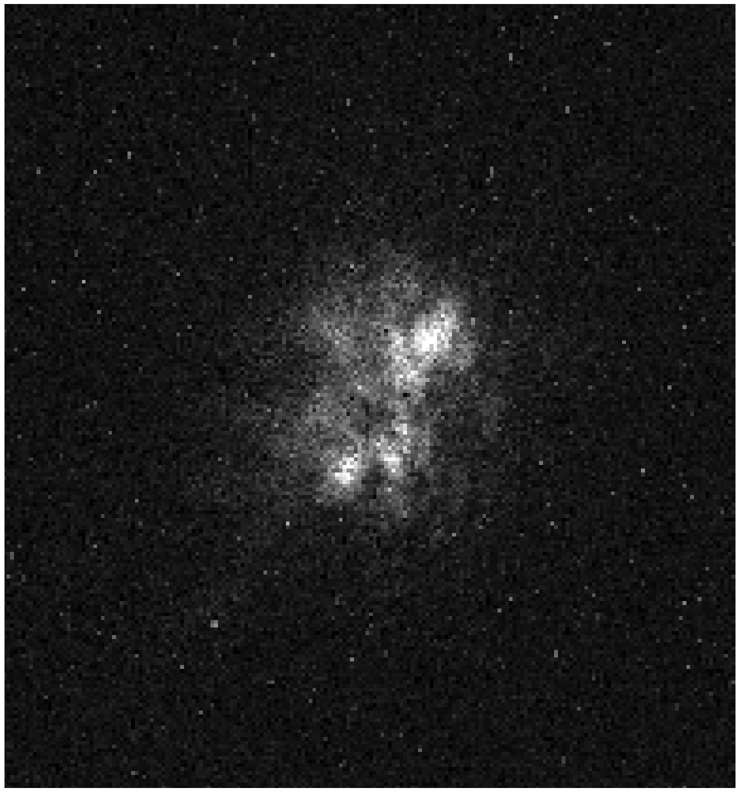

Figure 1. MWO Speckle Image of WDS 18181-0120 (0.02 second exposure).

Table 1. USNO Double Star data for WDS 18181-0120

Date	ρ (")	θ (°)	Observer
1991.25	0.133	350.0	Hipparcos (1997)
2013.643	0.086	318.7	Gili, R. (2022)
2014.3021	0.0677	329.1	Tokovinin, A. (2015)
2015.7357	0.0786	160.7	Tokovinin, A. (2016)
2017.5332	0.0920	172.7	Tokovinin, A. (2018)
2018.2347	0.0963	175.3	Tokovinin, A. (2019)
2019.5361	0.1031	181.4	Tokovinin, A. (2020)

2. Equipment and Methods

Data for WDS 18181-0120 was collected by the 60-inch telescope at the Mount Wilson Observatory on 2023.4873 (June 27, 2023). The telescope was used in its bent Cassegrain mode. 1000 images of 18181-0120 were taken with 20 millisecond exposure with a ZWO ASI 6200MM Pro camera fitted with a Astronomik ProPlanet 642 BP 2850002585 (IR pass) filter with a midpoint transmission at 750 nm. Five hundred images were also taken of HD 166991, using 20 millisecond exposures to be used as a reference star. The PlateSolve software was used to determine the pixel scale of .0306 arcseconds/pixel and rotation angle of 178.997° (Harshaw et al. 2017). Using these values, each of the three authors did five reductions each at both 128 and 256 pixel sized images using Speckle ToolBox (STB), then the mean ρ, mean θ, and standard deviation were calculated and are shown in Table 2.

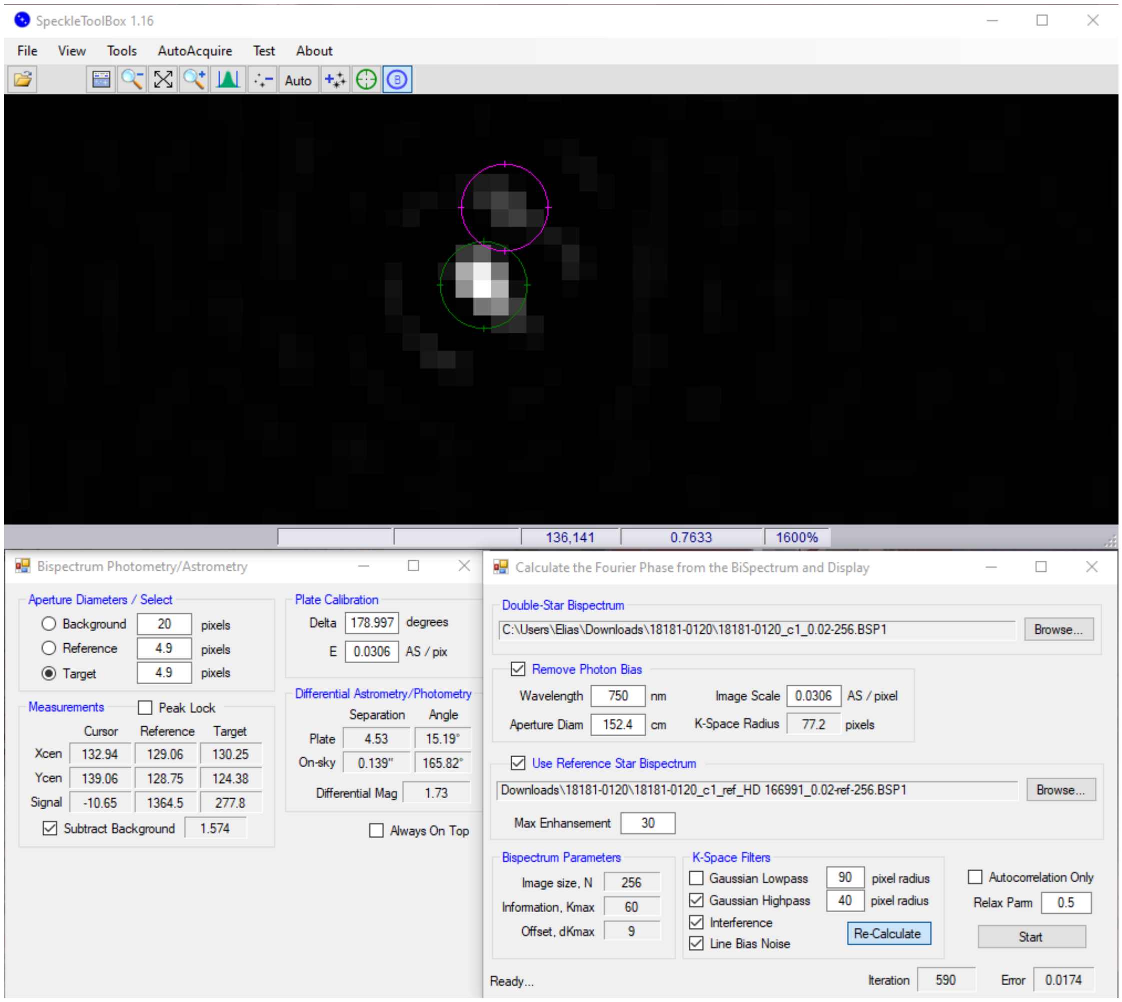

Figure 2: Screenshot of a 256 pixel STB data reduction on 18181-0120

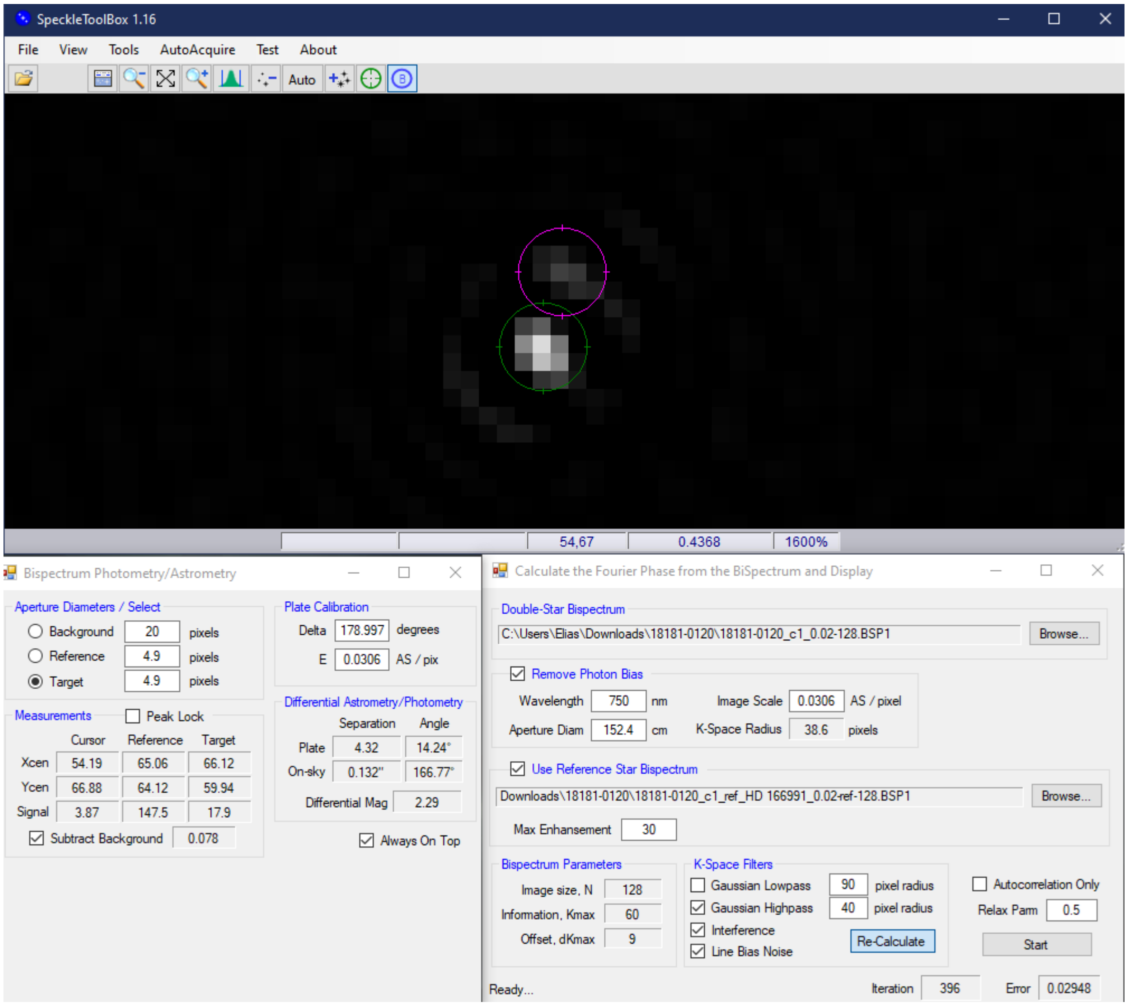

Figure 3: Screenshot of a 128 pixel STB data reduction on WDS 18181-0120

3. Data

The average values of ρ and θ calculated from the reductions (repeated 15 times) are shown in Table 2. The values for ρ and θ shown in columns 6 and 7 are extrapolated from the 6th orbit projections for 2023.4873. The standard error was calculated by dividing the standard deviation by the square root of the number of measurements.

Table 2. Average calculated values of ρ and θ for WDS 18181-0120 (HDS 2587) on 2023.4873

Pixels	ρ (")	Standard Error (")	θ (°)	Standard Error (°)	Extrapolated ρ (")	Extrapolated θ (°)
128	0.1357	9.28×10^{-4}	195.87	.876		
256	0.1357	1.57×10^{-3}	197.04	.806		
Average	0.1357	8.96×10^{-4}	196.46	.595	.118	195.61

The values found were plotted onto the orbital plot of WDS 18181-0120 from the Sixth Catalog of Visual Binary Stars displayed in Figure 4.

4. Discussion

The binary exhibits one discrepancy with respect to the 6th Orbit Plot in historical θ and ρ measurements, with the specific outlier being the Gili 2013 measurements (see Table 1 and Figure 4) (Gili et al. 2022). Subsequent observations by Tokovinin (2016, 2018, 2019, 2020) offer a more consistent orbital path. Our Mount Wilson Observatory observation is plotted as "MWO" in red.

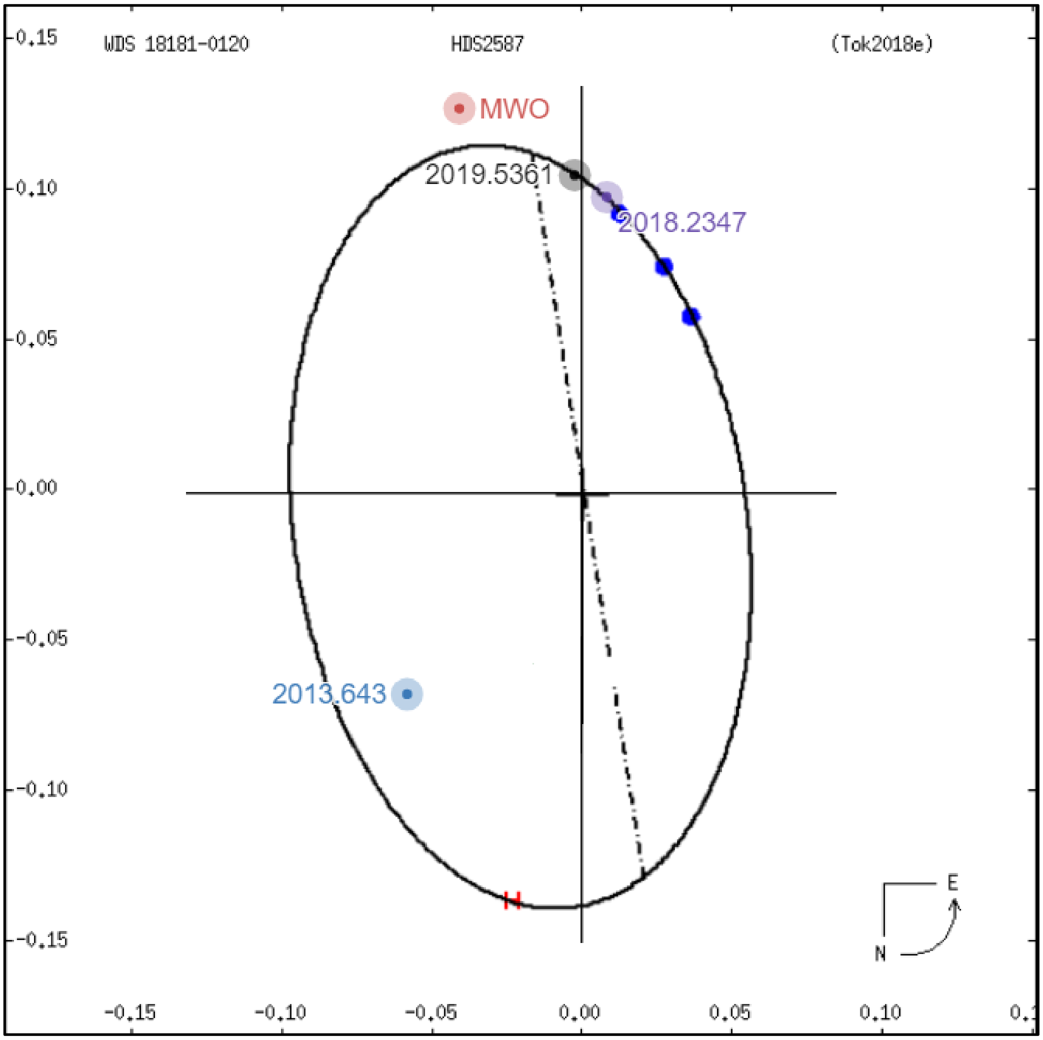

Figure 4: Plotting of Gili 2013, Tok 2018, Tok 2019, and the Mt. Wilson Observatory data onto the Sixth Catalog of Visual Binary Stars orbit for 18181-0120

Our observation fell outside the path displayed in the orbital plot of WDS18181-0120 from the Sixth Catalog of Visual Binary Stars (see Figure 4). The authors' measured θ of 196.46° differs by 4% from the interpolated value of 195.61°, and the observed ρ exceeds the interpolated value of 0.113" by 15%. If our observation is correct, it would mean the orbit is wider and the period somewhat longer than originally calculated.

5. Conclusions

Speckle techniques can accurately measure sub-100 mas separations and position angles, and represent a relatively accessible means to measure multiple systems. Remote access to large aperture, near professional-grade telescopes, coupled with free tools for Speckle Interferometry, have revolutionized binary star research. This combination of tools have made it possible for first-time researchers to contribute scientifically valuable binary star observations. Given the relatively short period of the WDS 18181-0120 system, and the small number of observations currently available, near-future observations could further establish the orbital path using the same methods. A larger number of observations could force the 6th Catalog of Binary Stars to revise the orbit.

Acknowledgements

This research has made use of the Washington Double Star Catalog maintained at the U.S. Naval Observatory.

This work has made use of data from the European Space Agency (ESA) mission Gaia (https://www.cosmos.esa.int/gaia), processed by the Gaia Data Processing and Analysis Consortium (DPAC, https://www.cosmos.esa.int/web/gaia/dpac/consortium). Funding for the DPAC has been provided by national institutions, in particular the institutions participating in the Gaia Multilateral Agreement.

This work used the SIMBAD service operated by Centre des Donnees Stellaires (Strasbourg, France), biblio-graphic references from the Astrophysics Data System maintained by SAO/NASA

This research made use of the Stelle Doppie database, maintained by Gianluca Sordiglioni.

Thanks to Rachel Freed and The Institute for Student Astronomical Research (https://www.in4star.org/) for helpful support.

Thanks to Russ Genet and Mark Harris for helpful comments.

References

Gili, R., Prieur, J.-L., Rivet, J.-P., Vakili, F., Scardia, M., Pansecchi, L., Argyle, R.W., Ling, J.F., Piccotti, L., Aristidi, E., Koechlin, L., Bonneau, D., Maccarini, L. & Serot, J. Measurements of visual double stars with PISCO2 at the Nice 76-cm refractor in 2013-2014. Astronomische Nachrichten, Volume 343, Issue 8, article id. e20224008 (2022) https://ui.adsabs.harvard.edu/abs/2022AN....34324008G/abstract

Harshaw, R., Rowe, D., & Genet, R. The Speckle Toolbox: A Powerful Data Reduction Tool for CCD Astrometry. . The Journal of Double Star Observations, Volume 13, Number 1, January (2017)

Hipparcos Catalog, ESA SP-1200, 1997 (incl. Hp photometry, vol. 10)

Labeyrie A. (1970) Attainment of Diffraction Limited Resolution in Large Telescopes by Fourier Analysing Speckle Patterns in Star Images. Astron. & Astrophys. 6, 85-87. https://adsabs.harvard.edu/pdf/1970A%26A.....6...85L

McCudden, P., Genet, R., Willie, E, Dugan, L., Risin, S. Known Binaries Excel Spreadsheet. The Journal of Double Star Observations, Volume 18, Number 4, October (2022).

Tokovinin, A., Mason, B.D., Hartkopf, W.I., Mendez, R.A., & Horch, E.P. Speckle Interferometry at SOAR in 2014. The Astronomical Journal, Volume 150, Issue 2, article id. 50, 17 pp. (2015). https://arxiv.org/abs/1506.05718

Tokovinin, A., Mason, B.D., Hartkopf, W.I., Mendez, R.A., & Horch, E.P. Speckle Interferometry at SOAR in 2015. The Astronomical Journal, Volume 151, Issue 6, article id. 153, 9 pp. (2016)

https://arxiv.org/abs/1603.07596

Tokovinin, A., Mason, B.D., Hartkopf, W.I., Mendez, R.A. & Horch, E.P. Speckle Interferometry at SOAR in 2016 and 2017. The Astronomical Journal, Volume 155, Issue 6, article id. 235, 11 pp. (2018). https://arxiv.org/abs/1804.10553

Tokovinin, A., Mason, B.D., Mendez, R.A., Horch, E.P. & Briceno, C. Speckle Observations and Orbits of Multiple Stars. The Astronomical Journal, Volume 158, Issue 4, article id. 167, 15 pp. (2019). https://arxiv.org/abs/1908.11445

Tokovinin, A., Mason, B.D., Mendez, R.A., Costa, E. & Horch, E.P. VizieR Online Data Catalog: 2019 SOAR speckle interferometry of binary stars (Tokovinin+, 2020). VizieR On-line Data Catalog: J/AJ/160/7. https://ui.adsabs.harvard.edu/abs/2020yCat..51600007T/abst

Robotic Speckle Interferometry Studies of WDS 04215-2544

R. Shane Christopher[1], S. Stephen Rajkumar Inbanathan[1], Mark Harris[2], Russell Genet[3], Rachel Freed [3] and Paul McCudden[4]

[1] The American College, Madurai, India
[2] Oorsprong Science, Roswell, Georgia, USA
[3] Eastern Arizona College, Payson, Arizona, USA
[4] Colorado Mountain College, Steamboat Springs, Colorado, USA

Abstract

The separation and position angle of the known binary system WDS 04215-2544 was measured using the Speckle Interferometry method with the fully robotic 1.0-meter Planewave Instruments telescope, located at the El Sauce Observatory in the Atacama Desert of Chile. The November 2022 results are Separation $\rho = 0.5 \pm 0.1$ and Position Angle Theta θ = 246.3° $\pm$ 0.3. These are in line with 6th Orbit Catalog (Mason et al 2023) ephemeris projections for 2022 and 2023.

Introduction

Binary Stars

Binary star systems provide a unique opportunity to study stellar evolution. By observing the interaction between the two stars in a binary system, astronomers can better understand how stars evolve, exchange mass, and transfer energy (Tauris & Heuvel 2023). This knowledge contributes greatly to modern astrophysics.

Astronomers identify and catalog binary star systems through various surveys and observations. These systems are discovered through direct imaging, spectroscopic measurements, photometric variations, or astrometric techniques. Each binary is classified by its properties, such as spectral type, component star separation, period, eccentricity, and component masses. Photometric observations can track brightness, spectroscopic observations can measure radial velocities and determine orbital parameters, and high-resolution imaging can resolve the individual stars within the system.

Known Binary Stars Project

The Known Binary Stars project (Genet et al 2023) obtained observations of WDS 04215-2544 using a robotic 1.0-metre Planewave Instruments telescope, one of the largest aperture research telescopes currently in production. Located at the telerobotic El Sauce Observatory in Chile's Atacama Desert, this telescope is one of a growing array of remote access telescopes in one of the best astronomic viewing locations on Earth.

Figure 1: Left: Fully automatic El Sauce Observatory powered with solar panels. Right: The 1.0-meter Planewave Instruments robotic telescope used for these studies is located in one of the enclosures.

The purpose of the overall project was to determine the accuracy, precision, and limitations of robotic astrometry for 1-meter telescopes. Binary star data from the Sixth Catalog of Orbits of Visual Binary Stars (Matson et al 2023) was used as the starting point. A spreadsheet list (McCudden et al 2022) was filtered to obtain observable candidates, and a number of these were observed in the fall of 2022. WDS 04215-2544 was selected from the observed binaries based on a review of the orbital plots of past observations.

Speckle Interferometry

Speckle interferometry (Labeyrie 1970) is a technique used to study binary or multiple stars using high magnification. It involves obtaining many short-exposure images and analyzing the changes or "speckles" caused by atmospheric turbulence, as shown in Figure 2.

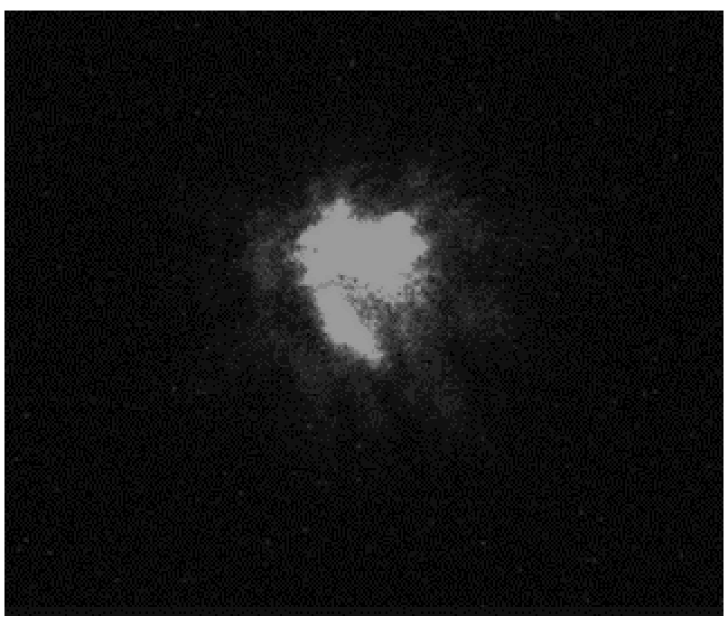

Figure 2. Example of a short exposure speckle image of WDS 04215-2544.

The speckle analysis process includes collating thousands of such speckle images and using multiple Fourier transformation steps and correlation to re-construct images. This process effectively removes much of the atmospheric turbulence of an Earth-based telescope system. The re-construction of the optical image comes close to reaching the optical diffraction limit of the telescope, given the telescope's aperture and camera system configuration, with most of the atmospheric turbulence effect removed by the special mathematical processing. The Speckle Toolbox software developed by Dave Rowe (Harshaw et al. 2017) was used to process the speckle images. Astrometric measurements of key binary star parameters were produced including component separation (Rho) and position angle (Theta).

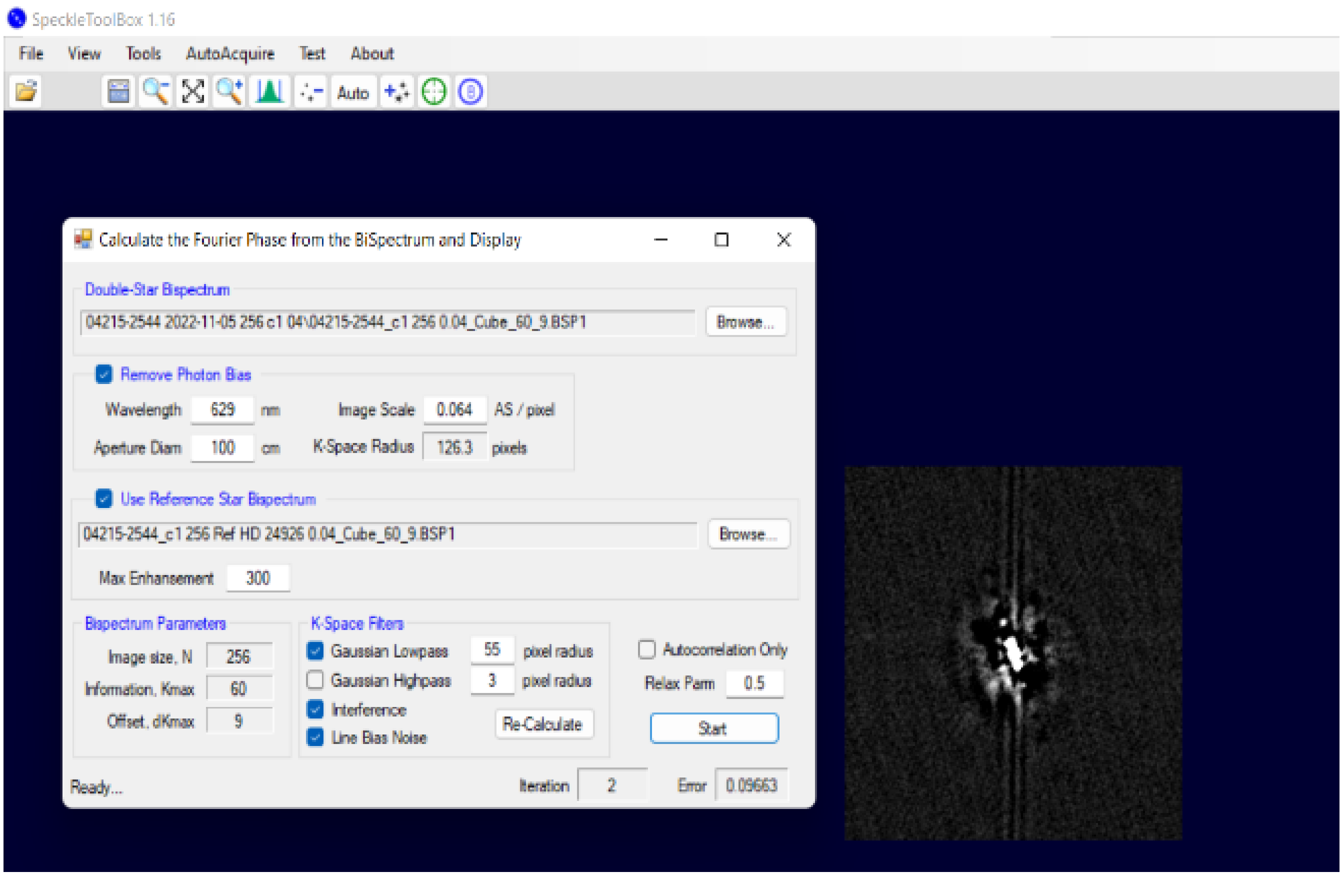

Figure 3: Bi-spectrum Phase Reconstruction of WDS 04215-2544 using the Speckle Toolbox enables special processing of high-resolution imaging at high magnification.

The main steps and associated equipment involved in the speckle interferometry process are as follows:

FITS Cube: A high-speed camera is used to capture short exposure images of the binary star system. These images document the continuous changes caused by air turbulence. The software pulls these images into an overall matrix of all the FITS speckle images.

Bispectrum Processing: Double Fourier transform and correlation processing is performed on the acquired speckle images to eliminate the atmospheric turbulence effects, including deconvolution using a single reference star automatically selected during the speckle observing session (Genet et al 2023).

Bispectrum Phase Reconstruction: Reconstruction step uses an interactive procedure to reproduce the image.

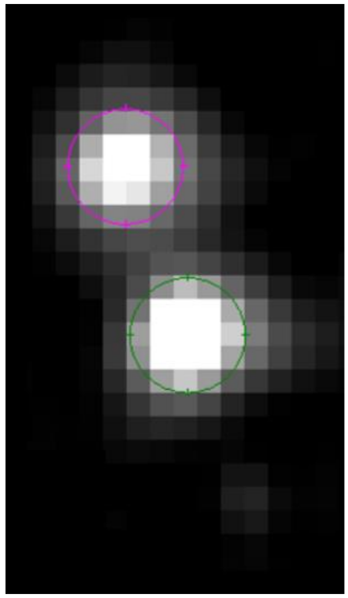

Figure 4. Final Phase Reconstruction of WDS 04215-2544 showing the Primary A star closest to the middle of the image and the Secondary B star to the top left. A small faint artifact of the Speckle Interferometry process is shown towards the bottom right.

WDS 04215-2544

The spectral class of a star is determined by its surface temperature and spectroscopy which categorizes stars into different types represented by letters (Cannon. 1895). The spectral class of the components of a binary star system can vary significantly. Each component star can have its own spectral class.

WDS 04215-2544 was discovered in 1879 by Sherburne Wesley Burnham with a 0.2-meter telescope equipped with a micrometer. Both component stars (Table 1) are F-type stars, and the binary currently has a projected orbital period of 81 years. The key system and component parameters are as follows (Matson et al 2023):

Table 1: Key parameters of WDS 04215-2544

WDS 04215-2544	Value	Spectral Class	Magnitude	Rho ρ "	Theta θ^0
6th Orbit 2022.0 Projection				0.487	243.6
6th Orbit 2023.0 Projection				0.5	246.4
Primary Star		F2V	7.26		
Secondary Star		F2V	6.56		
Constellation	Eridanus				
Discoverer	BU 744AB		Alternative Names	HIP 20347	
RA (Decimal)	65.38038		Tycho 2 6460-03129-1	HD 27710	
Dec (Decimal)	-25.72844		CP-26 520	HR 1374	
Distance	191.64 ly		CD-26 1642	ADS 3159	

Instrumentation, Automation, and Methods

Speckle interferometry observations of WDS 04215-2544 were obtained with a PlaneWave Instruments PW1000 telescope with a 1-meter aperture, using the Known Binary Project configuration set up by Hardy et al (2023). The filters (Sloan g', r', z', and i' filters) and the QHY600MM-Pro CMOS camera are installed on their own speckle interference port. The focal length of 12,038 mm provides an image scale of 0.065 arcseconds/pixel. The AltAz telescope's image is stabilized with a field counter rotator that maintains a nearly constant direction with respect to celestial north. Small night-to-night deviations require a plate solution each night to determine the exact camera angle for that night. Software includes Night Imaging 'N' Astronomy (NINA), PWI-4 telescope control software, and a new NINA Speckle Interferometry Plug-in developed by Hardy and Bewersdorff (Hardy et al 2023). A full-frame image is created so that a region of interest (ROI) can be clearly defined around the target. A plate solution from the full frame is used to obtain the plate scale and camera angle for subsequent analysis. The NINA speckle plugin automatically calculates the optimum exposure time for images based on stellar magnitude. After taking 500 speckle images of the target star, the telescope moves to a nearby automatically selected reference star and repeats the whole process; taking 300 images with the same ROI size, before heading to the next target.

Data

Past Observations

An amateur astronomer, Robert Burnham was a court recorder in Chicago and searched for new double stars in his spare time. Almost 70 observations of 04215-2544 were made exclusively by refracting telescopes with micrometers between Burnham's discovery in 1879 and 1975. The majority of these observations were made by W. S. Finsen and W. H. van den Bos on the 0.7-meter Union Observatory refractor in Johannesburg, South Africa, and J. G. Voute on the 0.6-m refractor at Bosscha Observatory in Lembang, West Bangdung Regency, West Java. These observations are shown with + in Figure 1.

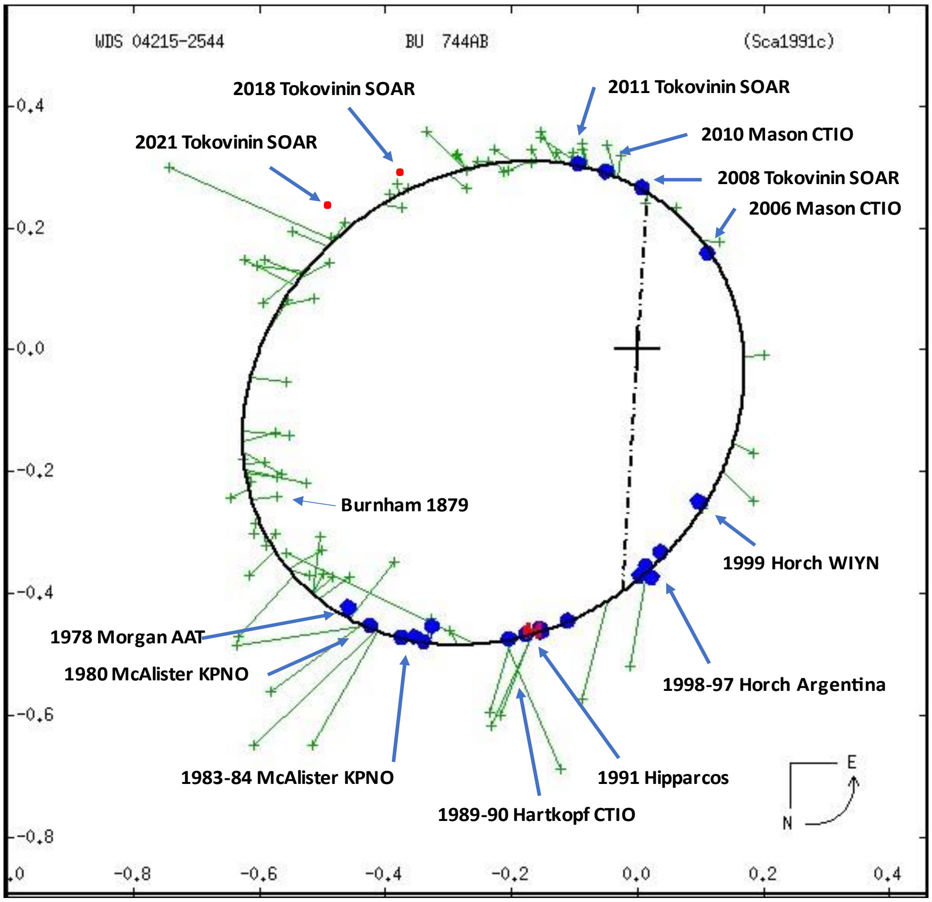

Figure 5: Orbital plot from the Sixth Catalog of Orbits of Visual Binary Stars (Matson et al 2023). Marco Scardia (1991), a French astronomer, calculated the orbit. We have added annotations and the two dot observations in the top left of Figure 5, using data from the Washington Double Star Catalog (2023) supplied to us by Rachel Matson.

The first speckle interferometry measurement of this binary was made in 1978 by B. L. Morgan et al (1982) from the Imperial College of Science and Technology in London. Their observations were made on the 3.9-meter Anglo Australian telescope at the Siding Spring Observatory in Australia. When it was commissioned in 1974, it was the largest telescope in the southern hemisphere. Observations were made with a high-speed film camera, while reduction was via a laser that illuminated each of the 500 or so frames.

Figure 6: The 3.9-meter Anglo-Australian telescope at the Siding Spring in Australia. It was one of the last large telescopes with an equatorial mount. Later large telescopes utilized alt-az mounts as they are much more compact.

The next speckle observations were obtained in 1980 by Harold McAlister et al (1983) with observations made on 35mm Tri-X film with a high-speed camera while riding in the Cassegrain focus of the 4.0-meter telescope at Kitt Peak National Observatory (KPNO). Similar observations were made in 1989 and 1990 by William Hartkopf et al (1993) with the 4.0-meter Victor Blanco telescope at Cerro Tololo Interamerican Observatory (CTIO) in the Chilean desert. These two 4.0-meter telescopes are twins. Their design and construction were supervised by David Crawford, Assistant Director of KPNO.

The Hipparcos astrometric space telescope was launched by the European Space Agency in 1989 and operated until 1993. It took four years to analyze the data with what was then the world's largest computer complex. The result was the *Hipparcos Catalog* (1997) which contained precise astrometric data (including distances) of over 100,000 stars. One of these was WDS 04215-2544.

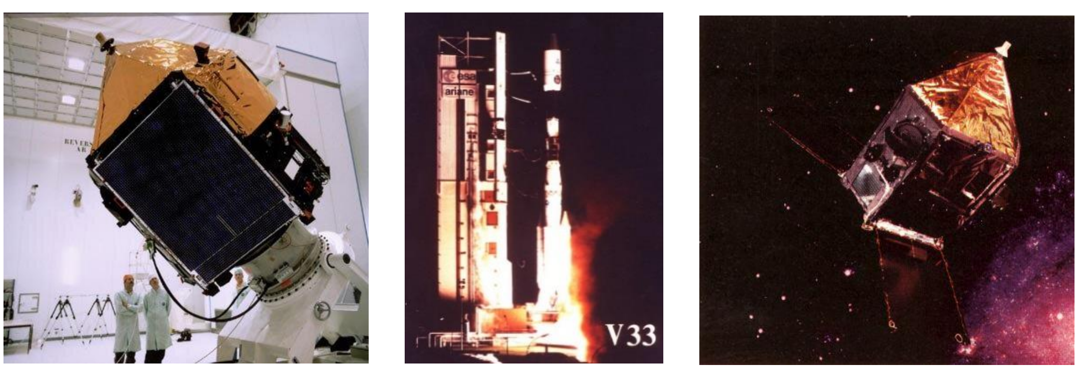

Figure 7: The Hipparcos space telescope, which was launched in 1989, obtained precise astrometric measurements of over 100,000 stars.

Elliot Horch made speckle observations in Argentina in 1998-97 and in 1999 with his advanced speckle camera on the 3.5-meter WYIN (Wisconsin, Yale, Indiana, National Optical Astronomy Observatories) located on Kitt Peak (Horch et al.). This pioneering telescope, devised by R. Kent Honeycutt at Indiana University, utilized an alt-az mount and had a thin primary mirror that was warped into exact shape by 66 computer-controlled actuators.

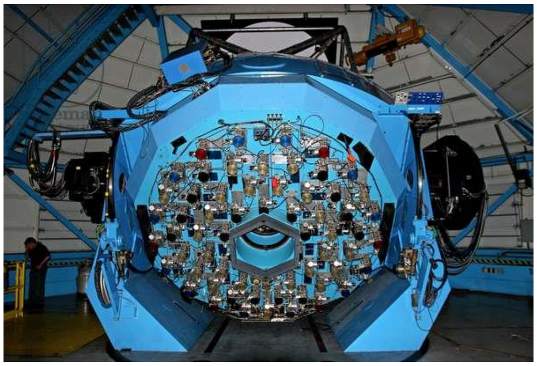

Figure 8: The rear of the WYIN telescopes is covered with actuators that shape the mirror. The octagon-shaped dome is small for a telescope this size thanks to the alt-az mount and short-focus primary mirror.

In 2006, Brian Mason et al (2009) used the 4.0-meter telescope at Kitt Peak National Observatory to observe WDS 04215-2544. In 2008, Andre Tokovinin made his first speckle interferometry observation of this binary with the 4.1-meter Southern Astrophysical Research (SOAR) telescope in Chile, located near CTIO. Tokovinin's initial SOAR speckle observations were made with the same, small, front illuminated Andor Luca emCCD camera used by several astronomers on much smaller telescopes.

Figure 9: The Southern Astrophysical Research (SOAR) telescope in Chile.

Further speckle interferometry measurements were made in 2010 by Hartkopf et al (2012) and in 2011 by Tokovinin et al (2012). The last two speckle measurements were made in 2018 by Tokovinin et al (2019) and in 2021 by Tokovinin et al (2022). These observations are shown in the top left-hand side of the original plot (Figure ~~1~~5).

Our New Observation

The equipment and procedures used to obtain our observation have been described in Section 2 and in much detail by Hardy et al. The image in Figure 10 is a full frame, 60-second exposure with the Sloan Red r' filter. Because of the high magnification the field is small, just 10.37 x 6.92 arc-min. The plate scale and plate rotation angle were obtained through a long exposure image analyzed with the Plate Solve application developed by Dave Rowe (Harshaw et al period 2017). As shown in Figure 10, the stars were matched to catalogues, resulting in an image scale of 0.0650″/pixel and a plate rotation angle of 266.656°.

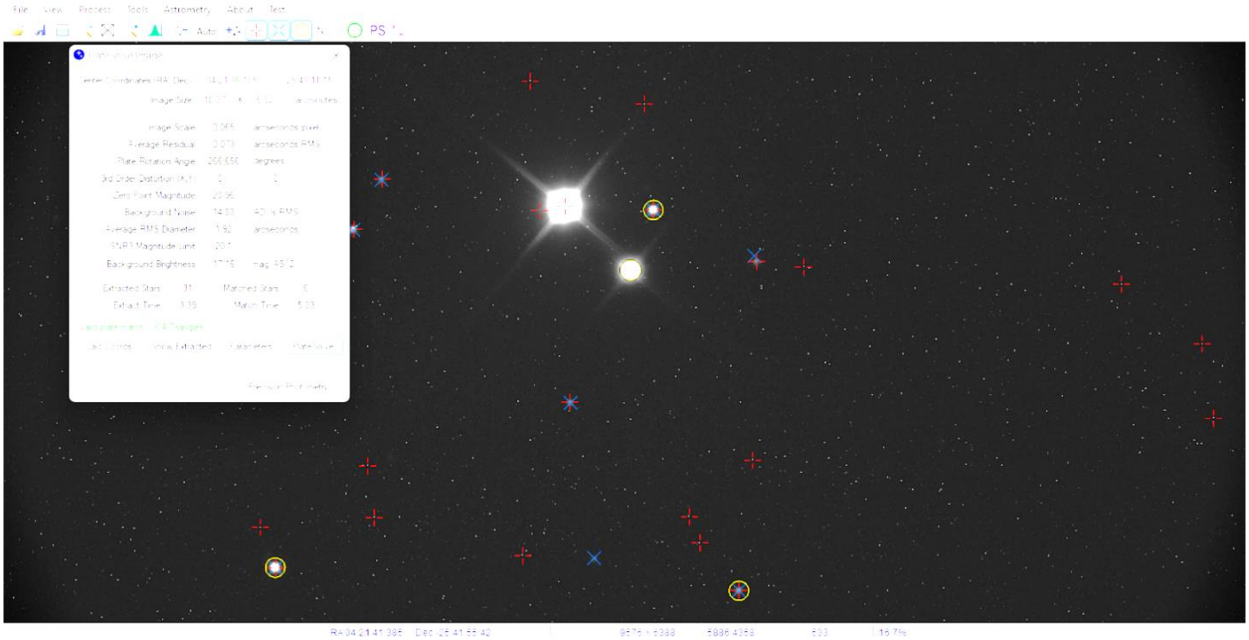

Figure 10: Plate solution for WDS 04215-2544, BU 744AB obtained 6 November 2022. The seeing (RMS FWHM Diameter) at that time was 1.92 arcseconds. The bright sky background was 17.16 mag per square arc second.

The final stage of the Speckle Interferometry process is running the bispectrum phase reconstruction or data reduction part of the process, as shown in Figure 11. Figure 11 also shows the measurement results by applying the Astrometry tool in the Speckle Toolbox, with centroids being applied around the component stars and a reference background area. Figure 12 shows the result tables of the measured parameters of the Astrometry Tool (left-hand side), along with the Reconstruction parameters used on the right-hand side.

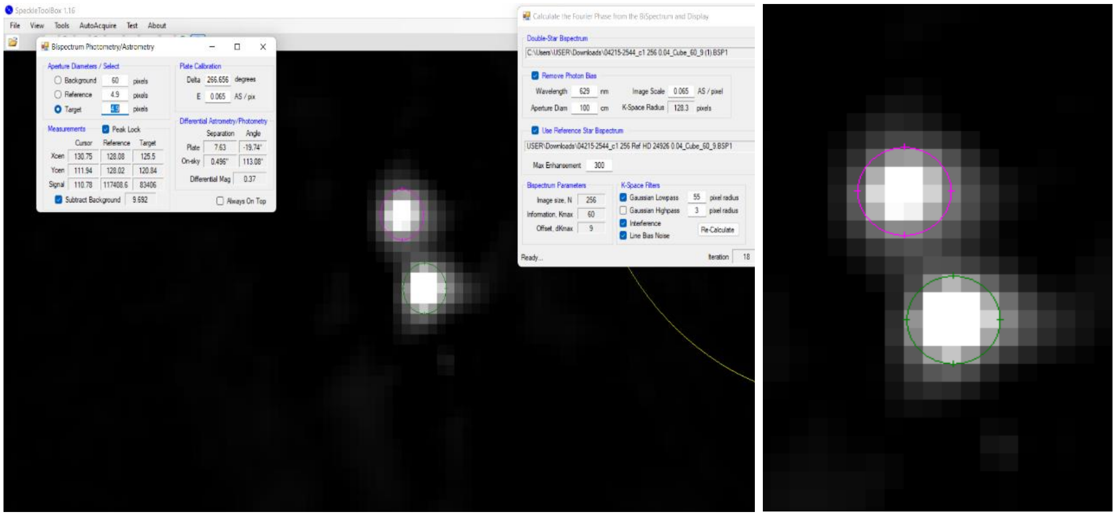

Figure 11: The Speckle Toolbox bi-spectral data reduction provides control and feedback to the user, as well as monitoring of integration and effective bi-spectral convergence results during recovery (Hardy et al 2023) The false autocorrelation lobe disappears. Image on right-hand side is after 18 iterations of the process.

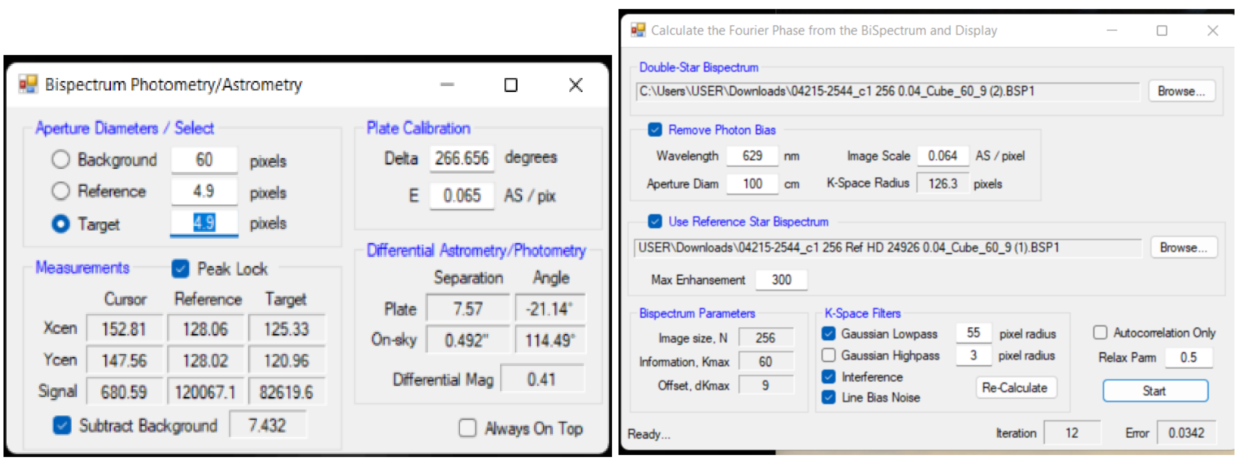

Figure 12: The measurement window provides inputs for calibration and measurement apertures, yielding astrometry and photometry results. The primary, secondary and background apertures seen above were manually centered on the image, guided by star centroid indicators when "peak lock" was checked.

Our repeated manual measurements of the final bispectrum image resulted in the following results for Rho and Theta as shown in Table 2.

Table 2: Our New Observation Results for Rho and Theta

	Measurements					Range		
Researcher	**Ref Pixels**	**Target Pixels**	**Rho "**	**On-Sky Theta**	**Theta °**	**Stat**	**Rho "**	**Theta °**

RSC	4.9	4.9	0.489	113.72	246.28	N	4	4
RSC	4.9	4.9	0.492	114.49	245.51	Mean	0.49	246.3
RSC	4.94	4.9	0.496	113.08	246.92			
RSC	4.9	4.9	0.497	113.53	246.47			

Orbital Period

Using much of the recent Speckle data, including our new observation, we re-calculated the estimated orbital period going as far back as we could in whole orbits from the most recent measurement epochs, measuring the epoch back in time where the position angles are next matched. The mean of these results provided a new estimated period of 80.3 ± 0.5 years, slightly shorter than the current 6th Orbit catalog's value of 81.0 years**.**

Discussion

Our new Rho and Theta measurements plural are in line with the 6th orbit catalog projections as shown in Table 3. After adding our 2022 speckle interferometry observation, shown as the X in the top left of Figure 13, we calculated a possibly slightly shorter orbital period using the latest speckle interferometry results.

Table 3: New Observation Measurements compared with 6th Orbit Projections

Measurement Source	**Theta °**	**Rho "**
6th Orbit Projected Ephemeris for 6th Nov 2023	246.0	0.5
Our New Observation Result on 6th Nov 2023	246.3+/0.3	0.5+/0.1

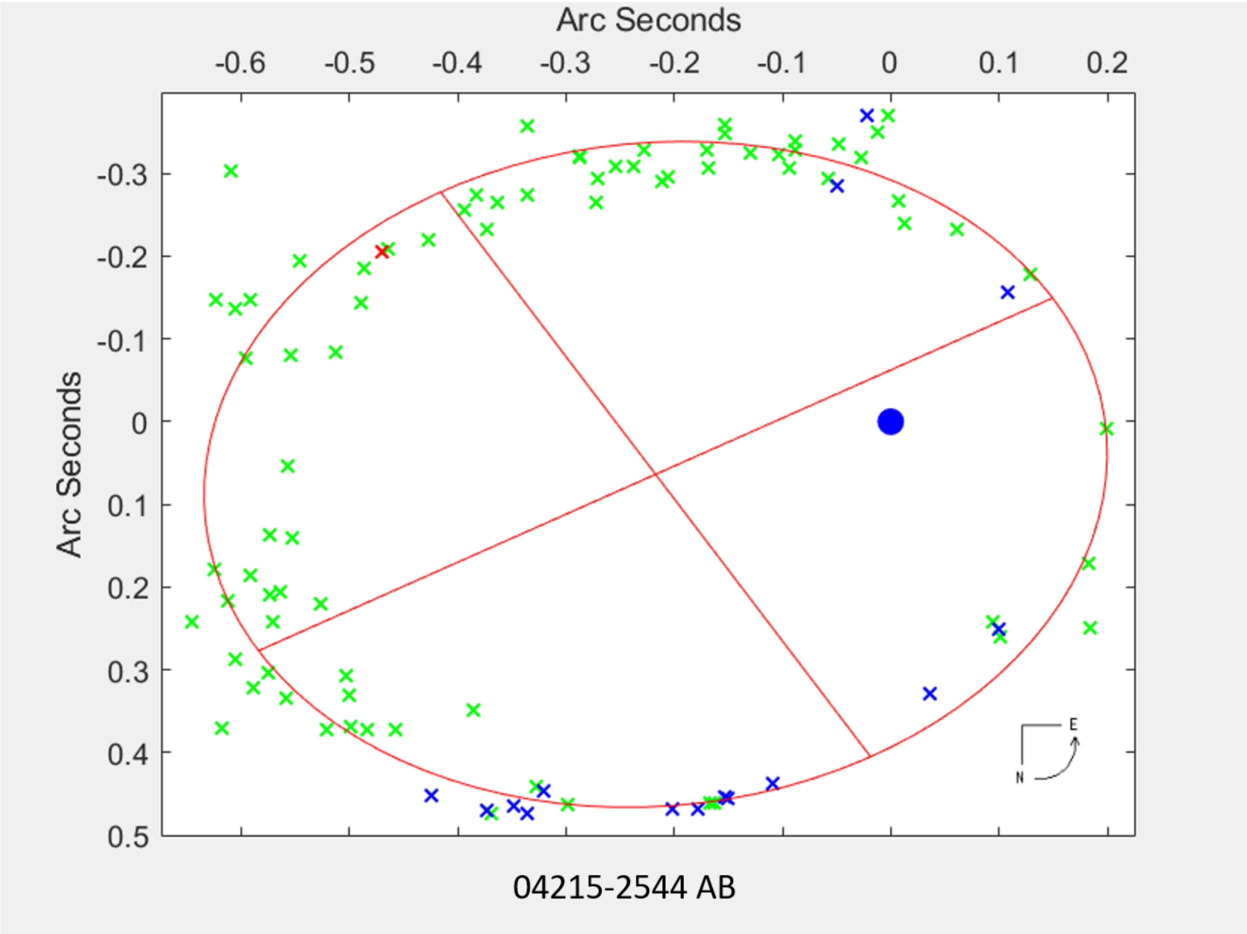

Figure 13: Our observation, shown as X is near the top left of the image close to the ellipse.

Conclusion

In conclusion, our new Rho and Theta measurements are very close to the 6th Orbit Catalog projections, even though the orbit might be slightly shorter overall than older historical data has previously shown.

Given that the measurement results are so close to the 6th Orbit Catalog projections, and the high signal to noise ratio in the reconstructed images, there are clear advantages in using speckle interferometry to measure binary stars with smaller telescopes.

Given the relatively short period of this star system it will be well worth repeating images over the coming years to provide further improved projections of the orbital period.

Acknowledgements

We are grateful to Mike Selby for granting us access to the 1.0-meter telescope and the El Sauce Observatory and for keeping the telescope in good shape. We also acknowledge the United States Naval Observatory for supplying us with the past data on WDS 04215-2544.

References

Burnham, S. W. 1887. Pub. Lick Obs 1, 24,45.

Cannon A.J, 1895, Archive of Harvard University Research Papers https://hollisarchives.lib.harvard.edu/repositories/4/resources/4134

Genet, R. Bewersdorff, L., Hardy, N., Harris, M., Armstrong, J., Wholly, R., Freed, R., McCudden, P., Calvin, M., Terrazas, M., Rajkumar Inbanathan, S., S., Christopher, S., Rowe, D., Dixon, S., Smith T., Giavarini, C., , Davis, M., Snyder, R., Wasson, R., Buchheim, R., Boyce, P., and Boyce, G.. Known Binary Speckle Interferometry with a 1.0-m Telescope in Chile, *Proceedings for the 42nd Annual Conference of the Society for Astronomical Sciences, 2023*

Hardy, N., Bewersdorff, L., Rowe, D., Genet, R., Wasson R., Armstrong, J., Dixon, S., Harris, M., Smith, T., Freed, R., McCudden, P., Rajkumar Inbanathan S., S., Davis, M., Giavarini, C., Snyder, R., Wholly, R., Calvin, M., Cotton, S., Carter, J., Terrazas, M., Christopher R., S., Kumar A., A., Naskath H., S., and Ronald Rabin A., M. 2023, Automated Speckle Interferometry of Known Binaries, *Journal of Double Star Observations* Vol 19 No 2

Harshaw R., Genet R, Rowe D. The Speckle Toolbox: A Powerful Data Reduction Tool for CCD Astrometry. 2017 Journal of Double Star Observations, vol.13, no. 1, p. 52-67.

Hartkopf, W.I., Mason, B.D., Barry, D.J., McAlister, H.A., Bagnuolo, W.G., & Prieto, C.M. 1993. AJ 106, 352.

Hartkopf, W.I., Mason, B.D., Tokovinin A., 2012. AJ 143, 42.

Hipparcos Catalog, ESA SP-1200, 1997.

Horch, E.P., Robinson, S.E., Meyer, R., van Altena, W., Ninkov, Z., & Piterman, A. 2002. AJ 123, 3442.

Labeyrie A. (1970) Attainment of Diffraction Limited Resolution in Large Telescopes by Fourier Analysing Speckle Patterns in Star Images. *Astron. & Astrophys.* 6, 85-87.

Mason, B.D., Hartkopf, W.I., Gies, D.R., Henry, T.J., & Helsel, J.W. 2009. *AJ* 137, 3358.

Matson, Rachel, Stephen Williams, William Hartkopf, and Brian Mason. 2023. Sixth Catalog of Orbits of Visual Binary Stars. U.S. Naval Observatory, Washington, DC. http://www.astro.gsu.edu/wds/orb6.html

McAlister, H.A., Hendry, E.M., Hartkopf, W.I., Campbell, B.G., & Fekel, F.C. 1983. *ApJS* 51, 309

McCudden, Paul, Russell Genet, Evan Willie, Liam Dugan, and Sophia Risin. 2022. Known Binaries Excel Spreadsheet. Journal of Double Star Observations, 18, 364.

Morgan, B.L., Beckmann, G.K., Scadden, R.J., & Vine, H.A. 1982. *MNRAS* 198, 817.

Rachel A. Matson, Stephen J. Williams, William I. Hartkopf & Brian D. Mason. 2023. Sixth Catalog of Orbits of Visual Binary Stars. U.S. Naval Observatory, Washington, DC.

Scardia, M. 1991. *Inf. Circ.* 114, 1.

Tauris T.M. and van der Heuvel E.P.J., Physics of Binary Star Evolution. From Stars to X-ray Binaries and Gravitational Wave Sources. ISBN: 9780691179087. Princeton University Press, 2023

Tokovinin, A., Mason, B., & Hartkopf, W. 2010. AJ 139, 743.

Tokovinin, A., Mason, B. D., Hartkopf, W. I. Speckle interferometry at SOAR in 2012 and 2013. 2014, AJ, 147, 123. ArXiv:1403.4970

Tokovinin, A., Mason, B.D., Mendez, R.A., Horch, E.P. & Briceno, C. 2019. AJ 158, 48.

Tokovinin, A., Mason, B.D., Mendez, R.A. & Costa, E. 2022. AJ 164, 58.

Observation and Investigation of 8 Physical Doubles in the Washington Double Star Catalogue

MD Dilshad Hossain, Siddharth Padakanti, Mahafujul Hamid Ananda, Kayla Oltman, Annie Chikelu, Yuqiao Zhang, Anaya Elias, Harris Massroor

University Of Saskatchewan, Saskatoon, Saskatchewan; mdh413@usask.ca

Abstract:

Eight physical double stars with separations between 8" and 20" were selected from the Washington Double Star Catalogue. Using the Afterglow tool, the position angles and separations were measured. The results were combined with data from GAIA DR3 to make orbital plots.

Introduction:

There were several constraints on the stars our team was able to study. During the months when this study was done, stars with a right ascension between 5 and 15 hours, and separation of 8'' and 20'' were observed. The target stars for this study were chosen with similar parallax and proper motion i.e., Physical Double Stars. To avoid pixel saturation, stars with a magnitude between 9 to 18 and relatively similar brightness (delta < 5) were chosen. This allowed us to get appropriate exposure time to capture both the primary and secondary stars. Using these constraints in *Stelle Doppie* for WDS Catalogue search, eight stars were selected. Those stars were: SKF2037 (WDS 05104+6020), GWP1113 (WDS 08557-1531), CRB 67 (WDS 05017+3324), HJ 3717 (WDS 05020-3935), KPP2106 (WDS 05037-7333), SKF2476 (WDS 05243-2149), UC 102 (WDS 07057+4827) and KPP992 (WDS 05005-6238).

Using ALADIN software, data from the SIMBAD data base, the VIZIER service, the GAIA DR3 data base, and other archives, the B-R and absolute Gmag, the luminosity, mass and temperature of the stars were estimated.

Instruments Used:

For our observations, six telescopes from Skynet Robotics Telescopes Network (SRTN) were used. Telescopes Prompt2 and Prompt5 in the Cerro Tololo Inter-American Observatory, Morehead telescope in Morehead, PROMPT-MO-1 in the Meckering Observatory, and finally, Prompt-USASK, USASK-14 in the Sleaford Observatory were used. All our observations were taken from Prompt2, Prompt5, PROMPT-MO-1, Prompt-USASK telescopes. The PROMPT2, PROMPT5, and Prompt-USASK telescopes had 0.4m apertures and 4,600mm focal lengths. The Morehead telescope has an aperture of 0.6m and focal length of 8600mm.The USASK-14 has an aperture of 0.4m and focal length of 3900mm. The images were taken with a 16-bit CCD with a flux range of 0 – 65353. A Hithru filter was used to allow long exposures to capture as many stars as possible. Five images with a dithering of 3X3 with 10 seconds spacing were taken for each pair of stars. Dithering helps get rid of photons of light lost on dead pixels on the lens by a controlled movement of the mount between successive exposures that very slightly modifies where photons land on the sensor on a pixel-by-pixel basis. Apart from Sleaford Observatory, all the Observatories are in barren locations and high altitudes. This allows the images to be less damaged by atmospheric *seeing* and pollution.

Measurements:

The measurements for this study were conducted using the Afterglow tool provided by SRTN. After ensuring that the images were not saturated, the images were stacked, and the separations and position angles were determined using the Afterglow tool. From which, we get a mean position angle and separation. The observed data is noted and shown in Table 2.

The resultant Proper Motion (rPM) was calculated following the method shown in Harshaw, 2016. rPM helps us understand if the stars share a common proper motion. rPM less than 0.2 is considered Common Proper Motion (CPM), between 0.2 and 0.6 is Similar Proper Motion (SPM) and above 0.6 is considered Different Proper Motion (DPM).

Table 1: Parallax and proper motion data for each system, including the proper motion ratio (rPM) calculated as the ratio of the PM difference vector magnitude to the magnitude of the longer of the component PM vectors.

System	Parallax of Primary (mas)	Parallax of Secondary (mas)	Proper Motion of Primary (mas/yr)	Proper Motion of Secondary (mas/yr)	rPM
SKF2037 (WDS 05104+6020)	11.47 ± 0.02	10.49 ± 0.01	(54.70 ± 0.01, -82.44 ± 0.01)	(54.58 ± 0.01, -80.78 ± 0.01)	0.017 (CPM)
GWP1113 (WDS 08557-1531)	4.57 ± 0.09	4.49 ± 0.17	(-74.71 ± 0.09, -4.46 ± 0.09)	(-75.35 ± 0.15, -7.98 ± 0.16)	0.047 (CPM)
CRB 67 (WDS 05017+3324)	13.28 ± 0.02	13.34 ± 0.05	(24.72 ± 0.03, -53.03 ± 0.2)	(26.60 ± 0.06, -53.56 ± 0.04)	0.033 (CPM)
HJ 3717 (WDS 05020-3935)	2.63 ± 0.01	2.63 ± 0.01	(25.10 ± 0.02, 18.62 ± 0.02)	(25.05 ± 0.01, 18.64 ± 0.01)	0.033 (CPM)
KPP2106 (WDS 05037-7333)	3.35 ± 0.01	3.38 ± 0.04	(5.22 ± 0.01, 36.25 ± 0.02)	(5.61 ± 0.05, 35.50 ± 0.06)	0.023 (CPM)
SKF2476 (WDS 05243-2149)	2.83 ± 0.03	2.21 ± 0.14	(-14.02 ± 0.02, 32.52 ± 0.03)	(-14.00 ± 0.10, 32.56 ± 0.13)	0.002 (CPM)
UC 102 (WDS 07057+4827)	11.65 ± 0.04	11.70 ± 0.03	(22.49 ± 0.03, -81.08 ± 0.03)	(22.97 ± 0.03, -79.17 ± 0.03)	0.023 (CPM)
KPP992 (WDS 05005-6238)	7.06 ± 0.02	6.99 ± 0.05	(15.01 ± 0.02, 44.78 ± 0.02)	(14.62 ± 0.06, 43.69 ± 0.07)	0.025 (DPM)

Table 2. Measurements of eight double stars made between January-February 2023.

System	Date	Number of Images	Position Angle (°)	Standard error on Position Angle	Separation (")	Standard Error on Separation
SKF2037 (WDS 05104+6020)	2023.08	5	218.3	0.02	15.30	0.015
GWP1113 (WDS 08557-1531)	2023.09	5	67.5	0.06	18.97	0.007
CRB 67 (WDS 05017+3324)	2023.11	5	177.9	0.13	19.26	0.186
HJ 3717 (WDS 05020-3935)	2023.07	5	196.4	0.10	12.88	0.013
KPP2106 (WDS 05037-7333)	2023.07	5	8.9	0.02	17.00	0.016
SKF2476 (WDS 05243-2149)	2023.07	5	326.7	0.08	19.38	0.028
UC 102 (WDS 07057+4827)	2023.11	5	59.2	0.10	19.834	0.013
KPP992 (WDS 05005-6238)	2023.04	5	48.6	0.22	8.01	0.035

Plots:

Previous measurements for each system were requested from the US Naval Observatory. Using the historical data along with our current data, we plot a graph to witness any formation of orbit. If any forward curve is formed, that would suggest stars are orbiting and with future observations, a predicted orbit may be formed. But more importantly, it would suggest that the star system is a binary star system.

Each plot is labelled by the discover code of the system. Note that the historical data are plotted in Figure 1 chronologically using colour. The darker the colour, the more recent the data. The measurements are plotted as a circle and the measurements taken by us are the green square with an x. The other red square is the measurement we obtained from Gaia. Observing any trends from the plotted graph we can estimate if the stars are likely to be gravitationally bound.

Figure 1: Measurement of each system (labelled by their discover code) in accordance with the historical data. The darker circles are more recent measurements than the lighter circles. Our measurements are green squares with an x in the middle, while the Gaia collected data is the red square.

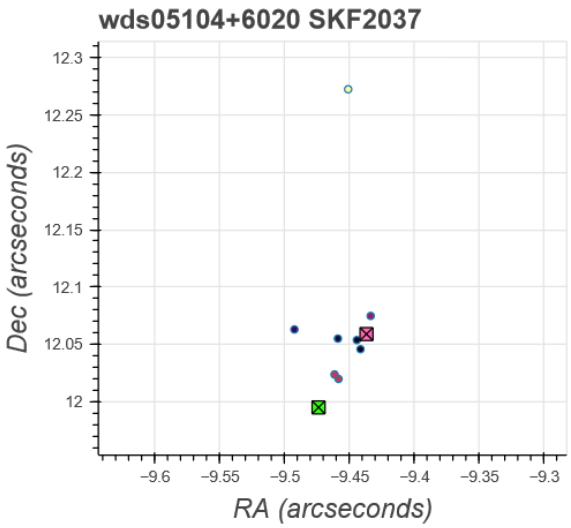
wds05104+6020 SKF2037
Dec (arcseconds)
RA (arcseconds)

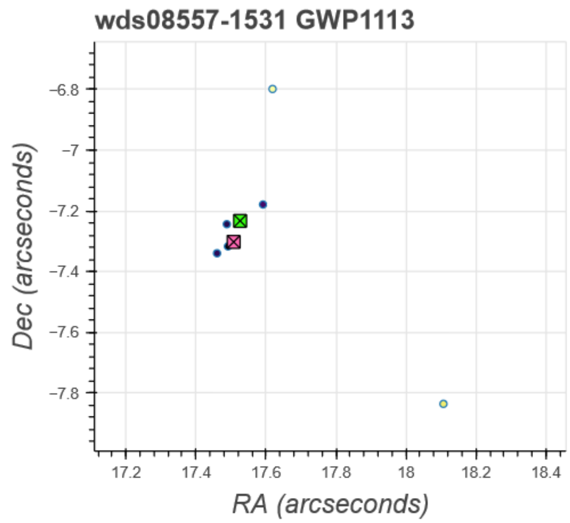
wds08557-1531 GWP1113
Dec (arcseconds)
RA (arcseconds)

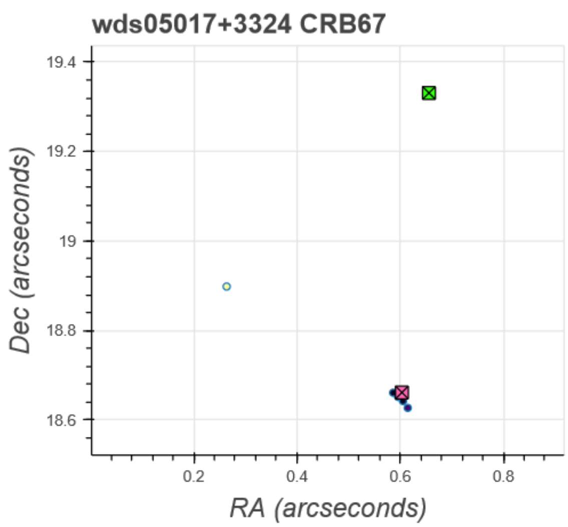
wds05017+3324 CRB67
Dec (arcseconds)
RA (arcseconds)

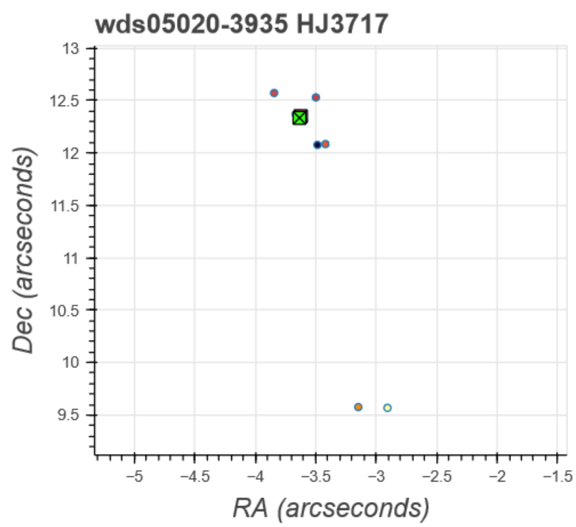
wds05020-3935 HJ3717
Dec (arcseconds)
RA (arcseconds)

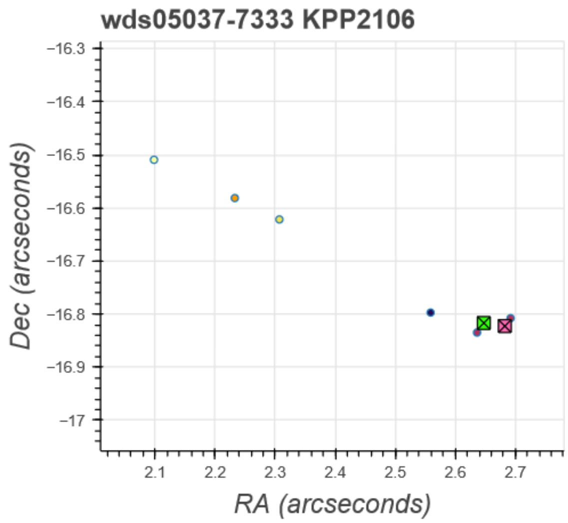

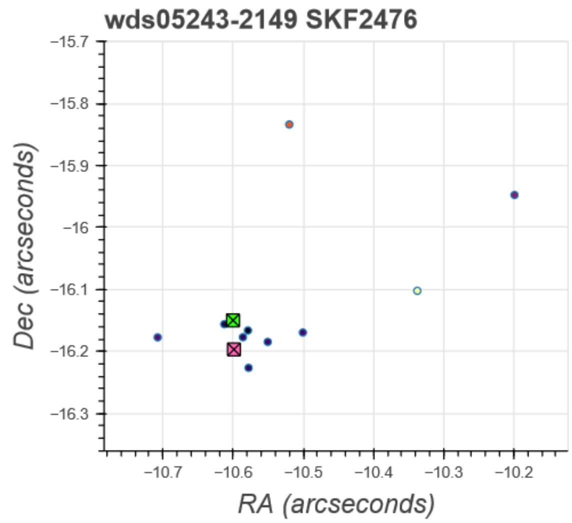

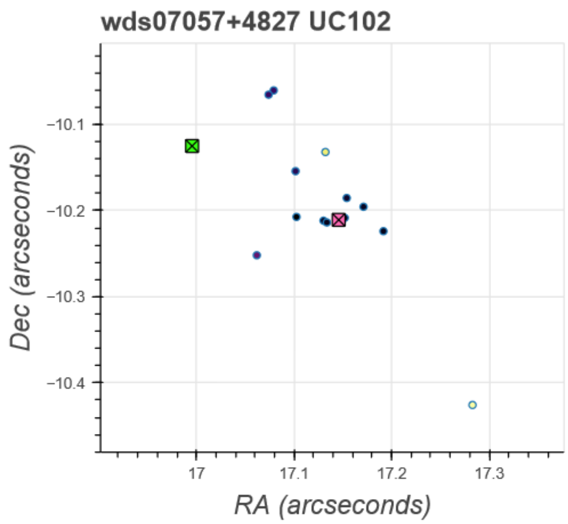

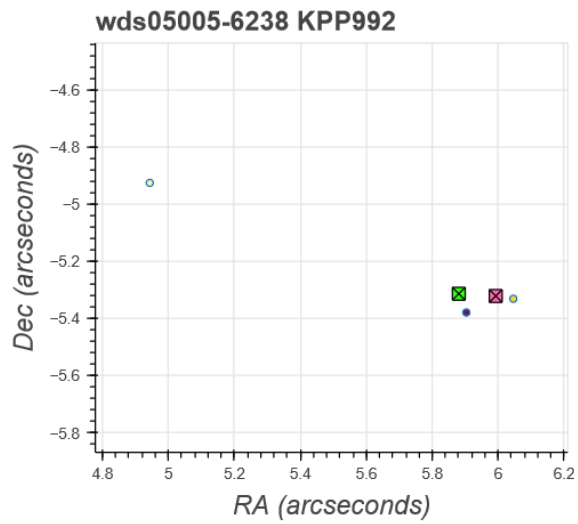

Analysis of the Double Stars:

If two or more stars have similar parallax and proper motion, they show signs that they might be related to one another in some way. However, just parallax and proper motion are not enough data to determine these conclusions. For our star system, they do not exhibit any sign of binary system behaviour. Amongst our eight double stars, all of them seem to have Common Proper Motion i.e., the double stars are moving through space relatively together.

However, the plot reveals no notable curvature. Thus, the historical data does not show any signs of stars orbiting each other. One thing to note in Figure 1 is that we have very few historical data of our stars so far. Notably the earlier measurements show high deviations from the newer data.

When historical data is insufficient to characterise a system as binary, one theory we can use is the system escape velocity. The two stars in each system need to be moving with a velocity less than the system escape velocity. The system escape velocity and the relative space velocity of the secondary star can be calculated using the equations presented in Bonifacio et al, 2020 and Caputo et al, 2020. The calculated data can be found in Table 3.

Table 3: System Escape Velocity and Relative Space Velocity of the secondary stars in each double star system.

System	System Escape Velocity (m/s)	Relative Space Velocity (m/s)
SKF2037	265.05	754.14
GWP1113	74.79	3716.99
CRB 67	73.82	696.46
HJ 3717	177.73	1153.95
KPP2106	82.56	1475.56
SKF2476	10.03	1945.01
UC 102	207.42	886.54
KPP992	93.41	1094.43

From Table 3, we find that the secondary star in every system is moving faster than the system escape velocity of the primary star. However, we must assume that calculation could have errors because they are estimated from so many imprecisely known values. Nonetheless, this gives some rough data to be used in future for further measurements.

Conclusion:

The systems that we examined and analysed do not exhibit much data implying a physical relationship. However, further observations need to be taken to find definitive conclusions on the nature of these double stars.

Acknowledgements:

This research has made use of the Washington Double Star Catalogue maintained at the U.S. Naval Observatory. The observations were conducted using the help of telescopes at Skynet Robotics Telescope Network (https://skynet.unc.edu) operated by out of the University of North Carolina at Chapel Hill supported by the National Science Foundation, North Carolina Space Grant, and the Mount Cuba Astronomical Foundation. The exploration and measurements of the data was done by the web-based application Afterglow maintained by the Skynet database. This work has made use of data from the European Space Agency (ESA) mission Gaia (https://www.cosmos.esa.int/gaia), processed by the Gaia Data Processing and Analysis Consortium (DPAC, https://www.cosmos.esa.int/web/gaia/dpac/consortium). Funding for the DPAC has been provided by national institutions, in particular the institutions participating in the Gaia Multilateral Agreement. This research has made use of "ALADIN sky atlas" developed at CDS, Strasbourg Observatory, France.

Special thanks to Dan Reichart for providing us access and documentations on the telescopes and tools at Skynet Robotics Telescope Network. This work makes use of observations taken by 0.4 Prompt2, Prompt5, PROMPT-MO-1, PROMPT-USASK, USASK-14, Morehead telescopes of Skynet Robotics Telescope Network located in Cerro Tololo, Morehead, Meckering and Sleaford. We especially appreciate Daryl Janzen's advice, inputs, and directions on our paper. Also, we would like to express our gratitude to Daryl Janzen for evaluating drafts of this work and providing numerous insightful suggestions for improvement, all of which have been incorporated into this final edition.

References:

- Gaia Collaboration et al. (2016b): The Gaia mission (provides a description of the Gaia mission including spacecraft, instruments, survey and measurement principles, and operations).
- Gaia Collaboration et al. (2022k): Gaia DR3: Summary of the contents and survey properties.
- Bonifacio, B., C. Marchetti, R. Caputo, and K. Tock. (2020). Measurements of Neglected Double Stars. Journal of Double Star Observations, 16(5), 411–423. http://www.jdso.org/volume16/number5/Bonifacio_411_423.pdf
- Harshaw, Richard, 2016, *"CCD Measurements of 141 Proper Motion Stars: The Autumn 2015 Observing Program at the Brilliant Sky Observatory, Part 3"*, Journal of Double Star Observations, Vol. 12, No. 4, 394-399. http://www.jdso.org/volume12/number4/Harshaw_394_399.pdf
- Caputo, Ryan, et al, 2020, *"Observation and Investigation of 14 Wide Common Proper Motion Doubles in the Washington Double Star Catalog"*, Journal of Double Star Observations, Vol. 16 No. 2, 173 – 182. http://www.jdso.org/volume16/number2/Caputo_173_182.pdf
- Reichart, Dan, et al, since 2004, Skynet Robotic Telescope Network, University of North Carolina. https://skynet.unc.edu/
- SIMBAD Astronomical Database. Unistra/CNRS.2020. https://simbad.u-strasbg.fr/simbad/
- Stelledoppie - Stelle Doppie - Double Star Database, Gianluca Sordiglioni. http://www.stelledoppie.it/
- The ALADIN interactive sky atlas - A reference tool for identification of astronomical sources. F. Bonnarel, P. Fernique, O. Bienaymé, D. Egret, F. Genova, M. Louys, F. Ochsenbein, M. Wenger, J. G. Bartlett Astron. Astrophys. Suppl. Ser. 143 (1) 33-40 (2000) DOI: 10.1051/aas:2000331

Astrometric Measurements of WDS 21143+2522 AB and WDS 21139+2512 in Vulpecula

Shannon Pangalos-Scott[1,5], Alex Vasquez[1,6], Rachael Rios[3], Clarissa Johansen[1], Sanat Vidwans[2], Ryan Geiser[1], Ryan Franz[1], Rachel Freed[4], Rebecca Chamberlain[1], Russ Genet[7], Joey Sandine[1], Sydney Stricker[1]

1. The Evergreen State College, Olympia, WA
2. Columbia Virtual Academy (CVA), Valley, WA
3. Academy for Academic Excellence, Apple Valley, CA
4. Institute for Student Astronomical Research, Sonoma, CA
5. Quadrivium STEAM & Astronomical Society, Olympia, WA
6. The Evoked Scion Institute, Lacey, WA
7. California Polytechnic State University

Abstract: New astrometric measurements for the binary systems WDS 21143+2522AB (POU5283) and WDS 21139+2512 (POU5276) were observed. Images were requested and received from the Las Cumbres Observatory Global Telescope (Image 3) of these systems on July 7th, 2022 from the observation node in Tenerife, Spain and individual images provided by team members. The program AstroImageJ was used to measure the PA and Sep of the secondary star to the primary within these systems. New astrometric measurements for WDS 21143+2522 AB are: PA 83.99° and a Sep of 15.89". For WDS 21139+2512, the PA was 108.17° and a Sep of 5.54". According to Gaia parallax data for these stars, it was concluded that these two systems are not gravitationally bound and are visual double star systems.

Introduction

The goal of this paper was to record the current position angle and separation of WDS 21143+2522 AB. According to *Stelle Doppie*, this system is located within the Vulpecula constellation in the northern hemisphere, both with uncertain classifications. Current images of this system were taken on July 7th, 2022, and recorded. While reviewing the images, it was apparent that a second double star system, WDS 21139+2512, was within the telescope's field of view. Therefore, measurements of the second system's current position angle and separation were also recorded.

WDS 21143+2522AB, which has an RA of $21^h\ 14^m\ 18.37^s$ and a DEC of +25° 22' 15.3", was discovered by French astronomer Abel Pourteau in 1893 (Smith, 2012). The magnitude of the primary star (A) in this system is 10.10, and the secondary (B) has a magnitude of 11.90, with a Δmag of 1.8. The first measurements of this system are recorded as having a separation (ρ) of 16.8", with a position angle (θ) of 92°. The most recent astrometric measurements of this system were in 2015, which recorded a separation (ρ) of 15.9" and a position angle (θ) of 84°. In total, there have been 13 observations of the primary and secondary (AB) stars in this system. Note: The WDS 21143+2522 has a tertiary (C) component that could not be resolved in our images.

Figure 1: Photograph by Sanat Vidwans . WDS 21143+2522AB (green) and WDS 21139+2512 (blue), taken on July 29th at 22:01 PDT, 2022 near Big Finn Hill park, Kirkland, WA. The equipment used was a 130mm Newtonian reflector telescope with a 650mm focal length and a ZWO ASI224MC camera.

WDS 21139+2512 was discovered later in 1898, also by Pourteau (Smith, 2012), and is located at RA $21^h\ 13^m\ 51.48^s$ and DEC +25° 11' 44.4". Like the other system, it was last observed in 2015. The magnitude of the primary star (A) is 11.28 and the secondary is 13.90, with a Δmag of 2.62. The initial measurements of this system are recorded as a separation (ρ) of 7.7" with a position angle (θ) of 104°. The most recent astrometric measurements of this system were recorded with a separation (ρ) of 5.8" and a position angle (θ) of 108°. In total, there have been 11 observations of the primary and secondary (AB) stars in this system.

Equipment and Procedure

WDS 21143+2522 AB was selected using the Stelle Doppie Database Selection Tool using the below parameters.

Table 1: Parameters used to select WDS 21143+2522 AB in the StelleDoppe Database Selection Tool.

	RA	Dec	Pri. Mag	Sec. Mag	Δmag	Sep.	Last Obs
Min	$14^h\ 00^m\ 00^s$	-90° 00' 00"	10	10	<3	5	2015
Max	$23^h\ 00^m\ 00^s$	+90° 00' 00"	12	14		10	

Once the original candidate was selected, an observation request was submitted using the Las Cumbres Observatory Global Telescope (LCOGT), a global network of telescopes that supports science and education. The images were taken on July 7th, 2022 between 01:54:35 and 02:00:23 UTC (JD 2459768.079572) by an LCOGT observation node located at the Teide observatory in Tenerife, Canary Islands, Spain (a similar observational node is shown in Figure 2). A total of ten images with a 10-sec exposure time were requested, using a Bessel-V (visible) filter, on one of the site's two, 0.4-m telescopes with an SBIG STL-6303 CCD camera. The initial target of the images was WDS 21143+2522.

However, due to the field of view of the telescope, it was found that WDS 21139+2512 was also within the images available.

Figure 2. A 0.4-m instrument is similar to the one at the Teide observatory used for imaging - this particular instrument is located at a Las Cumbres node at the Cerro Tololo observatory in Chile.

Astrometric measurements of both systems were taken using the measurement tool in AstroImage J (Collins et al., 2017) (Figure 3). Historical data for the position angle and separation was requested from Dr. Rachel Matson at the United States Naval Observatory (USNO) and compared to current astrometric measurements. From this, two historical data plots were made for each system. Finally, on VizieR, data from Gaia DR3 was found for the A and B components for WDS 21143+2522, and the A and B components for WDS 21139+2512.

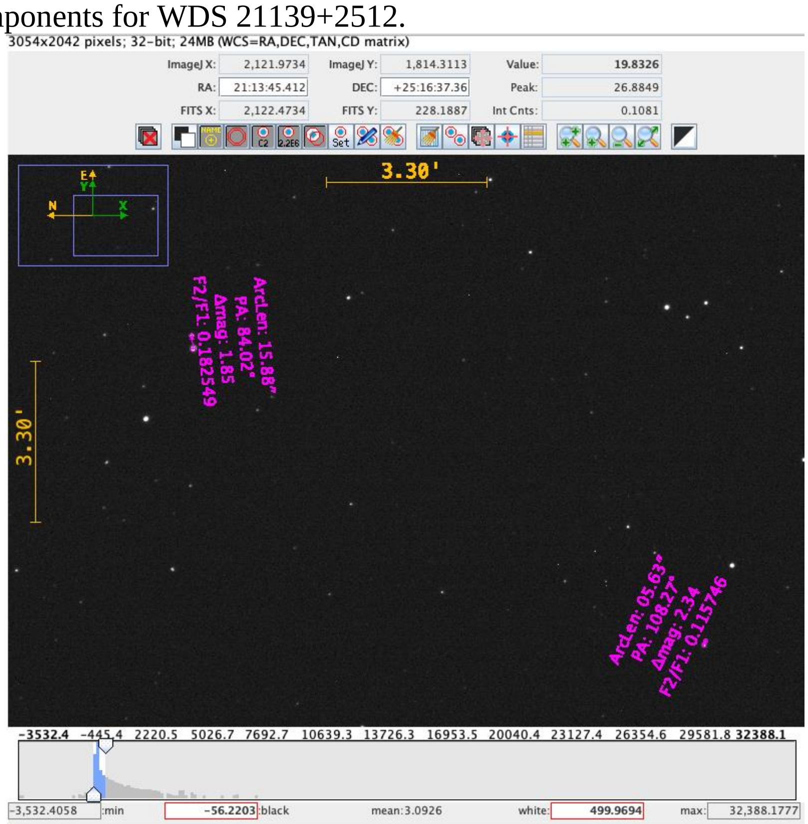

Figure 3. A screenshot of the AstroimageJ interface with the first of the ten images. Measurements of both star systems have been taken and the data is displayed as shown.

Historical data obtained from the USNO for WDS 21143+2522 AB (left) and WDS 21139+2512 (right), is shown in Table 2.

Table 2: Historical data (left) WDS 21143+2522 AB and (right) WDS 21139+2512. Separation (ρ) is measured in arcseconds, position angle is measured in (θ) degrees.

WDS 21143+2522 AB		
Epoch	**Sep "**	**PA °**
1893.70	16.79	92.0
1894.71	16.67	92.0
1897.73	15.95	91.5
1898.70	17.20	93.4
1982.90	15.88	87.0
2000.40	15.99	85.1
2001.70	16.03	85.3
2005.75	15.85	85.0
2009.88	15.99	85.9
2012.74	15.90	84.5
2013.65	15.90	84.5
2014.66	15.92	84.4
2014.79	15.90	84.4
2015.00	15.90	84.4

WDS 21139+2512		
Epoch	**Sep "**	**PA °**
1898.70	7.70	103.90
1982.90	6.13	116.70
2000.51	6.04	107.30
2001.70	6.03	107.00
2009.88	5.52	110.62
2012.76	5.71	107.95
2013.54	5.82	107.86
2013.64	5.79	107.94
2014.67	5.78	107.96
2015.00	5.81	107.96
2015.71	5.80	107.92

Results

Current measurements representing the separation and position angle between the A and B components are displayed in Table 3. The mean and standard deviation for each set of images was also calculated.

Table 3: Data for (left) WDS 21143+2522, (right) WDS 21139+2512. Separation (ρ) is measured in arcseconds, with position angle (θ) measured in degrees, The average, standard deviation, and standard error of the mean (SEM) have been calculated.

WDS 21143+2522 AB		
Image	**Sep "**	**PA °**
1	15.88	83.96
2	15.87	84.03
3	15.90	84.08
4	15.89	84.00
5	15.89	83.89
6	15.90	83.94
7	15.91	84.01
8	15.91	83.95
9	15.89	84.01
10	15.84	84.04
Average	**15.89**	**83.99**
SD	**0.06**	**0.02**
SEM	**0.02**	**0.01**

WDS 21139+2512		
Image	**Sep "**	**PA °**
1	5.63	108.27
2	5.68	107.49
3	5.60	108.27
4	5.56	108.05
5	5.65	108.40
6	5.60	107.91
7	5.35	108.39
8	5.14	109.35
9	5.63	107.98
10	5.60	107.60
Average	**5.54**	**108.17**
SD	**0.16**	**0.52**
SEM	**0.05**	**0.16**

Discussion

In the following graphs (Figures 4 & 5) the red circle at (0,0) represents the A component, the gray triangles represent the historic relative position of the B component, and the green triangles represent the observed position of the B component according to our newest measurement. Older historical data points are a light shade of gray, and newer points are darker.

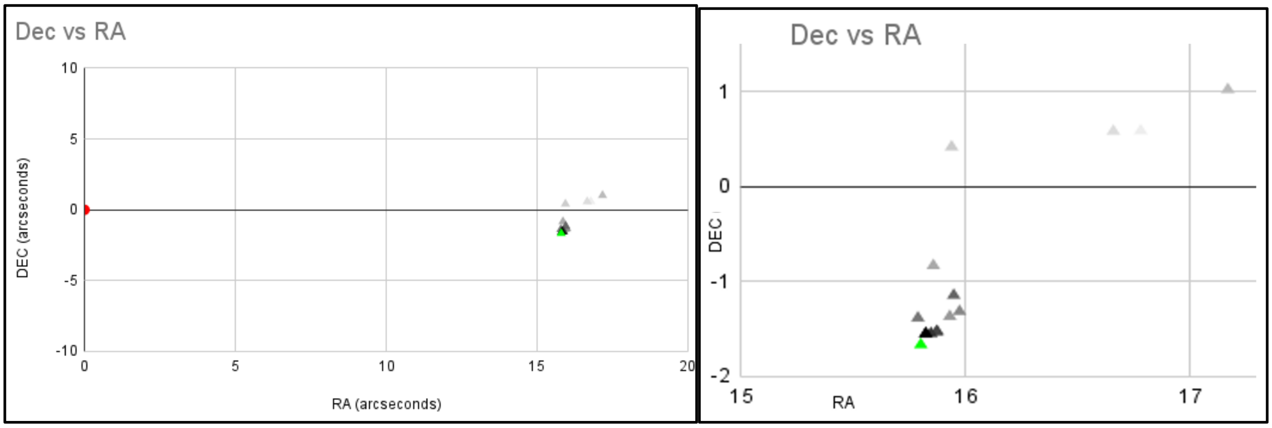

Figure 4. Historical data for WDS 21143+2522 AB. (left) Shows the A component relative to the B component. (right) Shows a zoomed-in representation of the graph, note that the RA marking begins with 15. The saturation of the gray triangle on historical points is a sliding scale, light for the oldest measurements, and darker for the most recent, except for the new data point, which is marked with green.

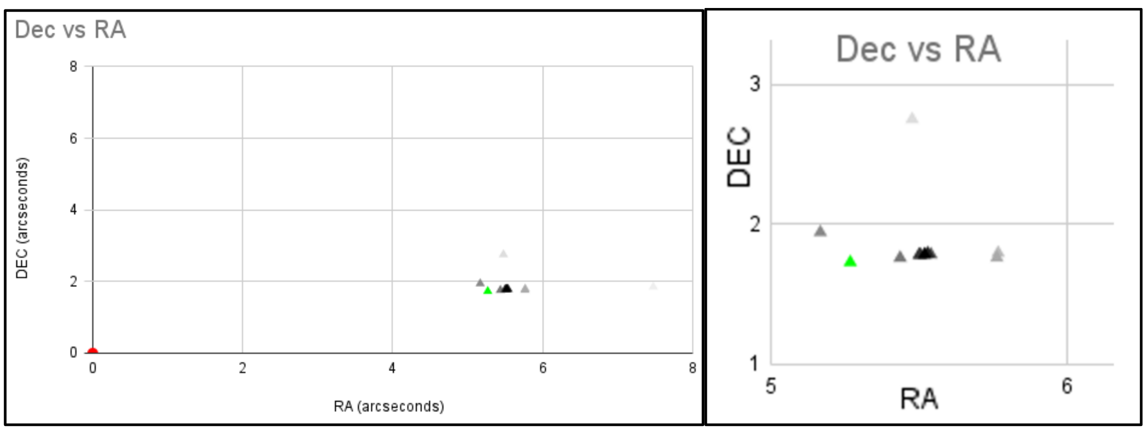

Figure 5. Historical data for WDS 21139+2512. (left) Shows the A component relative to the B component. (right) Shows a zoomed-in representation of the graph, note that the RA marking begins with 5 and DEC markings begin with 1. The saturation of the gray triangle on historical points is a sliding scale, light for the oldest measurements, and darker for the most recent, except for the new data point, which is marked with green.

From VizieR, data from Gaia DR3 was found for the A and B components for WDS 21143+2522, and the A and B components for WDS 21139+2512. This is displayed in table 4 below.

Table 4. WDS 21143+2522 AB Gaia DR3

Component	Parallax (mas)	PM RA (mas/yr)	PM Dec (mas/yr)
A	3.11 ± 0.02	-9.53 ± 0.02	-24.65 ± 0.01
B	2.17 ± 0.02	-16.36 ± 0.02	-9.00 ± 0.01

From the parallax values, WDS 21143+2522 A is 321.048 parsecs from Earth, and WDS 21143+2522 B is 459.812 parsecs from Earth. Based on these values WDS 21143+2522 A and WDS 21143+2522 B have a spatial separation of 28,622,129.57 AU, According to Richard Harshaw (2018), very few binaries have separations that are more than 3,000 AU, and most are closer than 1,000 AU. He also states that two stars separated by one parsec are probably too far to be gravitationally bound, even if they are massive. Since this system has a separation of tens of millions of AU, it is exceedingly unlikely that these two stars are gravitationally bound.

For WDS 21143+2522 AB, the proper motion values are -9.53 ± 0.02 in RA and -24.65 ± 0.01 in DEC for the A component and -16.36 ± 0.02 in RA and -9.00 ± 0.01 in DEC for the B component. These values do not show any similarities, especially for the proper motion values in the DEC axis (Table 4). In the historical data and graph of such data, no defined orbital trajectory is shown. The separation remains variable, but is generally decreasing over time. The position angle also shows a trend down over time, and is less variable then the separation.

Table 5. WDS 21139+2512 Gaia DR3

Component	Parallax (mas)	PM RA (mas/yr)	PM Dec (mas/yr)
A	2.56 ± 0.13	11.85 ± 0.1	-12.30 ± 0.10
B	0.84 ± 0.02	-3.6 ± 0.02	-8.89 ± 0.01

Using the parallax values, WDS 21139+2512 A is 390.244 parsecs from Earth, and WDS 21139+2512 B is 1197.031 parsecs from Earth. From this, WDS 21139+2512 A and WDS 21139+2512 B has a spatial separation of 166,411,764.2 AU. This distance is more than five times greater than WDS 21143+2522, which has been determined to be almost certainly not gravitationally bound.

For WDS 21139+2512, the proper motion values are 11.85 ± 0.1 in RA and -12.30 ± 0.10 in DEC for the A component and, -3.6 ± 0.02 in RA and -8.89 ± 0.01 in DEC for the B component. They also do not show any similarities. For the proper motion in the RA axis, the two stars are traveling in opposite directions. In the historical data the separation decreases over time, this is shown in the historical data graph as the points get closer to 0,0. The position angle steadily increases over time except for one outlier observation is 1982. By purely observing the graph, this line may be considered as an orbital trend. However, from the parallax values, this simply means WDS 21139+2512 B is passing behind WDS 21139+2512 A as the former is more then four times further from Earth (Table 5).

Conclusions

Using the Las Cumbres Observatory portal and the Teide observatory in Tenerife, Spain, images were taken and astrometric data were collected on two separate binary star systems, WDS 21143+2522 AB and WDS 21139+2512. Historical data were then requested from the United States Naval Observatory and compared to the new astrometric measurements. For WDS 21143+2522 AB, the historical chart does not show a clear orbital trajectory. For WDS 21139+2512, the historical chart shows a straight line, which is subject to interpretation. However, the difference in parallax values from Gaia DR3 for both systems, WDS 21139+2512 and WDS 21143+2522 AB, are evidence that it is extremely unlikely that they are gravitationally bound and are simply visual double star systems.

Acknowledgments

We would like to give a very special thank you to Richard Harshaw, Kalée Tock, and Dr. Cheryl Genet for their tireless commitment to making science accessible for all. We would also like to thank Dr. Rachel Matson at the United States Naval Observatory for providing WDS historical data, as well as, the Washington Double Star Catalog, Stelle Doppie, and the Las Cumbres Observatory Global Telescope

Network for access to their telescopes for imaging. We are grateful to the European Space Agency and their mission, Gaia, for providing parallax values and proper motion values in both RA and DEC for all four of the stars listed above. Lastly, we would like to thank the educational institutions that have supported scientific research for students, the Institute for Student Astronomical Research, that facilitated this paper; The Evergreen State College, Columbia Virtual Academy, Academy for Academic Excellence, Quadrivium STEAM & Astronomical Society, and The Evoked Scion Institute.

References

Collins, K. A., Kielkopf, J. F., Stassun, K. G., & Hessman, F. V. (2017). ASTROIMAGEJ: Image Processing and Photometric Extraction for ULTRA-PRECISE ASTRONOMICAL Light Curves. The Astronomical Journal, 153(2), 77–89. https://doi.org/10.3847/1538-3881/153/2/77

Commander, Naval Meteorology and Oceanography Command. (2022). U.S. Naval Observatory. Retrieved August 3, 2022, from https://www.cnmoc.usff.navy.mil/usno/

Gaia DR3 content - Gaia - Cosmos. (2022). GAIA EARLY DATA RELEASE 3 (GAIA DR3). Retrieved August 3, 2022, from https://www.cosmos.esa.int/web/gaia/earlydr3

Harshaw, R. (2018). Gaia DR2 and the Washington Double Star Catalog: A tale of two databases. *Journal of Double Star Observations*, *14*(4), 734-740. http://www.jdso.org/volume14/number4/Harshaw_734_740.pdf

Smith, F. (2012). The Double Stars of Abel Pourteau. Journal of Double Star Observations. Retrieved July 30, 2022, from http://www.jdso.org/volume8/number4/Smith_v8_p243.pdf

Stelle Doppie - Double Star Database. (2022). Stelle Doppie. Retrieved August 3, 2022, from https://www.stelledoppie.it/index2.php

Teide | Las Cumbres Observatory. (2022). Las Cumbres Observatory. Retrieved August 3, 2022, from https://lco.global/observatory/sites/teide/

VizieR. (2022). VizieR. Retrieved August 3, 2022, from https://vizier.cds.unistra.fr/viz-bin/VizieR

Astrometric Measurements of WDS 13175-4625 DON 1104

Vanessa Harvey[1], Ann-Katrin Bock[1], Erin De Pree[2], Elan Lavie[3], Jennifer Krestow[1], Elizabeth Grimm[1], Nicholas Johnson[1], Michael Strane[1], Rachel Freed[4]

1. Glendale Community College, Glendale, California, USA, contact: *vharvey@glendale.edu*
2. Bates College, Lewiston, Maine, USA
3. El Cerrito High School, El Cerrito, California, USA
4. Institute for Student Astronomical Research, Sonoma, California, USA

Abstract

We present astrometric measurements of the double star system WDS 13175-4625 DON 1104 using the Las Cumbres Observatory Cerro Tololo and Siding Spring telescopes measured on March 14, 2023 and April 25, 2023, respectively. A position angle of 256.3° ± 0.48° and angular separation of 7.51" ± 0.069" were determined. Based on astrometric analysis as well as the parallax and proper motion values from Gaia DR3, we conclude that these stars are not gravitationally bound.

1. Introduction

In this paper we provide current astrometric measurements of WDS 13175-4625 DON 1104 with the objective of determining whether the double star system shows evidence of gravitational association. Only four measurements were made of this system in the past 114 years.

The Washington Double Star (WDS) Catalog through Stelle Doppie (Sordiglioni, 2023) was used to search for the candidate star using the following criteria: a component separation between 5 and 10 arcseconds, a primary star magnitude between 8 and 10, a delta magnitude (Δmag) of less than or equal to 3, an uncertain binary status, and a date of last observation less than or equal to the year 2015. The right ascension was chosen to be between 13 and 23 hours and the declination between −90° and +90°. WDS 13175-4625 DON 1104 met all our criteria except for Δmag. We chose a 5-magnitude separation between the primary and secondary stars for the system.

Since its discovery in 1909, there have been a total of four measurements for WDS 13175-4625 DON 1104. The primary star has a spectral type of M0/M1III indicating that it is a red giant star, and it has a magnitude of 8.48 in the visual. Its right ascension is 13h 17m 27.73s and its declination is –46° 24' 11.1" placing it in the constellation Centaurus. The secondary star has a magnitude of 13.50. The first angular separation measured in 1909 was 11.5" with a position angle of 259.7°. Its most recent measurement by Gaia in 2015 showed an angular separation of 8.1" and position angle of 256°.

2. Equipment and Procedures

The astrometric images of WDS 13175-4625 DON 1104 were captured by the Las Cumbres Observatory Global Telescope Network (LCOGT) 0.4-m telescope, using the SBIG 6303 charge-coupled device (CCD) camera at the Cerro Tololo Observatory in Chile on March 13, 2023 (2023.203) and Siding Spring Observatory in Australia on April 25, 2023 (2023.317). The images were calibrated, bias subtracted, and flat fielded by the LCOGT using the BANZAI pipeline.

Because of the five-magnitude difference between the component stars, care was taken to determine the exposure time such that the counts of the two stars fit within the dynamic range of the CCD camera. Initial test exposures of six frames at five and ten seconds each in the Bessell-V filter were made to determine the signal-to-noise of the secondary star and take initial astrometric measurements. Of these 12 measurements ten showed low signal-to-noise (< 100) for the secondary star, particularly the five second exposures. These were followed by test images at five and ten seconds in the infrared using the Pan-STARRS-z filter (central wavelength 8700-nm, bandwidth 1040-nm) to determine if the secondary star's signal-to-noise would be stronger at longer wavelengths. In these images in the infrared the secondary star barely appeared above the background for measurement. Images were also taken at five and ten seconds using the Bessell-B filter to determine if the signal of the secondary star would improve with observations at a shorter wavelength. The signal-to-noise of the secondary star did not improve with the blue filter as the secondary star also barely appeared above background for measurement.

Additional exposure times were taken at 20-, 25-, and 30-seconds. However, at these exposure times the peak measurements for the primary star were approaching the saturation level of the camera. It was then determined from observing the peak values of the primary star and signal-to-noise of the secondary star from all of the measurements that an exposure time of 10 seconds in the Bessell-V filter would yield a signal-to-noise of at least 100 for the secondary star while keeping the peak measurement of the primary star below the saturation level of ~64000 ADU (for the raw images) or 102400 e- (for the processed images). Thus, an additional 14 images were taken using these criteria at the Siding Spring Observatory. These measurements were added to the initial Cerro Tololo Observatory 10-sec exposures where the signal-to-noise was at least 100 for a total of 16 images for this study.

Images were analyzed using the AstroImageJ (AIJ) software suite (Collins et al., 2017). Angular separation and position angle of the stars were measured using the Howell centroid method (Howell, 1989). The object aperture was set to 6.0 pixels and the inner and outer radii of the background annulus were set to 30 and 40 pixels, respectively.

The AIJ astrometric measurements of position angle and angular separation were recorded, and the mean, sample standard deviation, and standard error of the mean were calculated. In addition, parallax and proper motion data was searched for in the Gaia Data Release 3 (DR3) catalog (Gaia Collaboration, 2015) and historical data for WDS 13175-4625 DON 1104 was requested from Dr. Rachel Matson at the U. S. Naval Observatory.

3. Data

Data was collected from the LCOGT 0.4-m telescopes using the SBIG 6303 CCD camera with the Bessell-V filter. The FITS files were reduced by LCOGT using the BANZAI pipeline and these processed images were analyzed using AstroImageJ (AIJ). A typical image, with measurements, is shown in Fig. 1.

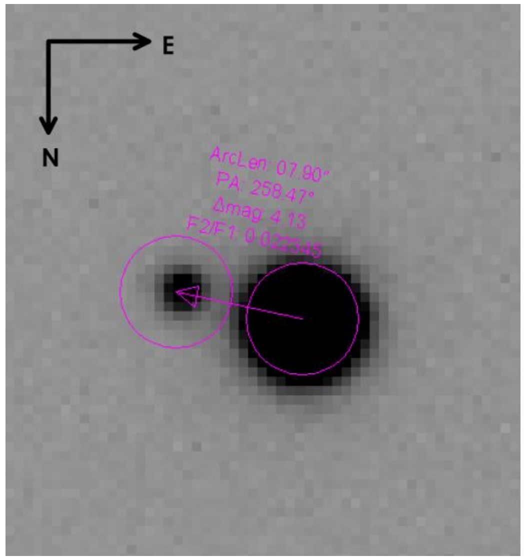

Figure 1: Example of an image of WDS 13175-4625 DON 1104 with measurements from AstroImageJ

Table 1 shows the mean, standard deviation, and standard error of the mean for the 16 images.

Table 1. Current results for WDS 13175-4625 DON 1104. The position angle is 256.3° ± 0.48° and the separation is 7.51" ± 0.069".

	Observatory	Dates	Images		PA (°)	SEP (″)
WDS13175-4625 DON1104	Cerro Tololo	2023.203	2	Mean (of all 16 images)	256.3	7.51
	Sliding Spring	2023.317	14	Sample Standard Deviation	1.9	0.30
				Standard Error of the Mean	0.48	0.069

4. Discussion

The historical data, shown in Table 2, for WDS 13175-4625 DON 1104 was requested from the U.S. Naval Observatory (Matson, 2023). The historical data consists of 4 data points starting in the year 1909 and ending in the year 2015. Table 2 shows the values for their position angle (PA) in degrees, separation (SEP) in arcseconds, as well as the measurement method used for the star system.

The historical data values for position angle and separation, shown in Fig. 2 along with our current measurement, were resolved to x-y coordinates (in arcseconds) using the following equations:

$$x(RA) = \rho\cos\theta \quad (1)$$

$$y(DEC) = \rho\sin\theta \quad (2)$$

where x is right ascension (RA), y is declination (DEC), ρ is the angular separation (SEP) and θ is the position angle (PA). The date for each measurement is shown. No orbital trend is observed.

Table 2. Historical and current measurements of WDS 13175-4625 DON 1104.

Date	PA (θ, deg)	Sep (ρ, arcsec)	x (RA, arcsec)	y (DEC, arcsec)	Measurement Method
1909.32	259.7	11.536	-2.06266	-11.3501	Pa: photographic, with astrograph
1929.24	258.4	10.42	-2.09523	-10.2072	Ma: micrometer with refractor
2000.22	261.2	7.8	-1.19329	-7.70818	E2: 2MASS (Two Micron All-Sky Survey)
2015	255.513	8.149	-2.03856	-7.8899	Hg: Gaia
2023.32	256.3	7.51	-1.93	-7.28	P: photographic technique

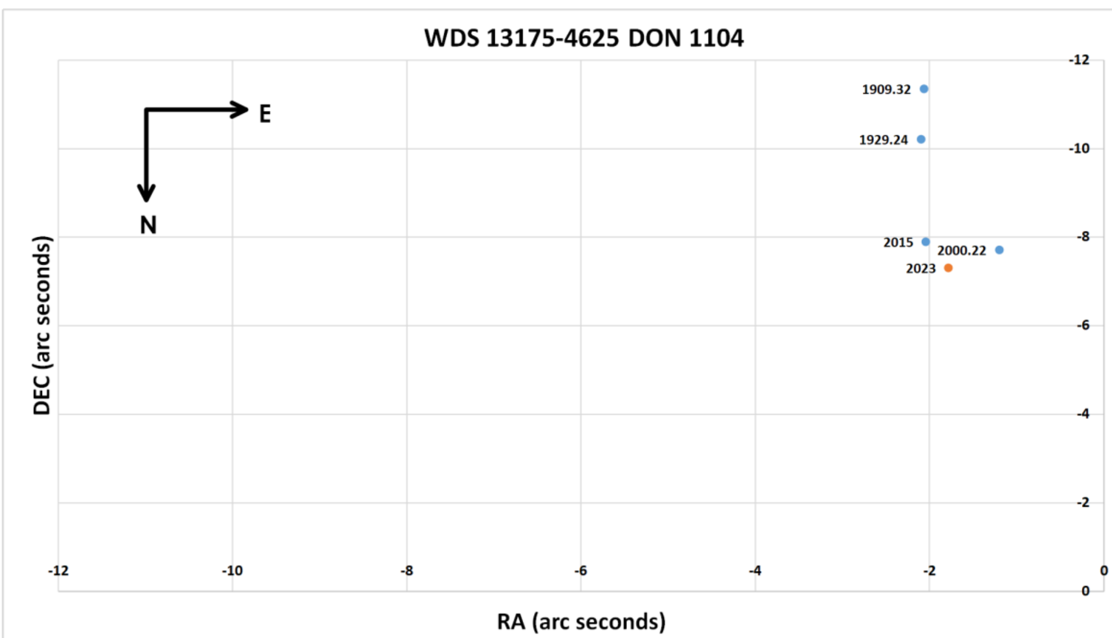

Figure 2: x (right ascension, RA) and y (declination, DEC) of the historical data (blue) and current data (orange)

To further investigate the movement of the secondary star, position angle versus time in Fig. 3 and separation versus time Fig. 4 were plotted. The position angle shows no clear relationship or trend with epoch progression. The separation, however, shows a decreasing linear trend with epoch progression. A linear fit to the data (Fig. 4) gives an R-squared of 0.96 showing a strong linear correlation indicating that the stars may be approaching each other.

Figure 3: Position angle versus time

Figure 4: Separation versus time

Using the VizieR astronomical catalog (Ochsenbein, 2000), the Gaia DR3 data (Gaia Collaboration, 2022) for the proper motion and parallax values were found and are provided in Table 3. Using the parallax equation,

$$\frac{1}{\text{parallax (in arcseconds)}} = \text{distance (in parsecs)} \quad (3)$$

the distance to each star was calculated and also included in Table 3. (Please note that accurately converting from parallax to distance is more complex than this equation (Luri, 2018), but it does give us a general estimate to work with.) The primary star is 683.4 parsecs (141 million AU or 2229 light-years) away while the secondary star is only 221.8 parsecs (45.7 million AU or 723.4 light-years) distant. There is a minimum separation of over 95 million AU, or 1500 light-years. Harshaw (2018) has noted that very few known binaries exceed separations of 3000 AU and stated that most of them are closer than 1000 AU.

Given the lack of orbital motion seen in the movement of the secondary and given the parallax and proper motion values for both stars provided by Gaia in Table 3, we conclude that these stars are not binary, nor do they show any other gravitational association.

Table 3. Parallax and proper motion from Gaia Data Release 3 (Gaia Collaboration, 2022) and the calculated distance.

Star	Parallax (mas)	Distance (pc)	Proper motion in right ascension (mas/year)	Proper motion in declination (mas/year)
Primary	1.4633	683.4 pc (2229 ly)	–17.383	–4.428
Secondary	4.5091	221.8 pc (723 ly)	13.428	–6.730

5. Conclusions

In this study, we have added additional measurements of position angle and separation for WDS 13175-4625 DON 1104. As a result of including this measurement and comparing the relative motion of the secondary star with respect to the primary star over the last 114 years as well as comparing the Gaia DR3 measurements of their parallax and proper motion relative to one another, we conclude that these stars are not gravitationally bound.

Acknowledgments

The authors would like to thank Nikolaus Volgenau of the Las Cumbres Observatory Global Telescope Network for his assistance, as well as the Las Cumbres Observatory Global Telescope for use of their observatories.

We would also like to thank the Glendale Community College Foundation for funding this research opportunity for the Glendale Community College students.

In addition, we thank Dr. Rachel Matson at the US Naval Observatory for supplying historical data for this study.

This research has made use of the Washington Double Star catalog maintained by the U.S. Naval Observatory, as well as data provided by Stelle Doppie. This work has made use of data from the European Space Agency (ESA) mission Gaia (https://www.cosmos.esa.int/gaia), processed by the Gaia Data Processing and Analysis Consortium (DPAC, https://www.cosmos.esa.int/web/gaia/dpac/consortium). Funding for the DPAC has been provided by national institutions, in particular the institutions participating in the Gaia Multilateral Agreement.

References

Collins, K. A., Kielkopf, J. F., Stassun, K. G., & Hessman, F. V. (2017). AstroImageJ: Image processing and photometric extraction for ultra-precise astronomical light curves. The Astronomical Journal, 153(2). Retrieved from https://iopscience.iop.org/article/10.3847/1538-3881/153/2/77.

Gaia Collaboration. (2016). The Gaia mission. Astronomy and Astrophysics, 595. DOI:10.1051/0004-6361/201629272.

Gaia Collaboration. (2022). Gaia Data Release 3: Summary of the Content and Survey Properties. *Astronomy & Astrophysics*. Retrieved from https://www.aanda.org/component/article?access=doi&doi=10.1051/0004-6361/202243940.

Harshaw, R. (2018). Gaia DR2 and the Washington Double Star Catalog: A Tale of Two Databases. *Journal of Double Star Observations.* Vol 14. No 4.

Howell, S. B. (1989). Two-dimensional aperture photometry: signal-to-noise ratio of point-source observations and optimal data-extraction techniques. Publications of the Astronomical Society of the Pacific, 101(640), 616. Retrieved from https://iopscience.iop.org/article/10.1086/132477.

Las Cumbres Observatory Network. (2023). Las Cumbres Observatory Observation Portal, https://lco.global/observatory/instruments/.

Luri, X., A. G. A. Brown, L. M. Sarro, F. Arenou, C. Bailer-Jones, A. Castro-Ginard, J. de Bruijne, T. Prusti, C. Babusiaux, and H. E. Delgado. (2018). Gaia Data Release 2: Using Gaia Parallaxes. *Astronomy & Astrophysics*, 616:A9. DOI: 10.1051/0004-6361/201832964.

Matson, R. (2023). Personal Communication. The Washington Double Star Catalog, Astronomy Department, US Naval Observatory.

Ochsenbein, F., Bauer, P., and Marcout, J. (2000). The VizieR database of astronomical catalogues. *Astronomy and Astrophysics Supplement Series*, 143(1):23–32. Retrieved from https://aas.aanda.org/articles/aas/abs/2000/07/ds1826/ds1826.html.

Sordiglioni, G. (2023). WDS 13175-4625 DON 1104. Retrieved March 6, 2023 from https://www.stelledoppie.it/index2.php?iddoppia=56461.

The Washington Double Star Catalog. (2023). Washington Double Star Catalog. https://crf.usno.navy.mil/wds.